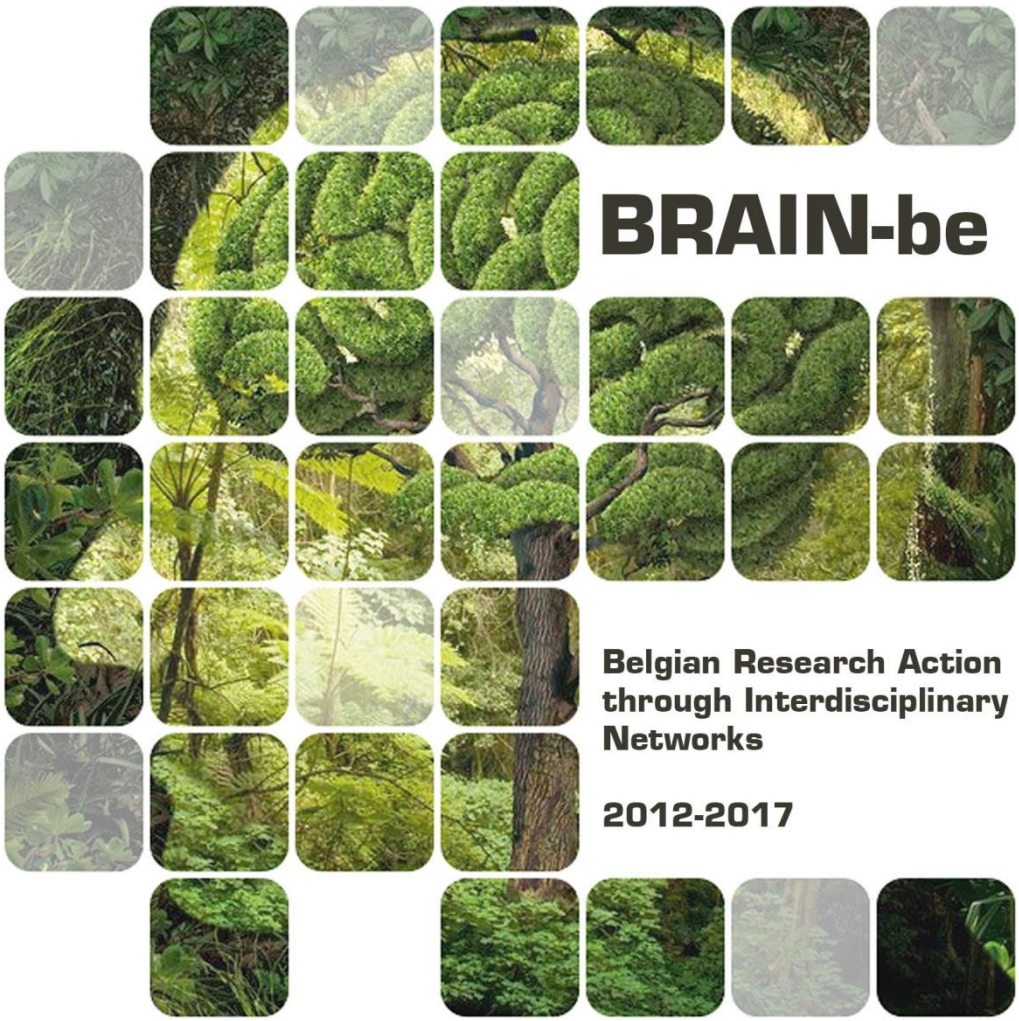

RESPONSE

Reactive transport modelling of point source contamination in soils and groundwater

Diederik Jacques (SCK CEN) – Vanessa Heyvaert (RBINS-GSB) – Marijke Huysmans (VUB) – Erik Smolders (KU Leuven) – Dirk Springael (KULeuven) – Bas Vanwesenmael (UCL) – Jan Walstra (RBINS-GSB)

Axis 2: Geosystems, universe and climate

belspo .be

NETWORK PROJECT

RESPONSE

Reactive transport modelling of point source contamination in soils and groundwater

Contract - BR/165/A2/Response

FINAL REPORT

PROMOTORS:

Diederik Jacques SCK CEN
Vanessa Heyvaert RBINS-GSB
Marijke Huysmans VUB
Erik Smolders KU Leuven
Dirk Springael KU Leuven
Bas Van Wesenmael UCL
Jan Walstra (RBINS-GSB)

AUTHORS:

Diederik Jacques SCK CEN
Vanessa Heyvaert RBINS-GSB
Marijke Huysmans VUB
Cas Neyens VUB
Erik Smolders KU Leuven
Dirk Springael KU Leuven
Bas Van Wesenmael UCL
Jan Walstra (RBINS-GSB)

Published in 2024 by the Belgian Science Policy Office
WTCIII
Simon Bolivarlaan 30 Boulevard Simon Bolivar
B-1000 Brussels
Belgium
Tel: +32 (0)2 238 34 11 - Fax: +32 (0)2 230 59 12
http://www.belspo.be
http://www.belspo.be/brain-be

Contact person: Aline van der Werf
Tel: +32 (0)2 238 36 71

Jacques, D., Heyvaert, V., Huysmans, C. Neyens, M., Smolders, E., Springael, D., Van Wesenmael, B., Walstra, J. RESPONSE Reactive transport modelling of point source contamination in soils and groundwater. Final Report. Brussels : Belgian Science Policy Office 2024 – 176 p. (BRAIN-be - (Belgian Research Action through Interdisciplinary Networks))

TABLE OF CONTENTS

ABSTRACT

Context

This project proposal deals with reactive transport modelling of contaminants in the unsaturated zone and in groundwater. Such modelling studies are typically very site-specific: depending obviously on the contaminant type and its transformation pathways, but also on the environmental conditions (groundwater depth, transient redox conditions, soil chemistry, climate, etc).

Point source contamination sites are omnipresent and in various forms, one of which is cemeteries. These involve the release of various compounds to the underground, such as arsenic and mercury (used in past embalming and burial practices or as wood preservatives), formaldehyde (from current embalming practices), heavy metals (from coffins), herbicides used for removal of unwanted herbs, bacteria and viruses, etc. Depending on local factors, some may ultimately threaten the quality of surface and groundwater resources.

There is a need for methods and tools for selecting potential point sources and assessment of contaminant fate and migration, taking into account site-specific features and characteristics without the possibility of relying on a large amount of precise site-specific information and measurements.

Objectives

This project aims to evaluate how available data on the properties of the environment and contamination can be used to assess the potential evolution of the contamination. Data can be used for different purposes. RESPONSE evaluates the use of data that is (publicly) available in (open) databases or the open (scientific) literature for:

- Assessing the susceptibility of a site to groundwater pollution,
- Setting up subsurface geological models as input to flow and transport models,
- Constraining a model describing the transport of leachate from a landfill,
- Deriving conceptual model and its implementation in (coupled) reactive transport models,

or the use of (limited) data that is collected at a specific site for:

- Screening the actual dispersion of contaminates from a point source,
- Gaining insight into contamination / metal remobilization after land change (flooding flood mitigation strategy by artificial wetlands),
- Gaining insight into the biodegradation of organic pollutants that originate from pesticides applied at given sites such as cemeteries.

Conclusions

Assessing the susceptibility of a site for ground water pollution. We carried out a screening at national scale for the suitability of monitoring schemes to detect the risk of pollution to the shallow groundwater of thousands of cemeteries and landfill sites and checked this suitability through site visits. Several georeferenced databases exist for this purpose. The most important criteria were: drainage class from the digital soil map, distance to water courses and slope of more than 4.5° in Flanders.

Setting up subsurface geological models as input to flow and transport models. Geological models are essential for the development of three-dimensional groundwater flow and transport models. When dealing with relatively small study areas (as is the case here for the point sources such as cemeteries and landfills) and a requirement of high-resolution spatial data (e.g. due to variability inherent to shallow Quarternary geology), publicly available data is lacking with sufficient levels of detail and therefore information from boreholes at the site itself and additional information (soil maps, digital elevation models) are essential.

Although publicly available data is crucial for building a geological model, specific site characterization and information seems to be inevitable as well.

Constraining a model describing the transport of a leachate from a landfill. The case study of this modelling study was a landfill leachate plume in a sandy phreatic aquifer potentially threatening a groundwater extraction site to the south of Leuven, Belgium. As a first step, a composite database was constructed from existing sources and included hydraulic head measurements, geochemical field parameters, and concentrations of geochemical species, among others. The data show elevated concentrations of several species indicative of groundwater pollution due to landfill contamination. A three-dimensional flow and transport model was built using site-specific data available in the open literature. the long-term average hydraulic head field and hydrogeological features can be simulated reasonably well. The general spatial trends in chloride (Cl) could also be reproduced; however, using only readily available chloride data could not reproduce the more detailed variations in the observations.

Model output as regards model complexity was studied for different aspects. Assuming a uniform variable recharge rate (instead of a spatially variable recharge rate) did not affect the flow model output. However, as the load of Cl from the landfill in the aquifer is directly related to the recharge rate through the landfill, Cl concentrations are sensitive to the assumed recharge, although differences are much smaller further from the landfill. Using a homogeneous instead of a heterogeneous hydraulic conductivity field does not greatly affect general plume characteristics. Uncertainties on source term magnitude and timing are often quite large for legacy landfills (and many other point sources). Uncertainties of timing and magnitude of the contamination source are quite important as they persist throughout time and space and affect concentration in receptors. On the other hand, source geometry might influence concentrations near the point source but can be dampened at larger distances or at longer time scales. Finally, also the degradation of dissolved organics by redox reactions was simulated with a limited number of site-specific information, but available measurements did not allow for validation of the simulations.

The case study gave insights into how available data and model abstraction can help build models. However, further research is required on the acceptable degree of data and process abstraction when modelling field-cases of subsurface flow and reactive transport. Although general suggestions are made with regard to sensitive model input and processes for several targets, a lack of specific data prevented a more refined identification of the required levels of data and model complexity. Obtaining an exact level of acceptable abstraction could, for example, be achieved by constructing a (or taking an existing) highly detailed and well-tested model with well-defined goals and adding (stripping) model complexity step-by-step while monitoring model performance to determine when acceptable results are achieved (forfeited). Furthermore, alternative sites and cases should be investigated to

determine the dependence of these general conclusions on the type of system (e.g. advection- or diffusion-dominated, transient or steady-state, the absence of large vertical gradients), pollution source, and type (e.g. leachate infiltration or subsurface storage, mobile versus sorbing contaminants) and system scale (e.g., field-scale and plot-scale). The latter might also influence the dominating processes, e.g., locally around a shallow pollution source; water-table fluctuations or reactive transport in the unsaturated zone can control the fate of contaminants, but for kilometre-scale long-term plume migration, these processes might become less important. If more knowledge on these subjects becomes available, conceptually simple models could be augmented by highly targeted insertions of model complexity. This could lead to a more accessible approach to modelling complex subsurface flow and transport.

Deriving conceptual model and its implementation in (coupled) reactive transport models. Implementing the HPx framework for coupled reactive transport modeling into the groundwater solute transport code MT3D-USGS resulted in a new versatile and powerful tool (MTHP) for assessing the fate and migration of organic and inorganic pollutants in subsurface saturated systems based on a mechanistic understanding of the governing processes including thermodynamic equilibrium calculations and microbiologically driven kinetic degradation processes. The new code was benchmarked for typical coupled reactive transport problems, including redox equilibria, cation exchange, mineral dissolution, and kinetic degradation networks in one- and two-dimensional transport problems.

To ease the use of complex biogeochemical models in coupled reactive transport models, user-friendly input forms were made for two important sets of processes without compromising on the versatility of the software. The first process is the microbiological-driven kinetic degradation of organic pollutants or organic matter for C-H-O components by a set of different electron acceptors (O(0), N(5), Mn(4), Fe(3), and S(6)) also linked to microbiological growth and death. The second process concerns the sorption of (heavy) metals to subsurface organic matter using the discrete humic-ion binding interaction model from Tipping, Lofts, and Sonke (2011) (model VII). Examples were provided to illustrate these models in a batch-type set-up and, for the first process, in a two-dimensional flow and transport set-up. The latter also illustrated the plume fringe concept.

The developed code and the two process implementations – all available in a public software repository – form a good starting point for developing (site-specific) models for assessing pollutant movement from point sources. Following the templates for these processes, other similar templates could be developed to capture additional processes or other emerging types of contaminants. Some limited work could be done to keep the tool (MTHP) current or use a similar framework for other codes with specific application domains. It is also needed to provide further suitable parameterisation of such models by laboratory studies, calibration and database development.

Screening the actual dispersion of contaminates from a point source Screening and monitoring was done around several selected cemeteries and landfills for measuring several heavy metals and organic compounds (pesticides, BTEX). Unfortunately, the monitoring scheme was not executed as initially planned due to various practical and logistical challenges, including staff availability, travel restrictions imposed by the COVID-19 pandemic and constraints caused by diminished groundwater levels during the dry summer months. BAM was monitored for Zillebeke and Villers-Deux-Eglises for a few sampling

dates and confirmed the presence of BAM at these sites. Monitoring data is summarized and available in Walstra et al. (2024).

Gaining insight into contamination / metal remobilization after land change (flooding flood mitigation strategy by artificial wetlands) Artificial wetlands are one of the measures considered in the strategy for flood mitigation in view of climate change. Intermitted flooding of these artificial wetlands may induce changes in the mobility of contaminants when a (hidden) point-source contamination (or any other type, such as a diffuse contamination) is present. In RESPONSE, the consequence of intermittent flooding on inorganic contaminants (heavy metals) was investigated using samples from the Grote Nete site. It was observed that a significant remobilization is possible under such land use changes. Therefore, it is important to assess consequences of land use changes for specific sites where contamination is present or expected to be present. This can be based on an experimental program and/or with numerical assessments based on mechanistic understanding of processes (of which some examples were developed in RESPONSE).

Gaining insight on biodegradation of organic pollutants that originates from pesticides applied at given sites such as cemeteries The research performed in RESPONSE showed the occurrence of multiple pesticide residues including pesticide transformation products like 2,6-dichlorobenzamide (BAM) in the groundwater near the examined cemeteries at concentrations higher than implemented threshold concentrations although it is not clear whether they originated from (former) pesticide use in the cemeteries. We decided to focus on BAM degradation since (i) it is a major recalcitrant groundwater organic micropollutant (occurring at trace concentrations) in Europe, and (ii) not much is known about its genesis as a transformation product in soil and about its fate/behaviour in natural systems while being extensively studied in the KU Leuven lab as a model for micropollutant biodegradation. The research performed, although not coming to fate modelling in soil, demonstrated some new aspects of the compounds' recalcitrance towards catabolism in groundwater systems when present at relevant environmental trace concentrations, i.e., occurrence of BAM degraders in natural soils is poor, degraders do not grow on the compound at low concentrations indicating that they should acquire the carbon/nitrogen for growth from other organics (i.e. other dissolved organic compounds (DOC)) and that BAM degraders, when present, have to compete for this DOC with other local resident organisms. As such, our research revealed new aspects of mechanisms of recalcitrance of organic micropollutants and bottle necks of organic micropollutant degradation in oligotrophic freshwater systems like groundwater. We are currently working on solutions to solve such bottle necks for instance for application in drinking water treatment systems treating micropollutant contaminated groundwater.

Keywords

REACTIVE TRANSPORT; POINT SOURCE; GROUNDWATER; INORGANIC POLLUTANTS; ORGANIC POLLUTANTS

1 INTRODUCTION

The RESPONSE project focuses on reactive transport of inorganic and organic contaminants in shallow groundwater environments (unsaturated zone and groundwater) and addresses research question related to better understand the physical, chemical, and biological processes that control contaminant transport in ground water in order to precise the reactive and non-reactive transport of contaminants in ground water with the ultimate goal of developing simulations to predict contaminant transport in ground water and to better characterize transport processes at the soil-groundwater interface, and improve their representation in models. RESPONSE aims to simplify the use of transport models of organic and inorganic contaminants for predicting the fate of pollutants in groundwater plumes and for predicting and monitoring plume behaviour. The project focuses on methodological developments enabling a more widespread and frequent use of reactive transport models in point source pollution problems. Processes are usually well understood in laboratory or at the pedon scale, but prohibitive data acquisition costs often hamper the use of appropriate numerical models in field-scale applications. RESPONSE will investigate to what extent information on plume extent and dynamics can be obtained using reactive transport models without site-specific data.

The development and application of models for point-source pollution problems requires different types of information:

- Identification of potential polluted point-sources – RESPONSE focusses on landfills and cemeteries as potential polluted point sources. Available datasets will be used to identify these sites and monitoring of some site will further confirm if pollutants are dispersed in the surroundings.
- Subsurface geological models are a key for building models for subsurface flow, transport and reactions.
- A calibrated water flow and tracer solute transport model is needed to assess the transport and dispersion of pollutants in subsurface systems.
- Software that can handle complex biogeochemical reaction networks coupled with the flow and transport models; given the complexity of such models, the heavy learning curve for implementing models in code, and the parameterisation, user-friendly templates as starting points will increase the applicability of such models.
- Information of processes and parameters; organic pollutants are often found around sites that uses pesticides (e.g. cemeteries). For example 2,6-dichlorobenzamide (BAM) was detected in groundwater samples at almost all examined sites and originates from the pesticide dichlobenil. Laboratory studies are needed to complement the information in literature on biodegradation.

2 STATE OF THE ART AND OBJECTIVES

Point source contamination sites are omnipresent and in various forms, one of which is cemeteries. These involve the release of various compounds to the underground, such as arsenic and mercury (used in past embalming and burial practices or as wood preservatives), formaldehyde (from current embalming practices), heavy metals (from coffins), herbicides used for removal of unwanted herbs, bacteria and viruses, etc. Depending on local factors, some may ultimately threaten the quality of surface and groundwater resources. Old unknown landfills and unknown legacy point soil contamination may pose risk of water use form aquifers downstream of the pollution, or might change from a dormant threat to an actual threat under changing land use conditions. One particular example is the construction of artificial wetland for the strategy of flood mitigation.

Coupled reactive transport models – flow and transport equations are solved together with models for (thermodynamic) equilibrium and kinetic reaction networks – are an emerging tool with offer an extreme versatile tool for addressing all kind of environmental pollution problems (Steefel et al. 2015). The versatility is due to the large amount of geochemical building blocks such as mineral dissolution and precipitation reactions, aqueous phase reactions, (multisite) surface complexation diffuse double layer or triple layer models, (multisite) ion exchange reactions, exchange between the aqueous and gaseous phase, and microbially mediated reactions that are available that are defined in a generic way adaptable to all kind of specific situations. It is therefore possible to simulate very complex processes governing metal contaminant transport. The speciation and mobility of metals is influenced by the pH, Eh, complexation with other dissolved compounds, sorption and ion exchange capacity of the solid phase and organic matter content. However, in the literature field-scale applications of reactive transport modelling usually require a tremendous amount of site-specific data (Mayer, Frind, and Blowes 2002; Bea et al. 2013).

One example for the unsaturated zone is the HPx code (Jacques et al. 2018; Šimůnek et al. 2024), which couples HYDRUS (Simunek et al. 2022) to PHREEQC (Parkhurst and Appelo (2013). HPx is specialized in variable-saturated soil systems and explicitly accounts for atmospheric boundary conditions and root water uptake.

Studies that investigate to what extent reactive transport models can be used successfully with a minimal amount of site-specific data are lacking. Moreover, reactive transport modelling studies most often consider the vadose zone and the aquifer as separate entities. Few studies effectively couple/integrate these two compartments and the impact of strong gradients/contrasting redox conditions at the soil/groundwater interface is rarely investigated (Salmon et al. 2014).

The objective of this project is to evaluate how available data of properties of the environment and contamination can be used to make an assessment on the potential evolution of the contamination. Data can be used for different purposes. RESPONSE evaluates the use of data that is (publicly) available in (open) databases or in the open (scientific) literature for the purpose of:

- Assessing the susceptibility of a site for ground water pollution,
- Setting up subsurface geological models as input to flow and transport models,
- Constraining a model describing the transport of a leachate from a landfill,
- Deriving conceptual model and its implementation in (coupled) reactive transport models,

or the use of (limited) data that is collected at a specific site for the purpose of:

- Screening the actual dispersion of contaminates from a point source,
- Gaining insight into contamination / metal remobilization after land change (flooding flood mitigation strategy by artificial wetlands),
- Gaining insight on biodegradation of organic pollutants that originates from pesticides applied at given sites such as cemeteries.

3 METHODOLOGY

3.1 General methodology

Figure 3-1 gives a general overview of the methodology in RESPONSE. At the left, four generic types of data sources are indicated. In the middle, the (types of) sites that were used in REPSONSE are indicated. The right column indicates the type of model that is developed.

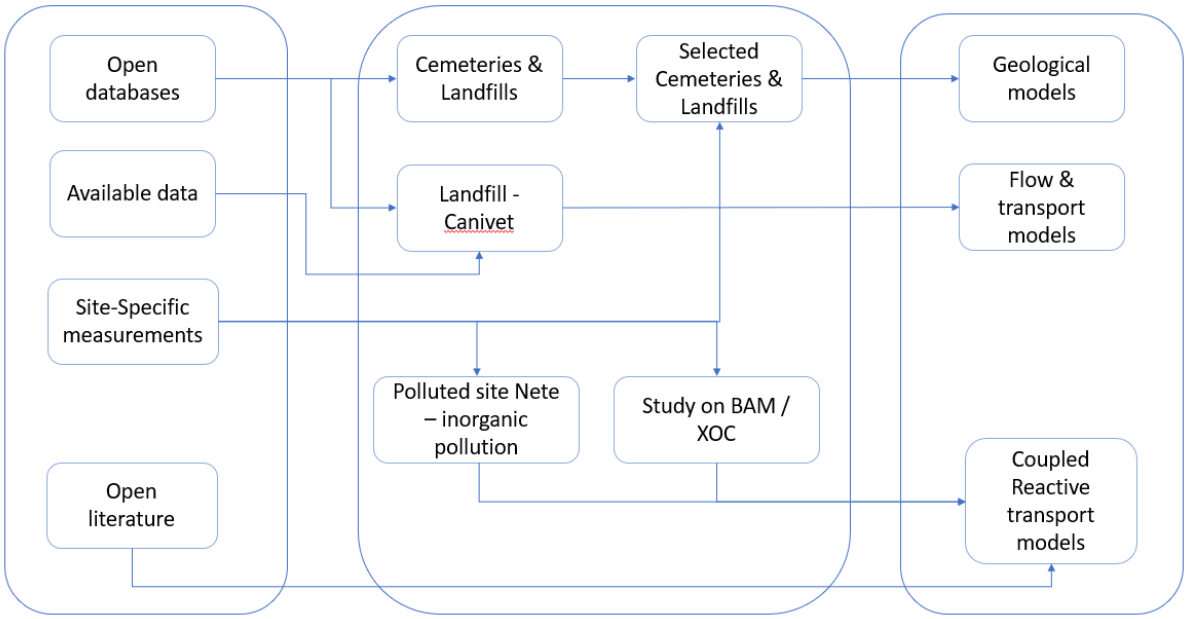

Figure 3-1 – Overview of methodology in RESPONSE with the data sources at the left, the sites in the middle and the models at the right (XOC: Xenobiotic organic compounds)

- The first purpose "to assess the susceptibility of a site for ground water pollution" uses open databases to identify sites (cemeteries and landfills in RESPONSE) that fulfil a given set of criteria that makes these sites susceptible for ground water pollution under the defined criteria. Additionally, a number of these sites are selected for further screening and model development. The methodology for selections of sites is described in section 3.2. Results are discussed in section 4.1.
- The second purpose "To set up subsurface geological models as input to flow and transport models" build further on the outcome of the previous purpose. Using additional open databases, geological models are built for the selected sites. The methodology is described in section 3.3.1.
- The third purpose "To constrain a model describing the transport of a leachate from a landfill" is developed for a case-study in which pollutants from a legacy landfill (Canivet) disperse in the aquifer system with the aim to evaluate a potential risk of reaching a downstream battery of drinking water production wells. A groundwater flow and transport model is developed and validated based on data that is publicly available or that is obtained from some specific sources – no detailed site-specific data collection campaign was performed. Some aspects of model simplification and abstraction which is inevitable when relying only on readily available data were evaluated. The data and methodology are described in respectively section 3.3.2.1 and 3.5.2; results in section 4.4.
- The fourth purpose "To derive conceptual model and its implementation in (coupled) reactive transport models" is first achieved via implementing a framework by which state-of-the-art

scientific knowledge and conceptual models on geochemical processes that affect the fate of pollutants in subsurface systems can be relatively easy integrated in flow and transport models for water-saturated systems. This framework is then applied to (i) the transformation of organic contaminants by a sequence of redox-mediated reactions and (ii) sorption of metals by organic material based on conceptual and mathematical models available in the open scientific literature. The data, *i.e.* the conceptual and mathematical models for the geochemical processes obtained via the open scientific literature, is described in section .The methodology for a coupled reactive transport model framework is described in section 3.5.3. Results are described in section 4.5.2.

- The fifth purpose "To screen the actual dispersion of contaminates from a point source" builds further on the first purpose by obtaining site-specific measurements of environmental variables and contamination levels in a screening phase followed by a monitoring phase. Methodology is described in section 3.3.1, results in section 4.1.1.
- The sixth purpose "Gaining insight on biodegradation of organic pollutants that originates from pesticides applied at given sites such as cemeteries" investigates the remobilization of inorganic contamination upon flooding which could occur in flooding mitigation strategies. The specific site is historical pollution at a site that will be transformed in an inundation area (the GN site in Figure 3-1). The site is described in section 3.3.3; experiments are given in section 4.6.1.
- The seventh purpose relates specifically to the organic organic pollutants. Since (i) 2,6-dichlorobenzamide (BAM) was detected in groundwater samples at almost all examined sites, (ii) BAM in groundwater is known to originate from transformation of parent compound dichlobenil (a widely used herbicide) in the vadose zone and (iii) BAM biodegradation is a major topic in the KU Leuven, it was decided to focus on BAM as a model compound. Original aim was to acquire information about the degradation rates of BAM in the investigated soils and the effects of additional DOC on BAM degradation to produce BAM dispersion models from vadose to aquifer integrating biodegradation activities. Methodology is described 3.4.3 in section and experimental results in section 4.6.2.

3.2 Screening and selection of historical municipal landfills and cemeteries

3.2.1 Preliminary selection of potential caste study sites

Screening and selection of the sites used a tiered approach:

i. A number of potential sites are identified by overlying existing information (mainly in a GIS-environment) with locations of civil cemeteries, military cemeteries and landfills.
ii. The suitability of this GIS analysis was checked in the field mainly regarding the access to the downslope area of the sites and the indications of shallow groundwater or the presence of hydromorphic soils.
iii. The site owners were contacted to request permission for the installation of piezometers.

As the focus is on shallow dynamic ground water systems, following criteria were taken for identification of potential sites:

i. The slope direction,
ii. A ground water depth of less than 2 meter

iii. An open landscape to limit external contamination.

The selection was based on a hierarchy of three criteria in decreasing order: i) presence of shallow groundwater approximated by the soil drainage class, depth to the groundwater from a map with existing piezometers and/or distance to a river, ii) soil type and geology in order to cover a variety of soil types and dominant substrates, iii) mean annual precipitation and land cover. All geographical data to make the selection are taken from electronic platforms, mainly from governmental authorities. In case the data is not available in a geographic system, the information is added to a geographic information system. In case data is present in tables or maps in digital reports, the information itself is digitized and incorporated in the geographic information system.

For the data on soils and geology, we used the Belgian soil map (https://geoportail.wallonie.be and https://www.dov.vlaanderen.be/page/bodemkaarten). For the substrate type we used http://www.onegeology.org. For the piezometers we used http://piezo.environnement.wallonie.be and http///data.inbo.be/watina. For the distance to the rivers we used the Belgian hydrological network (http://www.waterinfo.be and https://geoportail.wallonie.be. For the precipitation we used an interpolation by Meersmans et al. (2016). For the cemeteries we used http://memento-mori.be and http://www2.kamp-vogelsang.be. Finally, we used the databases of OVAM and SPAQUE for the landfill sites.

3.2.2 Screening of potential case study sites

The preliminary evaluation of potential case study sites involved the installation of multiple piezometers at each site, followed by examination of groundwater samples collected from these locations. The objective of this process was to identify a definitive selection of three case study sites for comprehensive monitoring, based on empirical evidence of contamination and presence of hydrological conditions favourable for the movement of contaminants through groundwater.

Initially, three shallow piezometers were installed at each location (Figure 3): two positioned downstream of the anticipated point source to capture the potential contamination plume, if it exists, and one located upstream to serve as a baseline for naturally occurring background concentrations of the compounds. This baseline is essential for determining the anthropogenic nature of the pollution.

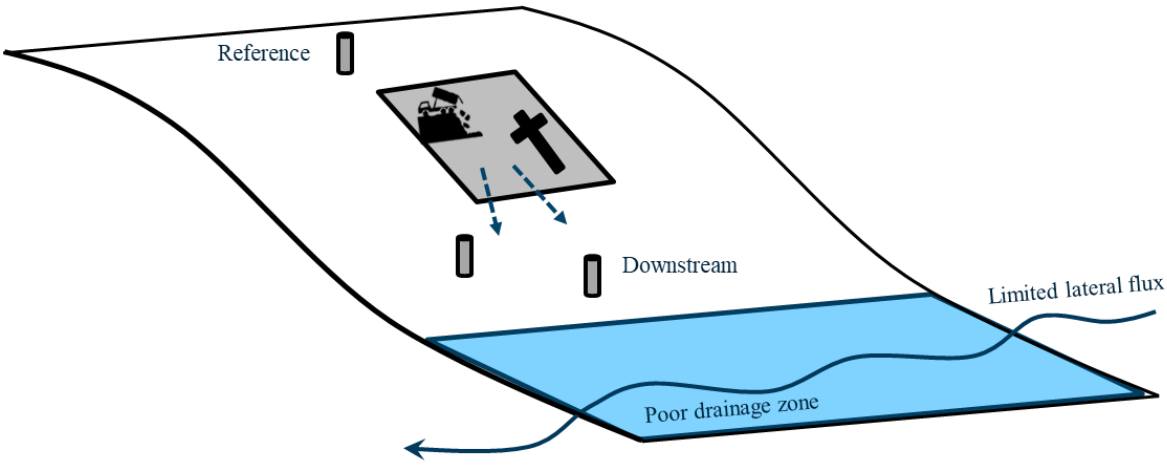

Figure 3-2 – The optimal positioning of piezometers at a test site for effective assessment of groundwater contamination.

The piezometers were installed in shallow boreholes, which were manually drilled to a maximum depth of 5 meters using a hand auger (Figure 3-3), and fitted with a filter extending up to 1 meter below the groundwater table. Detailed lithological description and facies interpretation of the borehole samples were conducted in the field. The lithological information obtained, subsequently served as supplementary input for the development of the geological models (section 3.5.1). Precise geographical coordinates were recorded using differential GPS.

Figure 3-3 - Drilling of shallow boreholes was accomplished through the utilization of a hand auger.

Groundwater samples were collected no sooner than two weeks after the installation of piezometers. At each sampling site, piezometric heads were measured using a portable water level meter to assess the direction and gradient of groundwater flow. Standard field parameters were acquired in situ through the use of a flow cell and calibrated field electrodes (Figure 3-4). Triplicate samples were collected utilizing low flow sampling techniques and employing various recipients for subsequent laboratory analysis.

The laboratory analyses were conducted by the team of KU Leuven, with a portion of the work being delegated to an accredited external company, i.e., De Bodemkundige Dienst. The chemical analyses primarily targeted heavy metals (KU Leuven) and organic compounds, i.e., pesticides (50 compounds) and all BTEX (Bodemkundige dienst).

Figure 3-4 –Extracting water samples from a piezometer and in situ measurement of field parameters using a flow cell and field electrodes.

In summary, the screening procedure included assessment of the following parameters:

- Piezometric heads
- Field parameters: pH, T, O_2, Eh, EC
- Inorganic elements: Fe, B, Na, Mg, Al, P, K, Ca, Cr, Mn, Co, Ni, Cu, Zn, As, Mo, Cd, Pb
- Electron acceptors: Fe(III), NO_3^-, SO_4^{2-}
- Organic compounds: DOC, DIC, SUVA
- Xenobiotic organic compounds (XOCs): BTEX, pesticides

Ultimately, three primary case study sites were selected for the monitoring phase of heavy metals, taking into account the presence of contamination, hydrological factors, and practical aspects such as accessibility. In addition, three sites were selected for initially studying BAM biodegradation.

3.3 Site-specific data

3.3.1 Sampling around selected cemeteries and landfills

Additional piezometers were installed at the selected case study sites, using the same methodology employed during the screening phase. The configuration was designed in a cone shape (locally adapted) to facilitate monitoring of groundwater quality both upstream and downstream of the contaminated area, as well as within the plume itself. This approach enabled the detection of the plume's movement across both spatial and temporal dimensions.

It was planned to monitor all locations over a period of three years, conducting measurements four times annually, to incorporate seasonal variability. The approach to sampling and analysis was adapted according to the particular research questions relevant at each site, focussing on either organic or inorganic contaminants. The data collected during the monitoring phase were expected to play a crucial role in the testing, improvement and validation of numerical reactive transport models.

3.3.2 The Canivet landfill site

The Canivet landfill site is a former landfill located in Haasrode south of Leuven (Figure 3-5). It is located at approximately 2.15 km south of the “Abdij” site where a large drinking water extraction site

(1642500 m³/y) is located (Watergroep 2015). An important question is how a potential plume with contaminants is spreading from the Canivet landfill to the Abdij site.

Data on the Canivet landfill is scarce. The Canivet site is a former sand quarry transformed in a municipal waste site in the years ~1980-1987 and closed in June 1987 with two sealing layers of concrete (no evidence found on the site). The totals surface area is 73195 m² with the current land use is a meadow (Van Keer, Bronders, and Smolders 2001); the vertical extent is unknown. North of the landfill, there is mainly an industrial zone that potentially contributes to ground water contamination. The well batteries at the Abdij site contain 24 wells drilled between 1931 and 1998 with well screens between 9 to 16m below surface.

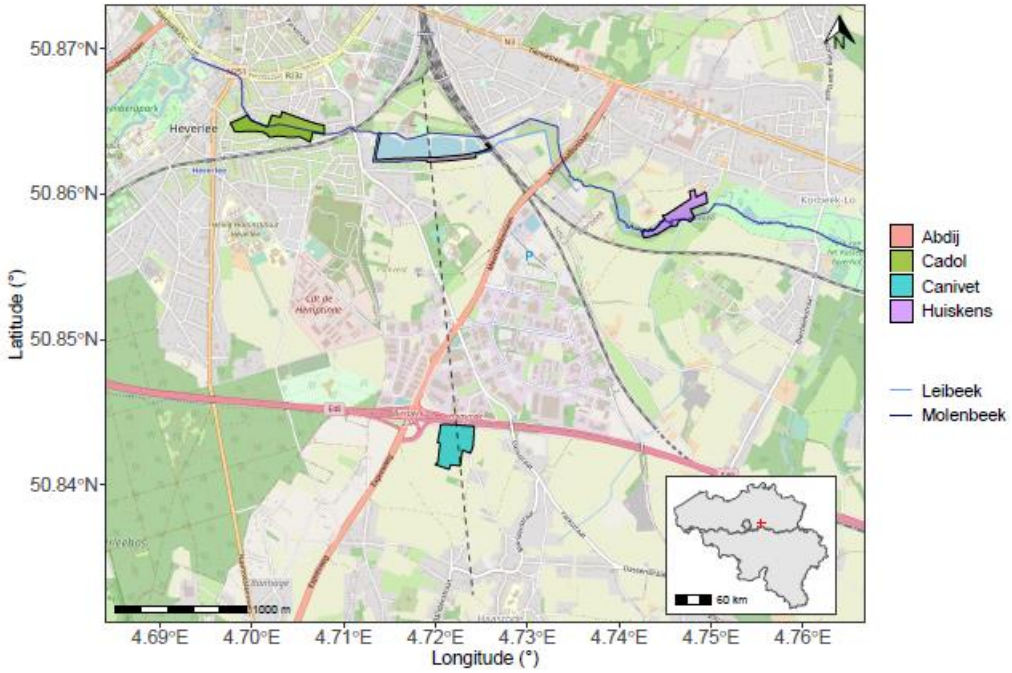

Figure 3-5 – Canivet case study: Major groundwater extraction sites south of Leuven, Belgium (Cadol, Huiskens, Abdij) and the location of the Canivet landfill. The dashed line represents the profile line used to draw a geological cross-section in Figure 3-6.

3.3.2.1 Geology and hydrogeology

The subsurface stratigraphy was obtained with data from Data Ondergrond Vlaanderen[1] – Geologisch 3D-model (v3) and GDI-Vlaanderen[2] and is shown in Figure 3-6. The topography and also the geological layers gently dip towards the north. Starting at the surface, following layers are present:

- A heterogeneous Quaternary cover comprised of loamy to fine sandy alluvial (*Allevium*) and eolian deposit (*Gent Formation)*. There are some indications of a coarser Holocene deposit of coarse sand and a base gravel deposited during the last ice age, specifically in the north part.
- On some hilltops, Tertiary deposits as the fine sands of the *Lede Formation* (Middle Eocene age) or the fine clayey sands of the *St-Huibrechts-Hern Formation* (Oligocene age) are present.
- The *Brussels Formation* consists of marine medium to coarse glauconite rich sands of Middle Eocine age with SSW-NNE oriented gullies due to a strong tidal influence in the depositional

[1] http://dov.vlaanderen.be
[2] Geografische data-infrastructuur Vlaanderen, https://www.geopunt.be/voor-experts/gdi-vlaanderen

system. This heterogeneous formation contains also local indurated sandstone banks and calcium-rich deposits.

- The *Kortrijk Formation* is an early Eocene marine clay.

Below the *Kortrijk Formation*, the *Hannut Formation* (marine formation, early Eocene to late Paleocene) is present.

The groundwater system is part of the Brulandkrijt groundwater system in the groundwater system classification of Flanders (VMM 2008). The hydrostratigraphy of the site consists of Quaternary deposits (HCOV 0100 (Meyus, Batelaan, and De Smedt 2000)[3]) and the Brussels formation (HCOV 0620). The Quaternary formation has a low permeability and only contribute to the phreatic system in the valleys. The Brussels formation is highly permeable and is the main driver of flow in the considered aquifer system. Note that the St-Huibrechts-Hern Formation (HCOV 0400) and the Lede Formation (HCOV 0610) are often situated in the unsaturated zone and, depending on the clay content, can behave locally confined. The Kortrijk Formation (HCOV 0920) and Hannut Formation (HCOV 1010) act as an aquiclude at the scale of this research.

The general flow direction is oriented NNW driven by the topography, pumping wells and surface water features; the Molenbeek drains the valley with deep unsaturated zones in the south (10-15 m) and expected ground water seepage conditions under natural circumstances at the ponds at the Abdij site. The estimated residence time from the Canivet site to the Abdij site is ~25 years.

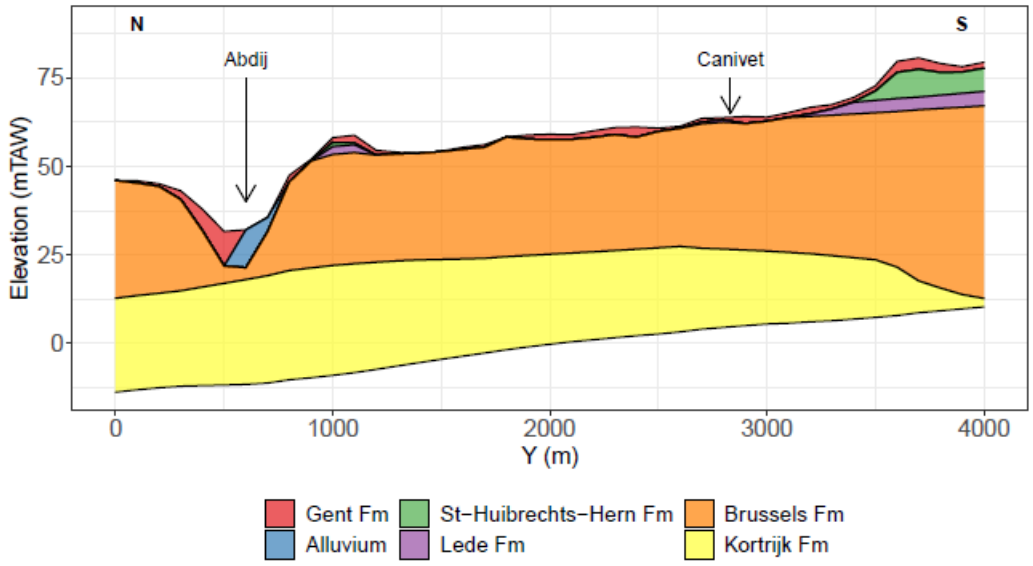

Figure 3-6 - Geological N-S cross-section of the profile line shown on figure 1. Source: DOV (2021a) and GDI-Vlaanderen (2021).

3.3.2.2 Data

Data concerning hydraulic heads, geochemistry, concentrations and pumping rates were obtained via private and public data sources including: wells measured by De Watergroep, a well from Flanders

[3] HCOV: Hydrogeologische Codering Ondergrond Vlaanderen (Meyus et al. 2000)

Environment Agency (VMM) and data collected in 1980's and 1990's around the landfill (Van Keer, Bronders, and Smolders 2001).

Hydraulic heads are available from about 50 wells with earliest measurement dating from mid 1980s and the most detailed measurements starting up from mid 1995' to 2000 (see Neyens (2022) for an overview of all data). Depth to water tables is ~10-15 m in the south and decreases towards the north with depths at 1-5 m. Temporal variations are less than 5 m although a long general decreasing trend of on average 2-3 meters over the last 15 years is observed.

Geochemical data are available from 14 wells. At the Abdij site (drinking water extraction), only composite samples are available for 2 batteries; thus 12 sampling points represent a single well. Data is available for the period 1990-2000 and after 2010. Figure 3-7 shows the measured major ion chemistry with data grouped in different locations. The water is rich in calcium and bicarbonate which is the dominant water type of the Brussels sands (Peeters 2010). Chloride concentrations are elevated over the entire study domain. There is also a spatial trend (specifically for Na and Cl): lowest values south of the Canivet, spike at the Canivet site, and decrease towards the Abdij site. In addition, data on metals (Figure 3-8), organic species and pesticides (only measured recently, Figure 3-9), nitrogen species (Figure 3-10), and general geochemical parameters (Figure 3-11) are available.

Figure 3-7- Canivet case study: Major ion concentrations (Neyens 2022)

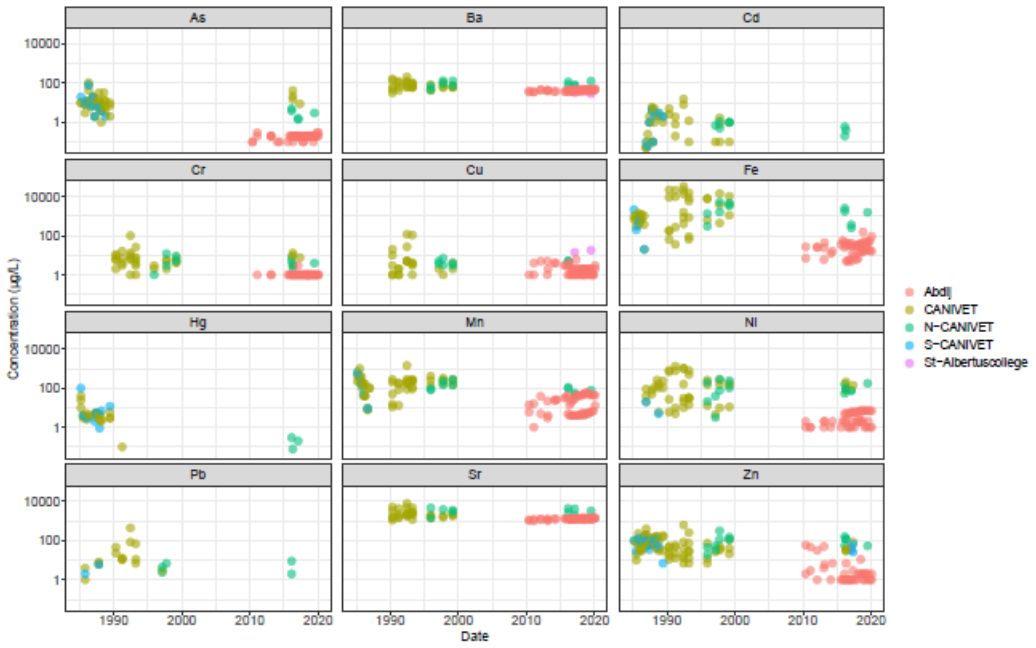

Figure 3-8 – Canivet case study: Metal concentrations (Neyens 2022)

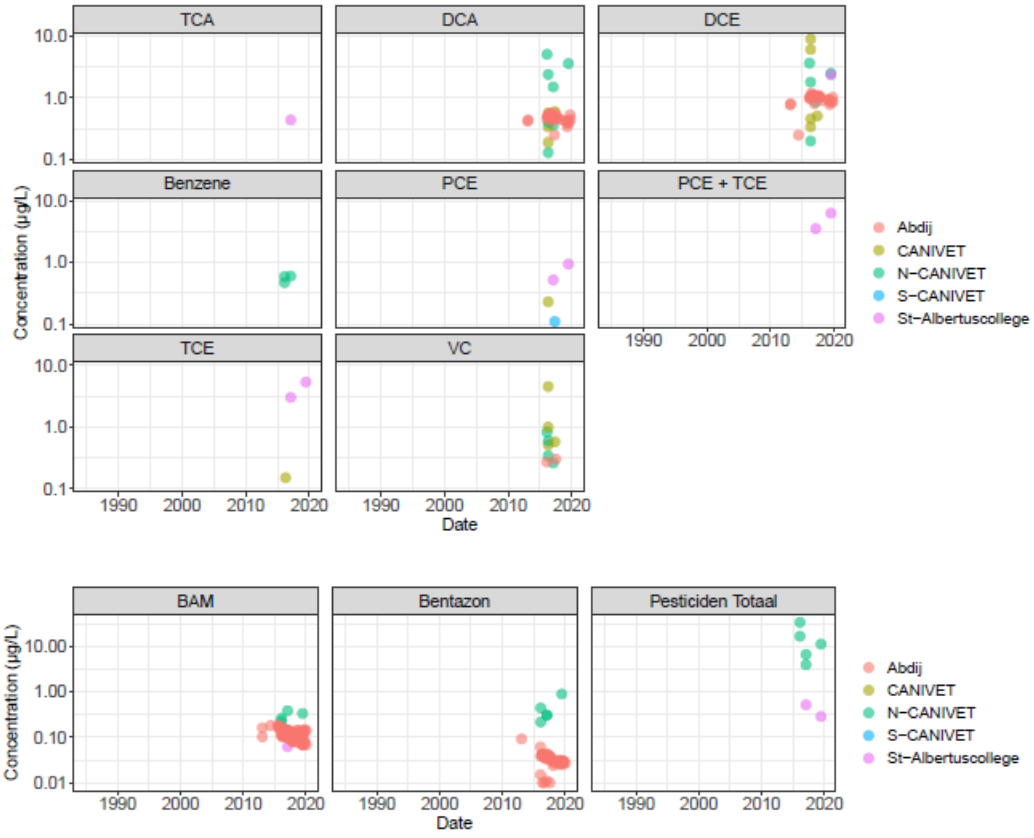

Figure 3-9 – Canivet case study: Organic species (Neyens 2022)

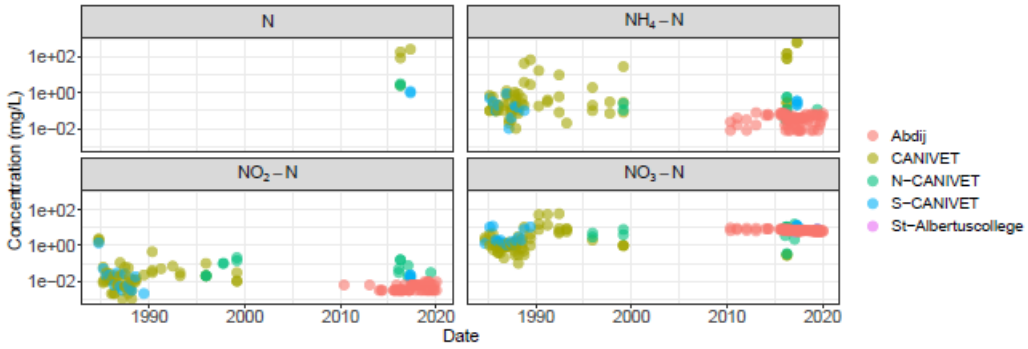

Figure 3-10 – Canivet case study: Nitrogen species (Neyens 2022)

Figure 3-11 – Canivet case study: pH, oxygen concentration and dissolved organic carbon concentration (Neyens 2022)

3.3.3 The Grote Nete site

In response to the escalating impacts of climate change, developing innovative flood mitigation strategies has become increasingly critical. In Flanders (Belgium), one such approach involves restoring former river meanders in the tributaries of the Scheldt River. This strategy, part of the long-term Sigmaplan project, is gaining recognition for its dual benefits: improving flood resilience and enhancing ecosystems. In addition to restoring meanders, the project includes constructing artificial wetlands that serve as sustainable flood management tools, offering not only floodwater storage but also ecological, recreational, and water quality benefits.

The Grote Nete River is one of the targeted waterways. In its basin, near Lier, certain riparian areas are contaminated with radionuclides (RN) and heavy metals (HM), a legacy of industrial pollution from the tributaries Grote Laak and Molse Nete until the 1980s. The Sigmaplan proposes to alter the land use of these contaminated areas by installing floodplains, potentially through breaching or natural degradation of river dykes. However, these changes could mobilize contaminants. Flooding the soil is expected to lower redox potential and alter the chemical forms of specific RN and HM, while increased water fluxes during flooding may enhance the migration of soluble contaminants. Therefore, understanding these chemical and physical processes is essential to evaluate the risks associated with the proposed land use changes.

To address these challenges, SCK CEN initiated a project to study the potential impacts of future land use changes across multiple domains. Within this framework, a PhD project was launched to investigate the geochemistry and bioavailability of radionuclides, heavy metals, and trace elements. One key component of this research was a column experiment simulating waterlogged conditions. Flooding of contaminated soils can significantly affect the mobility and bioavailability of inorganic contaminants, posing risks to ecosystems through dispersion into water bodies. Reliable assessments require pore water sampling methods that minimize oxidation artifacts and capture mobile colloids.

The column experiment aimed to evaluate different pore water sampling techniques under reducing (waterlogged) conditions and to examine the mobility and bioavailability of harmful contaminants. Intact soil cores (35 cm depth) were collected from a natural grassland site (initial pH 6.7, 8.9% organic carbon) and flooded. Pore water was sampled at various depths over three periods spanning up to 100 days. Inductively Coupled Plasma Mass Spectrometry (ICP-MS) was used to analyze 19 elements in the pore water solutions. Sampling techniques, including rhizon samplers, Diffusive Equilibrium in Thin-films (DET), and centrifugation, were assessed for their effectiveness under waterlogged conditions. Additionally, the experiment identified changes in contaminant mobility and highlighted the most problematic elements.

3.4 Organic species in the subsurface

3.4.1 Kinetic model for organic species degradation by oxidation reactions

Dissolved organic species will degrade (oxidized acting as an electron donor) by oxidation using a set of electron acceptors by micro-organisms. As oxygen is in terms of energy the most favourable electron acceptor, micro-organisms using oxygen will be more active under these conditions. Only when oxygen is depleted, micro-organisms using the next oxidant (nitrate) will become active and so on. Thus, a sequence of redox reaction for organic species degradation can be defined (Bhanja et al. 2019a; Bhanja et al. 2019b; Hunter, Wang, and Van Cappellen 1998; Nmor et al. 2022) as illustrated in Figure 3-12.

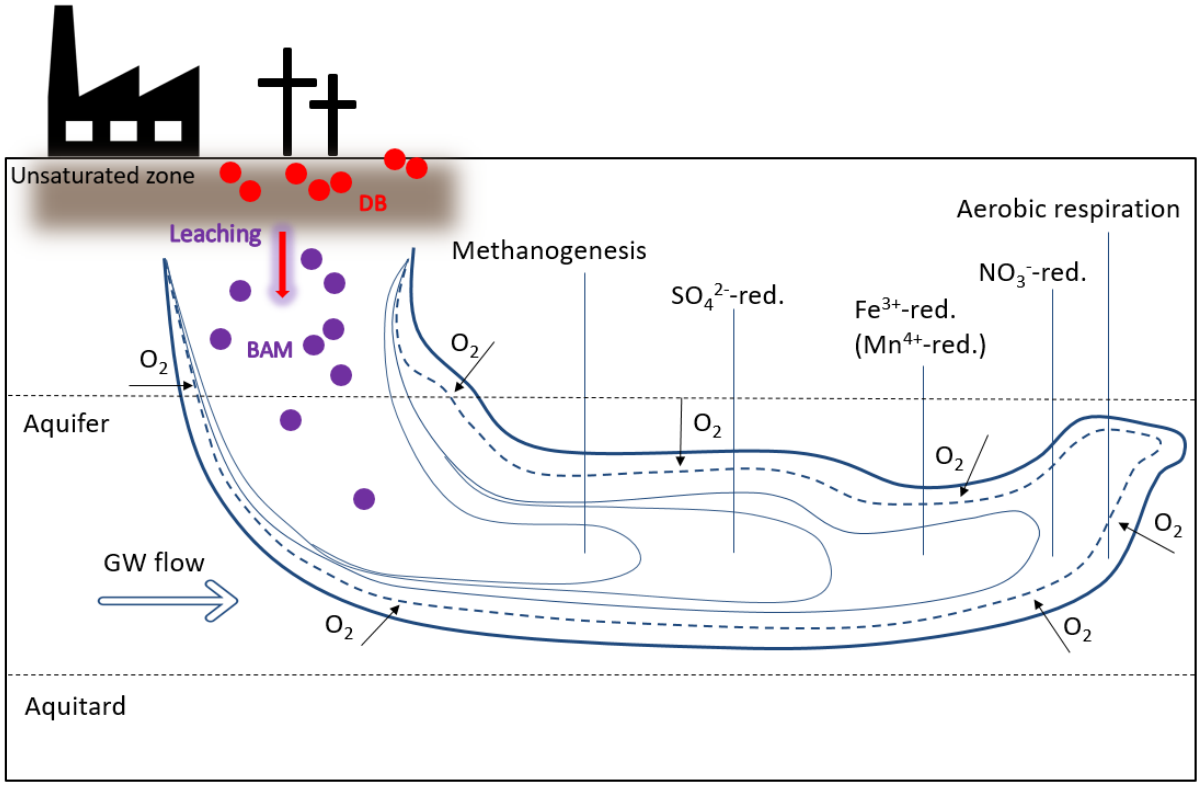

Figure 3-12 – Typically redox sequence when organics enter an aquifer.

A generic (but simply, as only C, H, and O are considered) formula for degradation of an organic species can be written as:

$$C_aH_bO_d^{\ Z} + (2a-d)H_2O \rightarrow aCO_2 + (4a+b-2d)H^+ + (-Z+4a+b-2d)e^- \quad (1)$$

The most energetically favourable electron except is oxygen:

$$O_2 + 4H^+ + 4e^- \rightarrow 2H_2O \quad (2)$$

with the overall reaction:

$$C_aH_bO_d^{\ Z} + sO_2 + (2a-d-2s)H_2O \rightarrow aCO_2 + (4a+b-2d-4s)H^+ \quad (3)$$

and $s = \dfrac{(-Z+4a+b-2d)}{4}$.

The next electron acceptor is nitrate:

$$NO_3^- + 2H^+ + 2e^- \rightarrow NO_2^- + H_2O \quad (4)$$

with the overall reaction:

$$C_aH_bO_d^{\ Z} + sNO_3^- + (2a-d-s)H_2O \rightarrow aCO_2 + sNO_2^- + (4a+b-2d-2s)H^+ \quad (5)$$

and $s = \frac{(-Z + 4a + b - 2d)}{2}$.

Next, reductive dissolution of pyrolusite occurs where manganese is the electron acceptor:

$$MnO_2 + 2e^- + 4H^+ \rightarrow Mn^{2+} + 2H_2O \quad (6)$$

with the overall reaction

$$C_aH_bO_d{}^Z + sMnO_2 + (2a - d - 2s)H_2O \rightarrow aCO_2 + sMn^{2+} + (4a + b - 2d - 4s)H^+ \quad (7)$$

and $s = \frac{(-Z + 4a + b - 2d)}{2}$.

Subsequently, iron is used as an electron acceptor with reductive dissolution of goethite:

$$FeOOH + e^- + 3H^+ \rightarrow Fe^{2+} + 2H_2O \quad (8)$$

with the overall reaction

$$C_aH_bO_d{}^Z + sFeOOH + (2a - d - 2s)H_2O \rightarrow aCO_2 + sFe^{2+} + (4a + b - 2d - 3s)H^+ \quad (9)$$

and $s = (-Z + 4a + b - 2d)$.

Finally, sulphate is used as the electron acceptor:

$$SO_4^{2-} + 8e^- + 9H^+ \rightarrow HS^- + 4H_2O \quad (10)$$

with the overall reaction

$$C_aH_bO_d{}^Z + sSO_4^{2+} + (2a - d - 4s)H_2O \rightarrow aCO_2 + sHS^- + (4a + b - 2d - 9s)H^+ \quad (11)$$

and $s = \frac{(-Z + 4a + b - 2d)}{8}$.

Note that the generic formula of the organic species can be extended to include other elements as N and P:

$$CH_2O(NH_3)_{N/C}(H_3PO_4)_{P/C} + H_2O \rightarrow aCO_{2NH} + 4H^+ + 4e^- + {}^{N}\!/\!_{C}\,NH_3 + {}^{P}\!/\!_{C}\,H_3PO_4 \quad (12)$$

where N/C is the stoichiometric coefficients of moles NH_3 per mole C and P/C is the stoichiometric coefficients of moles H_3PO_4 per mole C.

The rate equation for a microbiologically-controlled redox reaction is descried by a double Monod equation as (MacQuarrie, Sudicky, and Frind (1990),Essaid et al. (1995), Van Cappellen and Wang (1996), MacQuarrie and Sudicky (2001), Essaid et al. (2003), Appelo and Postma (2005)):

$$R = Q_{\max} B \frac{[E_{\mathrm{D}}] K_{\mathrm{D},0}}{K_{\mathrm{D}} + [E_{\mathrm{D}}]} \frac{[E_{\mathrm{A}}] K_{\mathrm{A},0}}{K_{\mathrm{A}} + [E_{\mathrm{A}}]} \left(\frac{K_{\mathrm{B}}}{K_{\mathrm{B}} + B} \right)^{\alpha} IT \tag{13}$$

where R is the degradation rate (M/L^3/T), $Q_{\max}$ is the maximum degradation rate (unit depends on inclusion or exclusion of the biomass term, see further), B is the biomass of the microbiological group that uses a given electron acceptor [M/L^3], $\frac{[E_{\mathrm{D}}] K_{\mathrm{D},0}}{K_{\mathrm{D}} + [E_{\mathrm{D}}]}$ is the Monod term for the electron donor, $\frac{[E_{\mathrm{A}}] K_{\mathrm{A},0}}{K_{\mathrm{A}} + [E_{\mathrm{A}}]}$ is the Monod term for the electron acceptor, [E_D] and E_A are the concentration of, respectively, the electron donor and acceptor [mol/l], K_D and K_A are the half-saturation constants for, respectively, the electron donor and acceptor [mol/l], $K_{D,0}$ and $K_{A,0}$ control if the dependency on respectively [E_D] and [E_A] are following the Monod term (value should equal 1) and first order-dependency by having a very large value of the half-saturation setting $K_{D,0}$ (or $K_{A,0}$) equal to the half saturation value (note that a zero-order dependency is obtained by setting the half-saturation to a very small value), I is an inhibition term to supress reactions when higher energy-yielding terminal electron acceptors are still present:

$$I = \prod_j \frac{K_{\mathrm{I},j}}{K_{\mathrm{I},j} + [\mathrm{TEA}_j]} \tag{14}$$

where $K_{I;j}$ is the half-saturation constant for the jth inhibitor and TEA_j is the concentration of the terminal electron acceptor with a higher energy yielding for all TEA with a higher energy yielding, $\left(\frac{K_{\mathrm{B}}}{K_{\mathrm{B}} + B} \right)^{\alpha}$ is a term to account for rate reduction when the microbial biomass is too large (e.g. effect of pore restrictions) where K_B is the half-saturation constant [M/L^3], and T is a factor accounting for temperature via e.g. the Arrhenius equation or a Q10 type of approach. If the effect of biomass is not considered, the unit of $Q_{\max}$ is [mol dm^{-3} T^{-1}]; if it is considered, the unit is [mol mB^{-1} T^{-1}] (mB is the mass of biomass).

Inclusion of a dynamic biomass model is via

$$R_{\mathrm{B}} = Y_{\mathrm{B}} \theta R_{\mathrm{DOM}} - b_{\mathrm{B}} B \tag{15}$$

where R_B is the rate of change of the biomass [M T^{-1} L^{-3}], Y_B is the yield factor [-], q is the water content, R_{DOM} is the rate of oxidation of dissolved organic matter for a given electron acceptor calculated using

Eq. (13), and b_B is the death rate [T^{-1}]. A different biomass rate equation can be included for each electron acceptor (thus, reflecting the dynamics of different microbiological groups).

3.4.2 Sorption of heavy metals on subsurface organic matter

Sorption of heavy metals on organic matter can be described in several ways ranging from empirical based approach (e.g., linear isotherms) to more sophisticated mechanistic models such as NICA-Donnan (Koopal et al. 2005) or the humic-ion binding model VII (Tipping, Lofts, and Sonke 2011). Within RESPONSE, Model VII was included in the modelling frameworks described in section 3.5.3.

The humic-ion binding model VII, applicable for both humic acids (HA) and fulvic acids (FA) has discrete binding sites for protons given rise to monodentate, bidentate and tridentate binding sites for metals. It postulates eight proton binding sites with four for stronger acidic groups representative for carboxylic acid groups (type A) and four for weaker acids as phenolic acids (type B). The 8 intrinsic equilibrium constants are defined by four parameters: pK_A and pK_B are the average pK values for respectively type A and B types, and ΔpK_A and ΔpK_B are measures for spread in the respective types. The abundance of each group within a given type is equal, and there are twice as much type A than type B. The intrinsic equilibrium constant for monodentate binding of metals is described with an average pK_{MA} (where M specifies a metal) whereas the logK_{MB} is calculated with a same relative binding strength as was observed for proton binding, i.e.:

$$\log K_{MB} = \log K_{MA}(\mathrm{p}K_B/\mathrm{p}K_A) \quad (16)$$

Each monodentate intrinsic equilibrium constant for each group within a single type is equal. Bidentate and tridentate sites are formed from the monodentate groups as follows (with 1-4 representing the groups in type 1 and 5-6 for groups in type B): bidentate 1-2, 3-4, 1-5, 2-6, 3-7, 4-8 and tridentate 1-2-5, 1-2-6, 1-2-7, 1-2-8, 3-4-5, 3-4-6, 3-4-7, 3-4-8. The number of sites is again related to the site of type 1 via a factor f_{prB} and f_{prT} for the bidentate and tridentate surfaces, respectively. The most abundant sites are the monodentate sites, but these are the weakest sites; on the other hand, the strongest tridentate sites are the least abundant. For each metal, sorption of the free metal (e.g. Cd^{2+}) and the first hydrolysis product (e.g. $CdOH^+$) are considered. Na^+ does not bind specifically in this model. Tipping et al. (2011) listed parameters calibrated on different dataset for different metals and different fulvic and humic acids and can be considered as generic parameters capturing some average behaviour.

The intrinsic equilibrium constants are corrected for electrostatics by a Boltzmann factor which in the model VII is mimicked by an empirical factor. Marsac et al. (2017) demonstrated the empirical relation can be implemented in PHREEQC using the constant capacitance surface complexation model with the capacitance dependent on the ionic strength. Alternatively, if the surface complexation model of the humic ion interaction model VII in PHREEQC needs to be combined with other type of surfaces (e.g. clays), the three plane model can be used (Marsac et al. 2017). In addition, a Donnan model is also included in model VII accounting only for counter-ion accumulation (i.e., non-specific binding of the cations to the humic or fulvic acid). In PHREEQC, this option is only available when the aqueous activity correction model is not calculated according to the specific ion activity theory (SIT) or PITZER.

3.4.3 Study of the biodegradation of BAM and other XOC

As mentioned, BAM was selected as a model groundwater XOC and micropollutant for studying XOC biodegradation. In a first instant, it was endeavoured to examine the occurrence of aerobic BAM biodegradation capacity at different selected sites. This was done by monitoring the degradation of BAM in minimal medium MMO inoculated with 0.5 g of top soil taken from the upper 5 cm at the soil surface and incubation as 25°C as earlier described (Nguyen et al. 2019). BAM degradation was monitored by monitoring BAM concentration in time using UPLC-UV-VIS as described (Raes et al. 2019). One only soil sample supported BAM biodegradation and that sample was used to enrich BAM degrading bacteria as described before (Nguyen et al. 2019). BAM degrading isolates were identified by sequencing its 16S rRNA gene amplicon as reported (Nguyen et al. 2019).

In addition, 150 mg soil samples along a vertical transect were tested in 96-well plates for the biomineralization of 8 different pesticide compounds by making use of [Ring-U-14C] labelled pesticide compounds as earlier described by (Vandermaesen et al. 2022). Soils examined originated from one agricultural land at Ter Munck, and one forest land at Wespelaar. At each site, 7 soil samples were taken at 0 – 3 m depth using a sterilized gauge with a handle and extension bars, and samples from several depths (0, 0.5, 1, 1.5, 2, 2.5, and 3 m at Ter Munck; 0, 0.1, 0.2, 0.4, 0.6, 0.8, 1.0, 1.25, 1.5 and 1.65 m at Wespelaar) were placed into sterile 1 L plastic soup pots. The soils were sieved at 2 mm sieve and 15O mg was used to inoculate the 96-well plates.

The BAM degrading isolate *Aminobacter* sp. MSH1 (Sorensen et al. 2007) was used to determine BAM degradation kinetics, growth kinetics on BAM and associated kinetic parameters at environmentally relevant concentrations as described by (Raes et al. 2024). To avoid growth on contaminating organic carbon in the medium, the experiments were performed in Assimilable Organic Carbon (AOC) restricted medium prepared as described by (Hammes and Egli 2007). Growth was monitored using flow cytometry while BAM concentrations using UPLC-MS/MS as described.

Finally, experiments were performed to examine how DOC and the presence of other resident microbiota affects biodegradation of BAM at low relevant environmentally concentrations by *Aminobacter* sp. MH1 in natural waters hypothesizing (i) that the presence of additional DOC as an auxiliary carbon source will support BAM biodegradation by increasing the biomass of the BAM degrader but that (ii) this can be counteracted by other bacteria that compete for the additional DOC. Monitoring of growth and BAM degradation occurred as mentioned above. As a model system, resident bacteria were obtained from sand filters treating groundwater in drinking water production systems while natural waters were local surface waters.

3.5 Models

3.5.1 Geological models

Geological data are essential in the development of a three-dimensional framework for numerical groundwater models, including defining the spatial boundary conditions and parametrization. For this purpose, the geological model should possess a sufficiently high resolution and adhere to established lithostratigraphic and hydrogeological standards, enabling the identification of lithologically uniform layers.

For each of the three case study sites a subsurface model was constructed, utilizing geological data sourced from the RBINS-GSB archives and DOV, including borehole descriptions and interpretations, and geological maps. In addition, new local field data obtained during the installation of the piezometers (03.3.1) were incorporated in the dataset. The model's lower boundary was defined by

the depth of the first aquitard, while the upper and lower extents of each geological unit were interpolated using geostatistical techniques in a GIS environment.

Considering the small dimensions of the case study site areas (500 x 600 meters) and the high spatial variability inherent to shallow Quaternary geology, the publicly available data was either insufficient in quantity (i.e. borehole information) or lacking the necessary detail (i.e. regional geological maps and models). Consequently, the incorporation of new boreholes and additional data resources (e.g. soil maps, digital elevation models), was essential for the development of a subsurface model that meets the required detail and accuracy (see process illustrated in Figure 3-13).

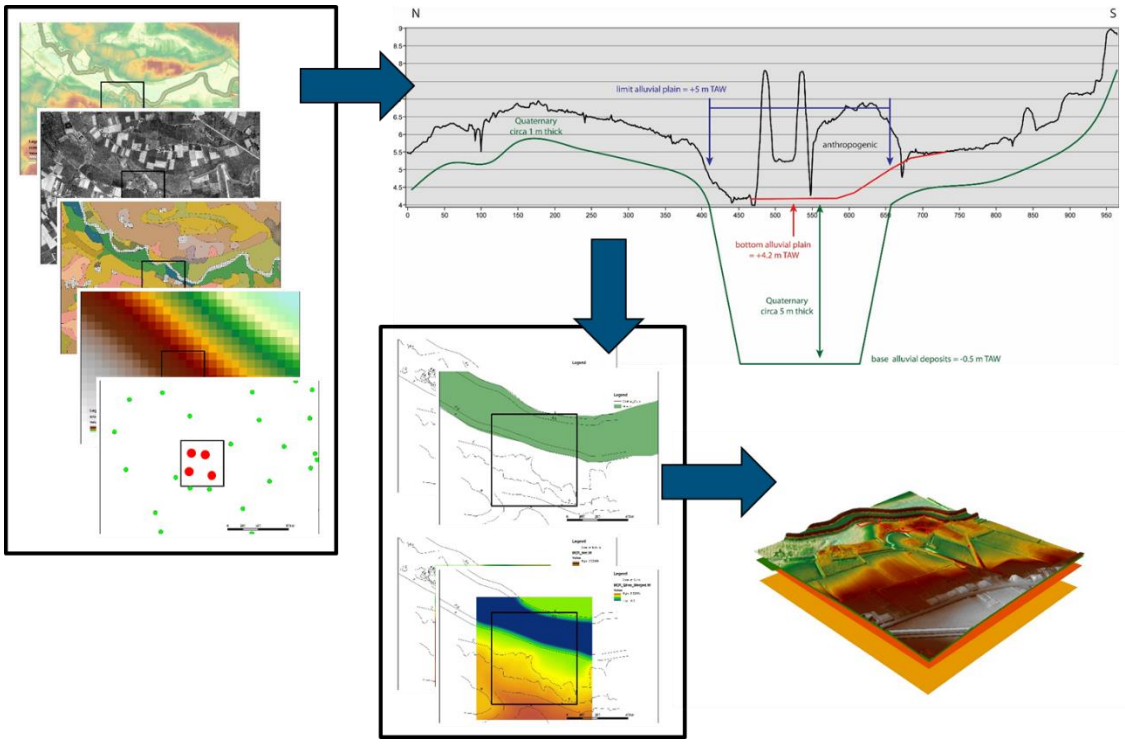

Figure 3-13- The process of developing a local high-resolution geological model involved the interpolation of the upper and lower boundaries of each geological unit; the accurate delineation of the extent of surficial deposits required incorporation of supplementary data sources and expert manual guidance.

3.5.2 Flow and Transport model

As described in the general methodology, flow and transport models are developed for the landfill site Canivet based on readily available data. The data was described in section 3.3.2; here the development of the flow and transport model is presented. The description of the methodology consists of two main aspects:

- Generic aspects on model building, and
- Elements specific to the site.

3.5.2.1 Objective of the flow and transport model

The objective of the flow and transport model for the Canivet landfill (section 3.3.2) is to describe the general features of the pollution, more specifically:

- To describe the spatial geometry of a potential pollution
- To assess the temporal evolution of a potential pollution
- To indicate contamination risk at the extraction site
- To determine and advise on shortcomings in the current dataset with respect to the risk

3.5.2.2 General mathematical model for flow and transport in an aquifer system

Water flow in a three-dimensional saturated aquifer system can be described by:

$$\frac{\partial}{\partial x}\left(K_{xx}\frac{\partial h}{\partial x}\right)+\frac{\partial}{\partial y}\left(K_{yy}\frac{\partial h}{\partial y}\right)+\frac{\partial}{\partial z}\left(K_{zz}\frac{\partial h}{\partial z}\right)+W=S_s\frac{\partial h}{\partial t} \quad (17)$$

where *x*, *y*, and *z* are the three axes on a Cartesian coordinate system [L], K_{xx}, K_{yy}, and K_{zz} are the values of the hydraulic conductivity tensor along the three axis [L T^{-1}], *h* is the hydraulic head [L], *W* represents sources and sinks per unit volume [T^{-1}], S_s is the specific storage term [L^{-1}], and *t* is time [T].

The transport of solutes is described with the advection-dispersion equation (Bedekar et al. 2016):

$$\eta\frac{\partial C}{\partial t}=\frac{\partial}{\partial i}\left(\eta D_{ij}\frac{\partial C}{\partial j}\right)-\frac{\partial}{\partial i}(\eta v_i C)+q_s C_s-q_s' C+\sum R \quad (18)$$

where η is the porosity of the porous medium [-], *C* is the aqueous concentration [M L^{-3}], *D* is the hydrodynamic dispersion coefficient tensor [L^2 T^{-1}], *v* is the average groundwater velocity vector [L T^{-1}], q_s is the volumetric flow rate per unit volume representing sinks and sources [T^{-1}], C_s is the concentration in the source and sink [M L^{-3}], q'_s is the volumetric transient storage flow rate per unit volume [T^{-1}], *R* is the rate of mass added or removed by geochemical processes [M L^3 T^{-1}] and *i* and *j* indicate the three axes *x, y,* and *z* of the coordinate system. The linear pore water velocity is obtained as:

$$v=\frac{q}{\eta} \quad (19)$$

where *q* is the Darcy flux obtained from the water flow equation (Eq. (17)). To account for chemical reactions, it can be assumed that chemical elements interact with each other or are independent from each other. The former will result in so-called coupled reactive transport and is discussed in section 3.5.3. The latter result in the advection-dispersion-reaction equation and account for chemical reactions as (non-)linear sorption isotherms or zero- and first-order decay reactions.

The partial differential equations must be solved by numerical algorithms for the complex geometries and conditions considered in this study. The numerical models implemented in MODFLOW-2005 for water flow and in MT3D-USGS (Bedekar et al. 2016) for solute transport are used in RESPONSE.

3.5.2.3 Site-specific aspects of the flow and transport model

To convert the generic equations defined above to a site-specific model and related to the objectives of the model as listed in section 3.5.2.1, several decisions on conceptual aspects, numerical aspects, parameterization and initial and boundary conditions have to be made. These decisions were made based on available data from literature, databases (at the level of Flandres) and some site-specific

data. However, no efforts were made to collect data at the site itself. Hereafter, the main site-specific components of the flow and transport model are listed.

Flow model

To assess the spatial and temporal evolution of the pollution in a groundwater system with a solute transport model (see below), Darcy's fluxes saturated thicknesses and volumetric boundary condition rates are required – these variables are obtained from a steady-state flow model. The flow model consists of following parts (further details are given in Neyens (2022)):

- Model area – The model area (Figure 3-14 left) is aligned with the general flow direction obtained from an available regional flow model (Watergroup 2015); the extent is chosen such that all required hydraulic features relevant for the model of the hydrogeological system are included (Figure 3-14 right). The top of the model area is defined by the surface topography (DTM at 25mx25m resolution from GDI-Vlaanderen (2021); the bottom is represented by the boundary between the Brussels Sands and the Kortrijk Formation (Figure 3-6) obtained from DOV (2021).
- Numerical aspects – The numerical cell size is 25mx25m (Figure 3-14 middle) chosen as a compromise between numerical accuracy (for both flow and transport model) and computational effort. The Quaternary deposits (Figure 3-6) were grouped in a single unit as a first numerical layer on the top. The St-Huibrechts-Hern formation and the Lede Formation were included in the Brussels sands; this group consists of 10 numerical layers.
- Parameter values – Within a single unit, the hydraulic conductivity field was assumed to be homogeneous and isotropic. The hydraulic conductivity values were taken from literature (0.1 m/d for the Quaternary deposits (literature values for similar fine-grained sediments from Fetter (2001)) and 10 m /d (Peters 2010)).
- Boundary conditions – Boundary conditions are showed in Figure 3-14 (right):
    - Extraction wells are included as Neumann-type boundary condition (constant fluxes) with medium pumping rates calculated from available extraction rates.
    - Surface water ponds are included as Dirichlet-type boundary conditions (constant head) with levels based on topography levels.
    - Molenbeek and brooks around the Abdij site are represented as river boundaries (Cauch-type of boundary) – parameterization (conductance values, vertical condictivities, riverbed thickness) were based on expert knowledge.
    - Groundwater recharge is assumed to be time-invariant but spatially variable. The estimate of the recharge was obtained from the long-term average groundwater recharge for Flanders at 50mx50m resolution from Zomlot et al. (2015).
    - Southern boundary considers an influx of groundwater from the upgradient areas via a Cauchy-type boundary condition with values derived from the regional model (Watergroup 2015).
    - No-flux boundary conditions were applied to the sides parallel to the flow direction and to the bottom of the model.

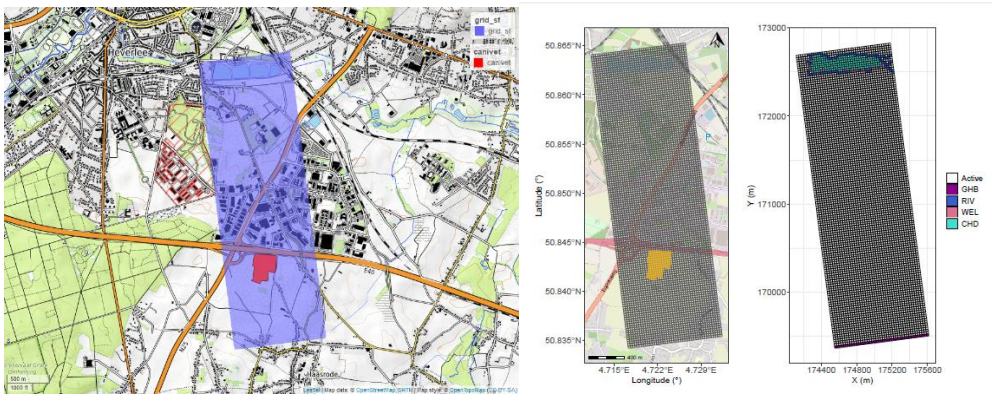

Figure 3-14 – (left) Alignment of the model area, (middle) numerical grid, (right) hydrogeological features as boundary conditions of the flow model (GHB = General-head boundary, RIV = River, WEL = well, CHD = constant-head. RCH (recharge) is applied over the entire domain (not shown)).

Transport model

The transport model is a 3D transient solute transport for a non-reactive solute (chloride) accounting for the solute transport processes by advection and mechanical dispersion for the time period 1980 - 2020. The model area and numerical grid was identical to those of the flow model. The other parts of the transport model are (further details are given in Neyens (2022)):

- Source term – the chloride which was present in the landfill started leaching as early as 1980 when precipitation percolates through the landfill. The source time is a highly uncertain aspect as neither exact location, geometry, concentration levels and timing are known. The geometry was based on the landfill cadastre as delineated by Van Keer, Bronders, and Smolders (2001). The simulation time was split in two periods: the first without landfill leaching and the second with leaching. The time of change from the first to the second period and the chloride concentration in the second period were estimated from available solute breakthrough data from the wells in the landfill itself (respectively 5.5 years, and 1432 mg/l).
- Transport parameters are derived from previous studies (uniform porosity of 20% based on Peeters (2010)) and expert knowledge/arbitrary choices (longitudinal dispersivity of 10m, horizontal and transverse ratios of 0.1 and 0.01, respectively).
- The recharge of chloride from the natural systems are represented by fluxes obtained by multiplying the recharge flux with the chloride concentration. The latter is estimated from available site-specific information (*e.g.*, observations in a shallow VMM well, observations in surface ponds close to the target domain, etc.).
- A guess of the initial chloride concentration in the domain is made by running the model for 40 years without the landfill leachate using a uniform chloride concentration of 50 mg/l at time 0.

3.5.3 Coupled Reactive Transport models

RESPONSE relies on two codes for coupled reactive transport:

- A first code is the existing HP1 and HP2 coupled reactive transport codes (Jacques et al. 2018) for one- and wo-dimensional flow and transport in variably-saturated media coupling HYDRUS 5.0 (Šimůnek et al. 2024) with PHREEQC (Parkhurst and Appelo 2013).

- A second code is developed within the framework of RESPONSE coupling MT3D-USGS (Bedekar et al. 2016) with PHREEQC, indicated by the acronym MTHP (section 3.5.3.3) via the HPx framework used also for HP1 and HP2 (section 3.5.3.2).

To facilitate the use of the somewhat complex geochemical models for organic species degradation (section 3.4.1) and sorption of heavy metals on organic matter (section 3.4.2), re-usable graphical user input forms are made available for HP1 and HP2 (section 3.5.3.4).

3.5.3.1 Generic model for coupled reactive transport

Coupled reactive transport models include (Steefel et al. 2015) (i) flow models for water transport (e.g. Eq. (17)), (ii) advection-dispersion equation for sol solute transport (e.g., Eq. (18)), (iii) advection-dispersion equation for heat transport, and (iv) geochemical processes with mixed thermodynamic equilibrium and kinetic process. The thermodynamic equilibrium model calculates aqueous speciation (i.e., aqueous complexes between different elements) and other processes such as sorption by exchange processes or surface complexation, mineral dynamics, and exchange with the gas phase. Processes as organic species degradation and microbiologically mediated redox reactions are examples of kinetically controlled processes (e.g. described by the set of equations in section 3.4.1).

The key difference with reactive transport models is that the source / sink term (R in Eq. (18)) does not depend on the concentration of the component only, but also on the concentration of the other components by e.g. forming aqueous species or competing for the same sorption sites. There exist different methods to integrate a geochemical model in the transport equation (Steefel, Yabusaki, and Mayer 2015). The models in this report are based on the non-sequential split-operator approach where, within one time-step, first the transport equation is solved (*i.e.*, Eq. (18) without R), and then R is calculated with the geochemical model solver. Thus, the transport solver considers coupling in the transport domain but no coupling in the geochemical domain (*i.e.,* transport of dissolved components depends only on the concentration of that dissolved component); the geochemical solver considers coupling in the geochemical domain but not in the spatial domain (*i.e.,* the geochemical speciation only depends on the amounts at the specific time and space). This method allows to couple different codes (a transport solver with a geochemical solver) in a rather simply way. The main disadvantage of this method is that small time steps are required to ensure mass balance and minimize splitting-operator errors (Jacques et al. 2006). Further mathematical equations are given in section 3.5.3.3 in which the development of MTHP is discussed.

3.5.3.2 The HPx framework

One of the most advanced coupled reactive transport codes for coupled reactive transport is the HPx framework (Jacques et al. 2018; Šimůnek et al. 2024). This framework was first used to couple the geochemical solver PHREEQC-2 (now replaced by PHREEQC-3, Parkhurst and Appelo (1999), Parkhurst and Appelo (2013)) to the HYDRUS codes for flow and transport in unsaturated media (Simunek et al. 2018; Šimůnek, van Genuchten, and Šejna 2016; Simunek, Sejna, and van Genuchten 2012) for one-dimensional and two-dimensional flow and transport problems (Jacques et al. 2008a, 2008b, 2006; Jacques et al. 2005, 2002; Simunek et al. 2013; Šimůnek, Jacques, and Šejna 2013; Šimůnek et al. 2009; Simunek et al. 2006; Jacques et al. 2018). The code was verified in different benchmarks (Jia et al. 2019; Xie et al. 2015; Greskowiak et al. 2015; Mayer et al. 2015). In essence, all capabilities of the most recent version of the geochemical solver are available. This means that the geochemical model for the coupled reactive transport problem can be set up the same way as in PHREEQC-3. However, the

(scripting) capabilities have been enhanced by introducing alternative scripting languages (for definitions of rates or output, an modern BASIC-like scripting language and PYTHON are implemented), use of global and inline variables, additional keywords for graphs and reactive transport options (Jacques et al. 2018).

The HPx framework (Figure 3-15) allows for a smooth hard coupling (*i.e.*, via the source code) between flow and transport solvers with geochemical solvers. For example, the framework has incorporated the alternative geochemical solver ORCHESTRA (Meeussen 2003) or can be used to couple sink/source models (*R* in Eq. (18)) written in Python with the transport solvers (*e.g.*, Laloy and Jacques (2022)). Similarly, alternative transport codes can be incorporated, as was done with MT3D-USGS in the RESPONSE project (see section 3.5.3.3).

Some components of the HPx framework are supported by Graphical User Interfaces (GUI). In essence, GUIs are available for HP1 and HP2 for both defining the flow, transport and geochemical input data. In addition, a GUI is available for pure geochemical calculations (no transport). This GUI can be used to implement more advanced geochemical models that are then subsequently used in MTHP (coupling MT3D-USGS with HPx).

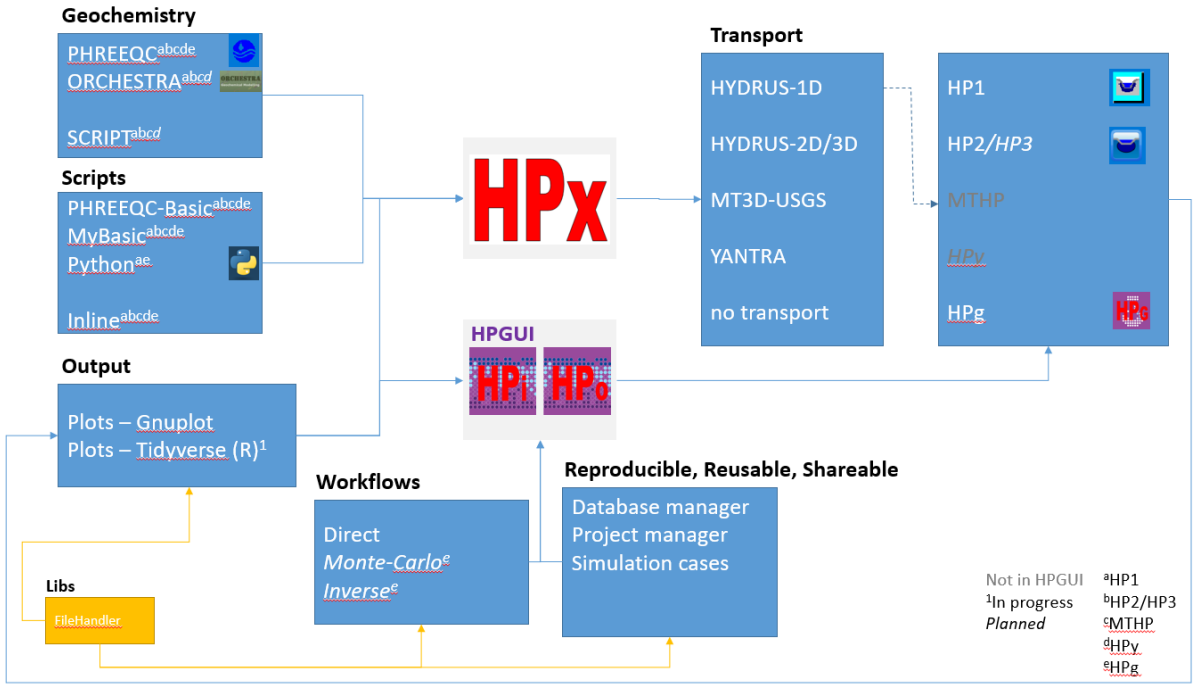

Figure 3-15 – The HPx framework

The HPx framework is coded in C++ transferring information from the flow and transport solver to the geochemical solver (water content, temperature, aqueous concentrations, auxiliary hydraulic parameters) and reverse (aqueous concentrations, effective flow and transport properties) at each time step and node. The standard operator-splitting approach (Jacques et al. 2018; Jacques et al. 2006) is used to calculate the coupled reactive transport equations. To speed up calculations, the OPENMP paradigm is implemented to distribute the geochemical calculations over different physical cores of a computer.

3.5.3.3 Extending MT3D-USGS with HPx

To be incorporated in MT3D-USGS, the transport equation Eq. (18) is written as:

$$\frac{\partial C_k}{\partial t} = L(.) + R_k \tag{20}$$

where *L(.)* is the transport operator (Bedekar et al. 2016) (Eq. (18) without the last term at the right hand side) with C_k is the total dissolved concentration (mol/L) of component *k*:

$$C_k = c_k + \sum_{j=1}^{N_S} \nu_{jk} c_j \tag{21}$$

where c_j is the concentration of an aqueous species, and ν_{jk} is the stoichiometric coefficient (*i.e.* the number of moles of the *k*th primary species in the *j*th secondary species). The concentrations of the aqueous species are calculated with the thermodynamic model based on thermodynamic data for the reaction equations:

$$\boldsymbol{A_j = \sum_{i=1}^{N_p} \nu_{ji} A_i} \tag{22}$$

where A_i and A_j are the chemical formulae of the primary and secondary species, respectively. When thermodynamic equilibrium is obtained (*i.e.* at the minimum of the Gibbs free energy of the system), the concentrations of the secondary species are obtained via the law of mass-action equation as:

$$c_j = \frac{\prod_{i=1}^{N_p} (\gamma_i c_i)^{\nu_{ji}}}{K_j \gamma_j} \tag{23}$$

where K_j is the equilibrium constant for the reaction and γ_i and γ_j are the activity correction coefficients for the primary and secondary species, respectively[2]. Activity correction coefficients relate the concentration of the species to the activities which are used in the definition of the equilibrium constant (activity $a_i = \gamma_i c_i$).

The geochemical reaction term in Eq. (20), R_i, accounts for heterogeneous equilibrium or kinetic geochemical reactions or homogeneous kinetic reactions. Homogeneous (aqueous) equilibrium reactions do not change the concentration of the primary species and therefore, there is no need to include them in a sink/source term in transport Eq. (20) for master species. Typical heterogeneous reactions taken into account in reactive transport models are (Steefel, Yabusaki, and Mayer 2015) ion exchange, surface complexation, aqueous-gas exchange, mineral dynamics, and solid-solutions; most of them treated both in equilibrium or kinetically-controlled. Typical homogeneous kinetic reactions are radioactive decay and (microbiologically mediated) kinetic degradation of, e.g. organics, or oxidation-reduction reactions.

A new package MCP (MultiComponent Package) was added to the original MT3D-USGS code using a similar versatile approach as in HPx, in order to set up the geochemical calculations. It defines the species, database and initial and boundary geochemical conditions of the simulation, and paths to the

geochemical input files. In the particular case of MTHP, MT3D-USGS and PHREEQC are, respectively, the transport and geochemical solver The code executable, manual and examples are available on https://github.com/dphjacques/MTHP. Examples of verification of the developed code are given in section 4.5.1.

3.5.3.4 The graphical user interface

The HPx framework comes with graphical user interfaces. The most advanced GUI is available for coupled reactive transport models performed with HP1 and HP2. The complete flow and transport problem can be defined in the advanced GUI of HYDRUS 5.0 (Šimůnek et al. 2024) with a specific dialogue window to define the geochemical model. The latter is also available for geochemical calculations and combined with options for visualization of calculation results; the GUI is indicated as HPGeochemistry. Note that there is no GUI for MTHP, but HPGeochemistry can be used to produce the input for the geochemical model.

Examples input forms and simulations are available on following platform: https://github.com/dphjacques/HPx-KRN for the model of microbial-driven kinetic degradation of organics (section 3.4.1) and https://github.com/dphjacques/HPx-SorptionModels for sorption of heavy metals on fulvic and humic acids (section 3.4.2).

The geochemical model for kinetic degradation of organic species presented in section 3.4.1 is a relative complex model with several rate equations, multiple parameters, and different options (temperature model, biomass, etc.). If the composition if the organic species changes (different C, H, O or N and P), kinetic statements in PHREEQC must be adapted. The GUI of HPGeochemistry allows to construct a relatively simple interface to set up the details of the geochemical model while underlying scripts will generate the specific PHREEQC input. Within RESPONSE, that aspect of the GUI has been elaborated, and specific input tables and templates have been made for the model described in section 3.4.1.

Figure 3-16 shows a screenshot of part of the input table form for the model described in section 3.4.1. The first input group (“Organic compound properties”) allows to define the stoichiometry of the organic species (Eq. (1)). The kinetic statements will subsequently be adapted according the stochiometric relations between electron doners and acceptors described by the various equations in section 3.4.1. The second input group (“DOC oxidation with O2”) allows to define the particular form of the rate equation (zero or first-order dependence, temperature effects, link to biomass) and specific parameters for electron donors and acceptors. Similar groups are available for the other electron acceptors; for those, also inhibition terms are included. Scripts convert the input from the form to PHREEQC input. An example of the KINETIC block readable by PHREEQC is shown in Figure 3-17. Files with the information on the input forms and the corresponding scripts are available in the github repository.

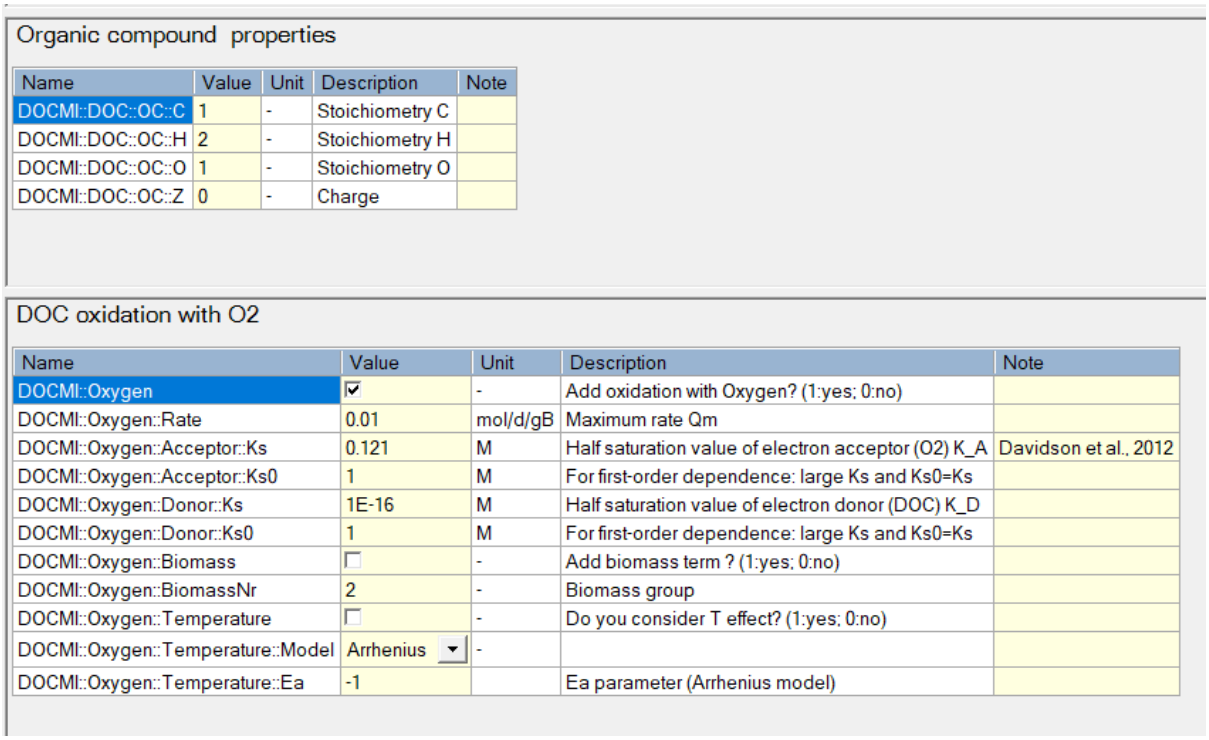

Organic compound properties

Name	Value	Unit	Description	Note
DOCMI::DOC::OC::C	1	-	Stoichiometry C	
DOCMI::DOC::OC::H	2	-	Stoichiometry H	
DOCMI::DOC::OC::O	1	-	Stoichiometry O	
DOCMI::DOC::OC::Z	0	-	Charge	

DOC oxidation with O2

Name	Value	Unit	Description	Note
DOCMI::Oxygen	☑	-	Add oxidation with Oxygen? (1:yes; 0:no)	
DOCMI::Oxygen::Rate	0.01	mol/d/gB	Maximum rate Qm	
DOCMI::Oxygen::Acceptor::Ks	0.121	M	Half saturation value of electron acceptor (O2) K_A	Davidson et al., 2012
DOCMI::Oxygen::Acceptor::Ks0	1	M	For first-order dependence: large Ks and Ks0=Ks	
DOCMI::Oxygen::Donor::Ks	1E-16	M	Half saturation value of electron donor (DOC) K_D	
DOCMI::Oxygen::Donor::Ks0	1	M	For first-order dependence: large Ks and Ks0=Ks	
DOCMI::Oxygen::Biomass	☐	-	Add biomass term ? (1:yes; 0:no)	
DOCMI::Oxygen::BiomassNr	2	-	Biomass group	
DOCMI::Oxygen::Temperature	☐	-	Do you consider T effect? (1:yes; 0:no)	
DOCMI::Oxygen::Temperature::Model	Arrhenius	-		
DOCMI::Oxygen::Temperature::Ea	-1		Ea parameter (Arrhenius model)	

Figure 3-16 – Screenshot of developed input form for kinetic models of organic species degradation.

```
DocOxygen
-formula Doc 1 O2 1 CO2 -1 H2O -1 H+ 0
-parms 0.01 1 1e-16 1 0.121
-m0 0
DocNitrate
-formula Doc 1 [N5]O3 2 CO2 -1 [N3]O2 -2 H2O -1 H+ 0
-parms 0.01 1 1e-16 1 0.00042 1e-08
-m0 0
DocIron::Goethite
-formula Doc -0.25 CO2 0.25 [Fe2] 1 H2O 1.75 H+ -2
-parms 0.01 1 1e-16 1 6.5e-06 1e-08 1e-08 1e-08
-m0 0.01
DocSulphate
-formula Doc 1 [S6]O4 0.5 CO2 -1 H[S2-] -0.5 H2O -1 H+ 0.5
-parms 0.0005 1 1e-16 1 0.0001 1e-08 1e-08 1e-08 1e-08
-m0 0

```

Figure 3-17 – Screenshot of PHREEQC input produced from the input form shown in Figure 3-16.

Previous version of the humic ion interaction model (e.g. model VI) described in section 3.4.2 have been included in PHREEQC (Appelo and Postma 2005). More recently, model VII was included in PHREEQC by Marsac et al. (2017) using the constant capacitance surface complexation model for the electrostatic factors. Creation of the input file for PHREEQC is relatively complex because of the numerous surface sites, species and capacities that need to be defined. A set of scripts and an input table are created within RESPONSE to ease incorporation that model in geochemical and coupled reactive transport. The developed input form is shown in Figure 3-18.

HA-FA: Sorption & Buffering

Humic Ion-Binding Model VII (for HA & FA)

Properties organic matter

Name	Value	Unit	Description	Note
OM::Sorption	☐		Do you consider sorption on OM?	
OM::WeightPercentage	2	%		
OM::FractionFA	0.6		Fraction of Fulvic Acids	

Humic VII - General Parameters

Name	Value	Unit	Description	Note
HumicVII::SurfaceType$	CC			
HumicVII::DummySurface	1E6			

Parameters Humic Acid

Name	Value	Unit	Description	Note
HumicVII::HA::Database$	HumicVII_HA		Name of the datablock with the information	
HumicVII::HA::nA	0.0034	mol/gHA	Type A site (carboxylate) content ()	
HumicVII::HA::nB	0.0017	mol/gHA	Type B site (phenolate) content (mol/gHA) = nA/2	
HumicVII::HA::fb	0.5		Fraction of bidentate sites	
HumicVII::HA::ft	0.065		Fraction of tridentate sites	
HumicVII::HA::pKa	4.1		Intrinsic proton dissociation constant for type A sites	
HumicVII::HA::pKb	8.3		Intrinsic proton dissociation constant for type B sites	
HumicVII::HA::DpKa	2.6		Distribution terms that modifies pKA	
HumicVII::HA::DpKb	3.1		Distribution terms that modifies pKB	
HumicVII::HA::SurfaceArea	1500	m2/g		

Figure 3-18 – Screenshot of developed input form for the humic-ion binding model VII for humic and fulvic (not shown) acids.

4 SCIENTIFIC RESULTS AND RECOMMENDATIONS

4.1 Selection of potential contaminated sites

A concise overview of selected site is given here – more details are available in Annex 6.1.

4.1.1 Cemeteries

Among 2330 **civil cemeteries in Wallonia** 12 cemeteries are at 20 meters maximum of a river and at 20 meters of a low drainage zone. The 12 cemeteries have been explored in order to verify the depth of the groundwater (< 2m). Among them several sites have been dismissed for different reasons:

- No groundwater < 2m
- Pollution from domestic waste in the sampling zone
- Owner of the pasture does not want to participate to the study
- Not possible to access to downslope zone

For 3 civil cemeteries, it was possible to find groundwater and the owner of the propriety agreed to give access to his pasture: Villers-deux-Eglises, Amberloup and Gozée (Fig. 4.1; Table 4.1).

Among 1578 **civil cemeteries in Flanders** 147 cemeteries are at 10 meters maximum of a low drainage zone. Among the 147 civil cemeteries, 85 cemeteries intersect a zone with a slope >4.5°. This threshold of slope has been taken after a classification of the slopes in Flanders (Meth: Jenks with 2 classes). We decided to include this criterion because the landscape in Flanders is relatively flat and it is easier to determine the flow accumulation (and the ideal position of the piezometers) if there is a clear slope. It was not possible to use the same second order criteria than in Wallonia because there are too many rivers or drainage channels in Flanders. The 85 cemeteries have been checked individually on ArcMap in order to verify the flow direction, the accessibility or the environment around the cemetery. It has decreased the number of sites to 17 civil cemeteries. All of them have been visited. After the visit, 10 civil cemeteries have been retained. Among the 10 Study sites, 2 have been selected (Kruishoutem and Erpe-Mere) by the RESPONSE researchers to install piezometers and 1 has been kept has a backup site (Haacht) (Fig. 4.1)

Among 63 **military cemeteries in Wallonia** 4 cemeteries are at 20 meters maximum of a river and at 20 meters of a low drainage zone. The 4 cemeteries have been explored in order to verify the depth of the groundwater (< 2m). Among them, several sites have been dismissed for different reasons:

- No groundwater < 2m
- Not possible to access to downslope zone
- Territory ruled by an foreign country

For 4 military cemeteries, it was possible to find groundwater and the owner of the propriety agreed to give access to his pasture. Among the 4 military cemeteries 2 have been retained and selected to install piezometers by RESPONSE researchers (Neuville-en-Condroz and Tintigny, Fig. 4.1).

Among 184 **military cemeteries in Flanders** 17 cemeteries are at 10 meters maximum of a low drainage zone. Among the 147 military cemeteries, 12 cemeteries intersect a zone with a slope >4.5°. This threshold of slope has been taken after a classification of the slopes in Flanders (Meth: Jenks with 2 classes). We decided to include this criteria because the landscape in Flanders is relatively flat and

it is more easy to determine the flow accumulation (and the ideal position of the piezometers) if there is a clear slope. It was not possible to use the same second order criteria than in Wallonia because there are too many rivers or drainage channels in Flanders. The 12 military cemeteries have been checked individually on ArcMap in order to verify the flow direction, the accessibility or the environment around the cemetery. It has decreased the number of sites

to 4 military cemeteries. All of them have been visited. After the visit, 1 military cemeteries has been retained and is presented below. The military cemetery has been chosen by RESPONSE researcher to install piezometers (Fig. 4.1).

4.1.2 Landfills

Among 67 **landfills in Wallonia** (owned and managed by the SPAQuE), 13 landfills are at 20 meters maximum of a river and at 20 meters of a low drainage zone. Among the 13 landfills, 8 sites have been dismissed for different reasons:

- Difficult to define the flow accumulation (flat zone)
- Wet zone is on the plateau, upslope
- Phreatic level is too deep (from piezometric data received by SPAQuE)

The summary table below indicates: history of pollution, contamination measured, monitoring by piezometers for the selected landfills. Among the 5 landfills, 3 have been selected by the RESPONSE researchers to install piezometers (Hensies, Perwez and Morlanwelz). The site of Genappe is kept as a back up site (Fig. 4.1).

Among 1127 **landfills in Flanders** (data given from OVAM), ~340 landfills are at 20 meters maximum of a river and at 20 meters of a low drainage zone. Among the 340 landfills, there are different types of sites that are managed differently by OVAM. Among them 34 sites have been monitored by OVAM. It means that reports and data exist but only few are digitalized. From that list, we selected 27 sites based on aerial photography. We received reports of 7 sites.

Among them, 4 landfills are interesting for our research project: Wervik, Berlaar, Wommelgem and Wevelgem (Fig. 4.1).

Some more details on the selected sites (cemeteries in Flandres and Wallonia, landfills in Wallonia) are given in the report given as an annex.

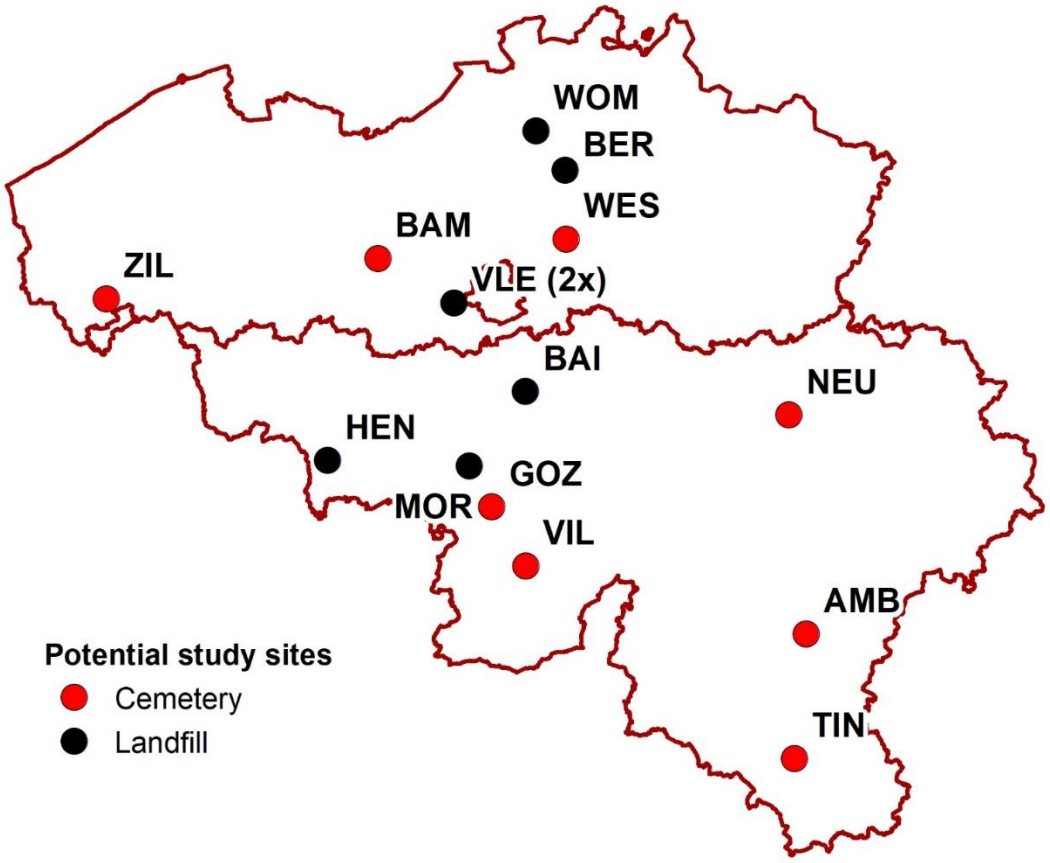

	Civ. Cemetery	Mil. Cemetery	Tot. Cemetery	Landfill	TOTAL
Vlaanderen	2	1	3	4	7
Wallonie	3	2	5	3	8
TOTAL	5	3	8	7	15

Figure 4-1. Locations of the selection of possible study sites, including cemeteries and historical landfill sites in Belgium.

Table 4-1 –Overview of the selected potential study sites.

N°	Location	Code	Region	Type
1	Gozée (Thuin)	GOZ	Wallonie	Cemetery
2	Morlanwelz	MOR	Wallonie	Landfill
3	Amberloup (Saint-Ode)	AMB	Wallonie	Cemetery
4	Tintigny	TIN	Wallonie	Cemetery (military)
5	Villers-Deux-Eglises	VIL	Wallonie	Cemetery
6	Hensies	HEN	Wallonie	Landfill
7	Neuville-en-Condroz	NEU	Wallonie	Cemetery (military)
8	Wespelaar (Haacht)	WES	Vlaanderen	Cemetery
9	Bambrugge (Erpe-Mere)	BAM	Vlaanderen	Cemetery
10	Berlaar	BER	Vlaanderen	Landfill
11	Wommelgem	WOM	Vlaanderen	Landfill
12	Zillebeke (Ieper)	ZIL	Vlaanderen	Cemetery (military)
13	Baisy-Thy (Genappe)	BAI	Wallonie	Landfill
14	Vlezenbeek A	VLEa	Vlaanderen	Landfill
15	Vlezenbeek B	VLEb	Vlaanderen	Landfill

4.2 Site specific data on contamination form point-sources

4.2.1 Screening of sites

During the screening stage, shallow piezometers were installed at the fifteen candidate study sites and subsequently sampled (see Table 4-2, see Annex 6.2 for more details).

Table 4-2. Overview of piezometer installation and sampling at the fifteen candidate study sites (few locations were not sampled due to lack of groundwater).

N°	Location	Code	Installation date	Sampling date	Sampled wells of
1	Gozée (Thuin)	GOZ	11/09/2017	22/01/2018	3 of 3
2	Morlanwelz	MOR	11/09/2017	16/01/2018	2 of 3
3	Amberloup (Saint-Ode)	AMB	12/09/2017	23/01/2018 & 10/04/2018	3 of 3
4	Tintigny	TIN	12/09/2017	23/01/2018	3 of 3
5	Villers-Deux-Eglises	VIL	20/09/2017	22/01/2018	3 of 4
6	Hensies	HEN	21/09/2017	16/01/2018	3 of 3
7	Neuville-en-Condroz	NEU	27/09/2017	30/01/2018	2 of 3
8	Wespelaar (Haacht)	WES	30/10/2017	07/12/2017	3 of 3
9	Bambrugge (Erpe-Mere)	BAM	09/11/2017		3 of 3
10	Berlaar	BER	15/12/2017 & 15/01/2018	15/01/2018 & 20/03/2018	2 of 3
11	Wommelgem	WOM	19/12/2017	15/01/2018 & 20/03/2018	3 of 3
12	Zillebeke (Ieper)	ZIL	17/01/2018	07/02/2018	3 of 3
13	Baisy-Thy (Genappe)	BAI	30/01/2018	20/02/2018	3 of 3
14	Vlezenbeek A	VLEa	06/02/2018	13/03/2018	3 of 3
15	Vlezenbeek B	VLEb	06/02/2018	13/03/2018	3 of 3

The measured values were compared against the reference station, known typical values in phreatic aquifers and intervention values – detected anomalies indicated the presence of pollution. Only a few sites showed metal contamination especially As and Pb. None of the sites showed contamination of BTEX compounds. The most detected organic contaminants related to pesticide use. The most

detected pesticide residue was BAM, a transformation product of the widely used herbicide dichlobenil. This compound was detected at 13 sites at concentrations ranging from 0.01 – 0.85 µg/L deviating from the Flanders threshold for groundwater contamination of 0.1 µg/L for pesticide residues at 4 sites, identifying it as an organic micropollutant (occurring at µg/L-ng/L concentrations). Other compounds that were encountered above the threshold were mecoprop (3 sites), bromacil (1 site), mecoporop (2 sites), metazachlor (4 sites), S-metalochlor (3 sites), and desethylatrazne (1 site).

Three primary case study sites were selected based on factors such as contamination levels, hydrological conditions and practical aspects like accessibility. They include a former landfill site in Berlaar, which exhibits heavy metal contamination, and two cemeteries located in Zillebeke and Villers-Deux-Eglises, both of which show notable concentrations of organic compounds commonly linked to pesticide use (see Table 4-3). Additionally, two other sites, Bambrugge and Wespelaar, were reserved for soil sampling related to BAM degradation experiments conducted by KU Leuven. Furthermore, two extra sites, Haacht and Lier, not part of the initial selection were incorporated into the project due to the availability of valuable external datasets.

Table 4-3. Selected study sites and the prominent contaminants present.

Location	Code	Type	Redox zonation	Inorganics	Organics
Berlaar	BER	Landfill	Y	As, Pb	(detected)
Zillebeke	ZIL	Cemetery	N	(As detected)	BAM, metazachlor
Villers-Deux-Eglises	VIL	Cemetery	N	-	BAM, bromacil, desethylatrazine
Wespelaar	WES	Cemetery	N	-	MCPP, metazachlor
Bambrugge	BAM	Cemetery	N	-	BAM

4.2.2 Monitoring and characterisation of of sites

During the monitoring stage, additional piezometers were installed at the three primary case study sites and periodically sampled (see Table 4-4, Figure 4-3, Figure 4-4). The monitoring scheme was not executed as initially planned due to various practical and logistical challenges, including staff availability, travel restrictions imposed by the COVID-19 pandemic and constraints caused by diminished groundwater levels during the dry summer months. BAM was monitored for Zillebeke and Villers-Deux-Eglises for a few sampling dates and confirmed the presence of BAM at these sites. Eventually, monitoring of the sites was discontinued, following the decision to change the study sites to Grote Nete and Canivet landfill site.

Details on the installation are given in Annex 6.2. An overview of the monitoring data that is not confidential is reported in: Walstra et al. (2024). Screening, monitoring and geological modelling of selected contaminated sites in Belgium. Contributions to the RESPONSE project. GSB report 2024 005, Scientific Reports Series, Royal Belgian Institute of Natural Sciences – Geological Survey of Belgium.

Table 4-4. Overview of piezometer installation and sampling at the three case study sites.

Location	Code	No. of sampling wells (total + additional)	Installation date (additional wells)	Sampling dates
Berlaar	BER	11 (+8)	19/07/2018 & 20/05/2019	13/12/2018, 07/03/2019, 20/05/2019, 24/09/2019,

Location	Code	No. of sampling wells (total + additional)	Installation date (additional wells)	Sampling dates
				25/10/2019, 12/12/2019
Zillebeke	ZIL	7 (+4)	05/09/2018	19/12/2018, 05/03/2019, 12/06/2019, 25/09/2019
Villers-Deux-Eglises	VIL	8 (+4)	04/07/2018, 05/07/2018 & 06/03/2019	05/12/2018, 06/03/2019, 11/06/2019, 11/09/2019

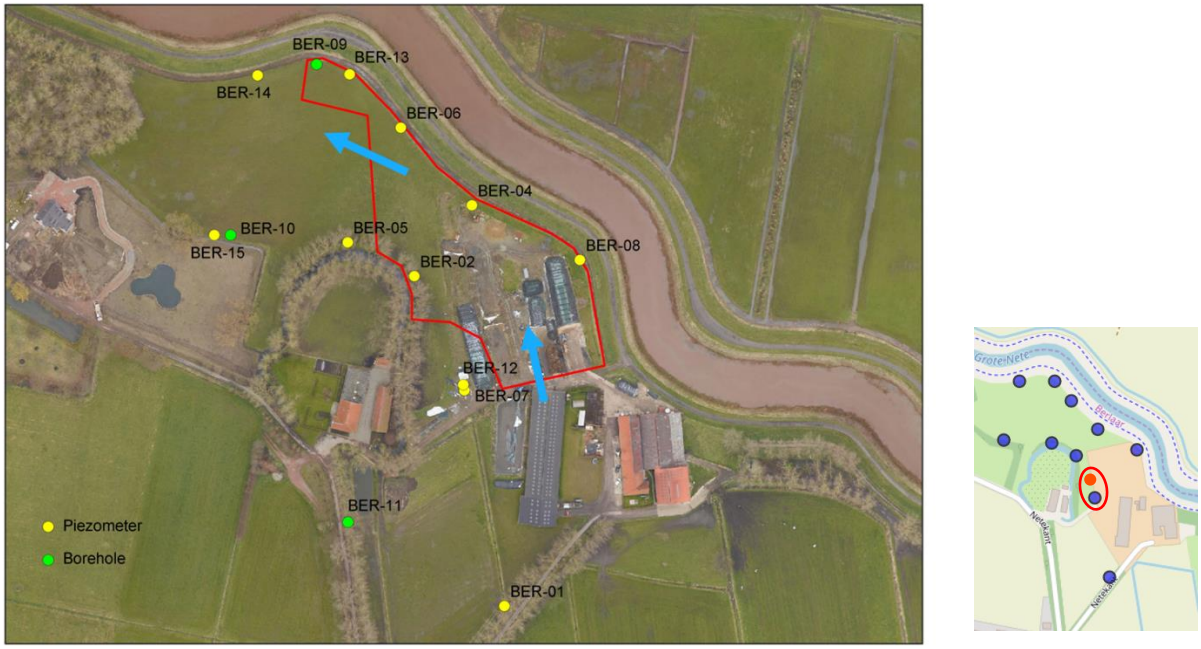

Figure 4-2. Placement of the piezometers (yellow dots) at the Berlaar site, along with a general indication of the groundwater flow direction (blue arrows). The additional boreholes (green dots) were carried out to gather localized data for the geological model. Small figure at the right indicates the position of the tracer test.

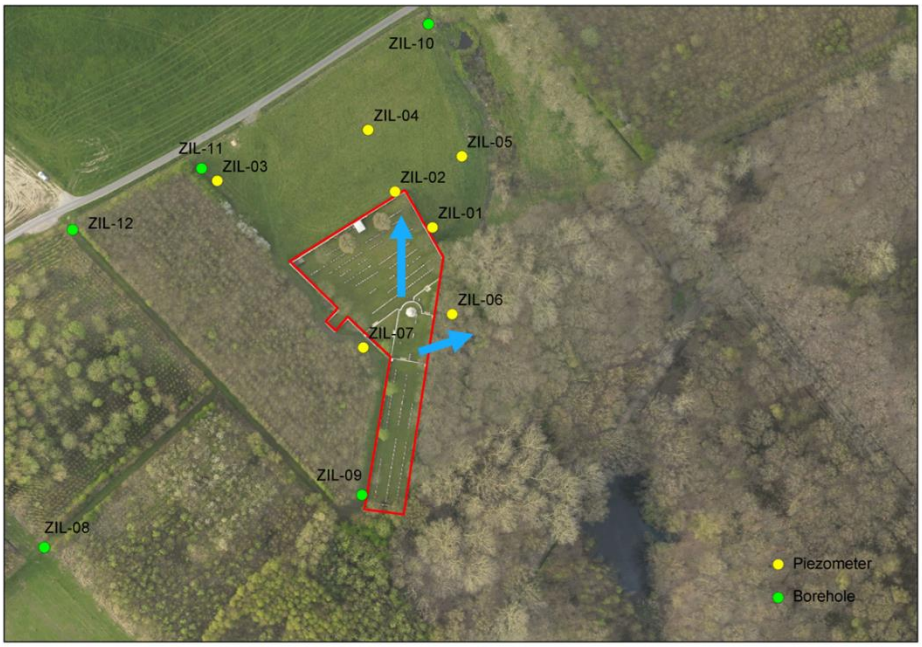

Figure 4-3. Placement of the piezometers (yellow dots) at the Zillebeke site, along with a general indication of the groundwater flow direction (blue arrows). The additional boreholes (green dots) were carried out to gather localized data for the geological model.

Figure 4-4. Placement of the piezometers (yellow dots) at the Villers-Deux-Eglises site, along with a general indication of the groundwater flow direction (blue arrows). The additional boreholes (green dots) were carried out to gather localized data for the geological model.

A tracer test was performed twice in Berlaar in the monitoring well BER-07 (Figure 4-2): one in June and the other in December 2019. The objective of this test is to derive an estimate of the longitudinal dispersivity for this site. NaCl was injected in BER-07, and electrical conductivity (EC) was continuously

measured with a logger installed in a monitoring well ~2 m further in the assumed groundwater flow direction.

The raw monitoring data of the summer test are presented in Figure 4-5. The breakthrough of the tracer at the monitoring point seems to occur after ~13-14 days. Then, the EC curve is characterized by a quite long tail. The monitoring data of the winter test are presented in Figure 4-6. It can be seen that the EC signal is very much influenced by the precipitation and consequent recharge. Interpretation of this tracer test requires first a trend decomposition on the EC signal, using the groundwater recharge estimated from the pressure head signal.

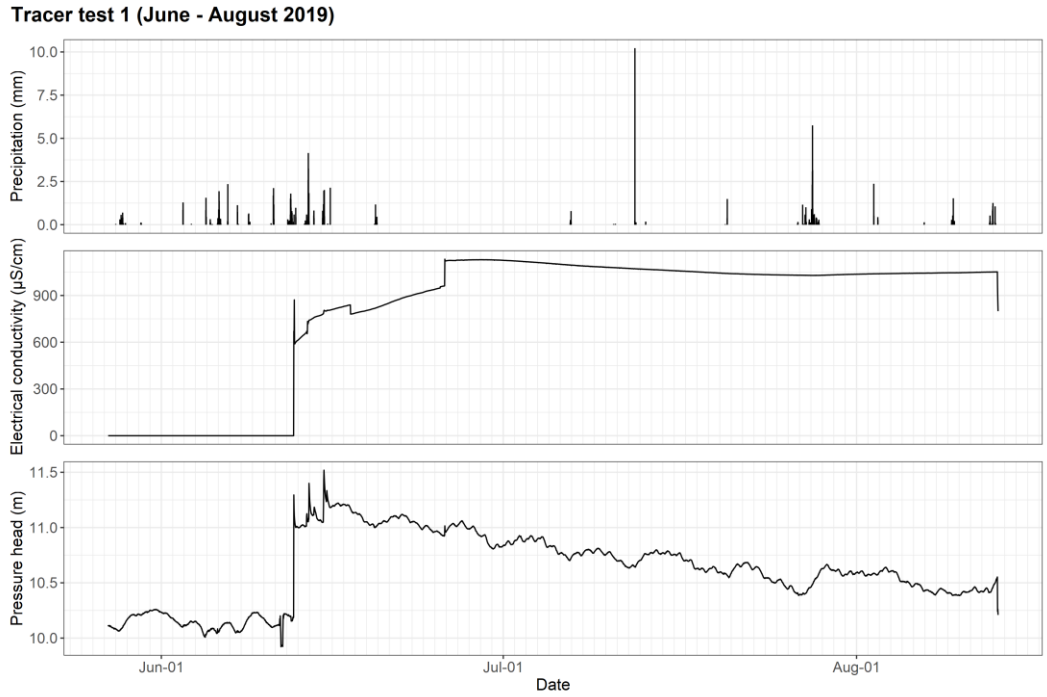

Figure 4-5 – Tracer test 1 in BER-07: precipitation (top; station VMM Herentals), electrical conductivity (middle) and pressure head (bottom) monitored ~2 m away from the injection point. The red circle indicates the interpreted breakthrough of the salt tracer at the monitoring point.

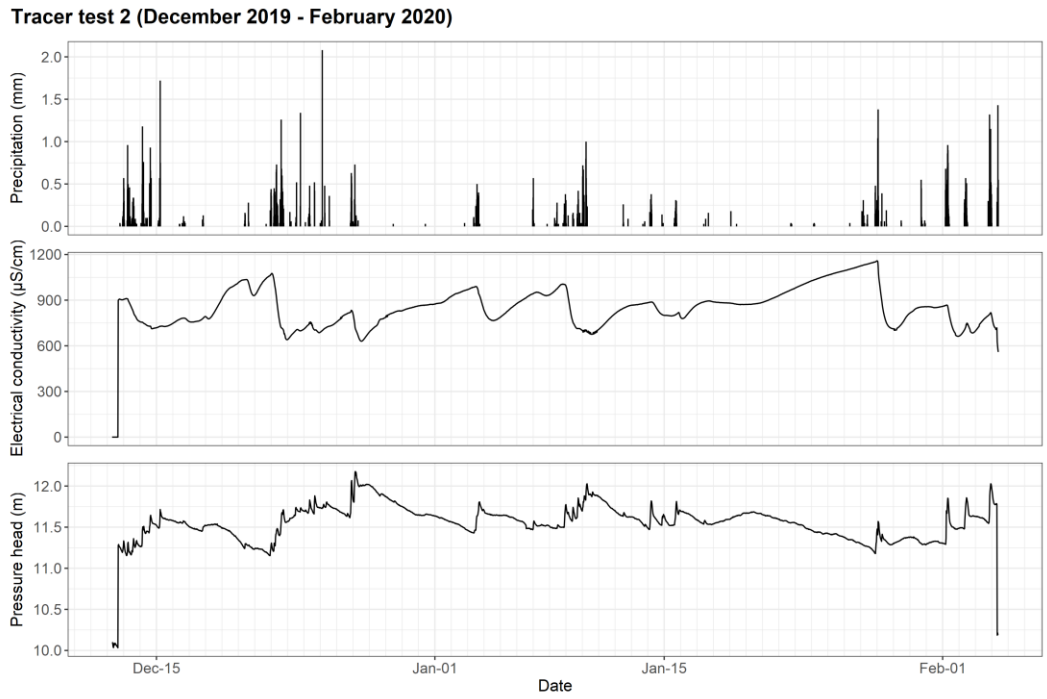

Figure 4-6 – Tracer test 2 in BER-07: precipitation (top; station VMM Herentals), electrical conductivity (middle) and pressure head (bottom) monitored ~2 m away from the injection point.

Sorption tests were performed on soil samples from different locations next to monitoring wells and three different depths. Figure 4-7 shows the resulting Kd values (L/kg) as a function of the As concentration measured in the nearby monitoring well. In general, soil samples above the groundwater table are associated with a lower Kd (except for BER-07). It is expected that changes in Kd when going from an aerobic to anaerobic system are strongly linked to the availability of biodegradable carbon. In anaerobic systems, As sorption will be more determined by sorption on (more crystalline) Fe oxides (Verbeeck, *pers. comm.*).

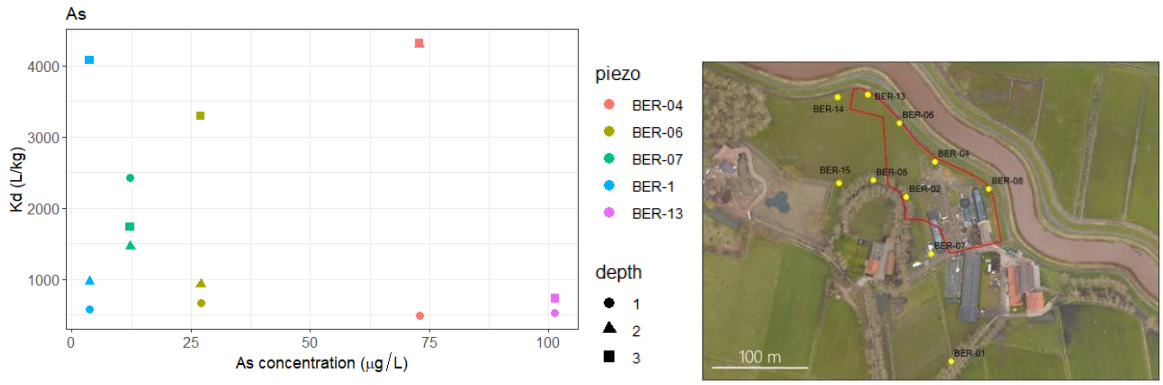

Figure 4-7 – Kd (L/kg) obtained for As from the sorption tests performed on soil samples from different locations and depths. Depth 1 (circles) is above groundwater table, depth 2 (triangles) is around the groundwater level and depth 3 (squares) is below the groundwater table.

Other field data collection included grain-size analysis on soil samples (at different depths) and slug tests on several piezometers. An example of the grain-size analysis at BER-07 location is shown in Figure 4-8. The grain-size analyses and slug tests are additional in-situ tests used to determine the amount of heterogeneity of K.

Investigating whether a heterogeneous K field would (significantly) improve simulation results is part of the overarching question on how complex the models have to be.

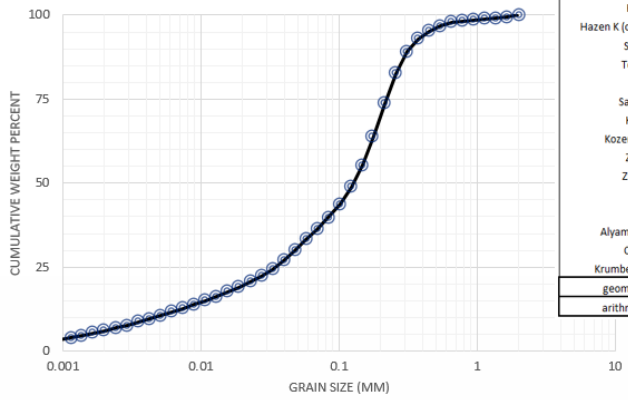

Estimation of Hydraulic Conductivity	cm/s	m/s	m/d
Hazen	.296E-04	.296E-06	0.03
Hazen K (cm/s) = d_{10} (mm)	.514E-04	.514E-06	0.04
Slichter	.584E-05	.584E-07	0.01
Terzaghi	.838E-05	.838E-07	0.01
Beyer	.336E-04	.336E-06	0.03
Sauerbrei	.891E-04	.891E-06	0.08
Kruger	.164E-04	.164E-06	0.01
Kozeny-Carmen	.203E-04	.203E-06	0.02
Zunker	.149E-04	.149E-06	0.01
Zamarin	.170E-04	.170E-06	0.01
USBR	.290E-03	.290E-05	0.25
Barr	.628E-05	.628E-07	0.01
Alyamani and Sen	.115E-02	.115E-04	1.00
Chapuis	.591E-06	.591E-08	0.00
Krumbein and Monk	.414E-03	.414E-05	0.36
geometric mean	.128E-03	.128E-05	0.11
arithmetic mean	.416E-03	.416E-05	0.36

From: A. Mondelaers

sample location	depth (m)	K (m/d)
BER-07	1.50	0.11
BER-07	1.90	0.11
BER-07	2.15	0.05

Figure 4-8 – Grain-size distribution and interpretation in terms of hydraulic conductivity, for samples collected close to BER-07 piezometer

4.3 Geological models of selected sites

4.3.1 Berlaar site

The geology of the Berlaar site is characterized by a limited anthropogenic layer, which includes the former landfill and the river embankments of the Grote Nete, underlain by Quaternary alluvial deposits that can reach a thickness of up to 5 meters, and glauconitic sands associated with the Diest and Berchem formations. The upper surface of the Boom aquitard is located approximately 15 meters beneath m.a.s.l. (see Figure 4-9 and Figure 4-10).

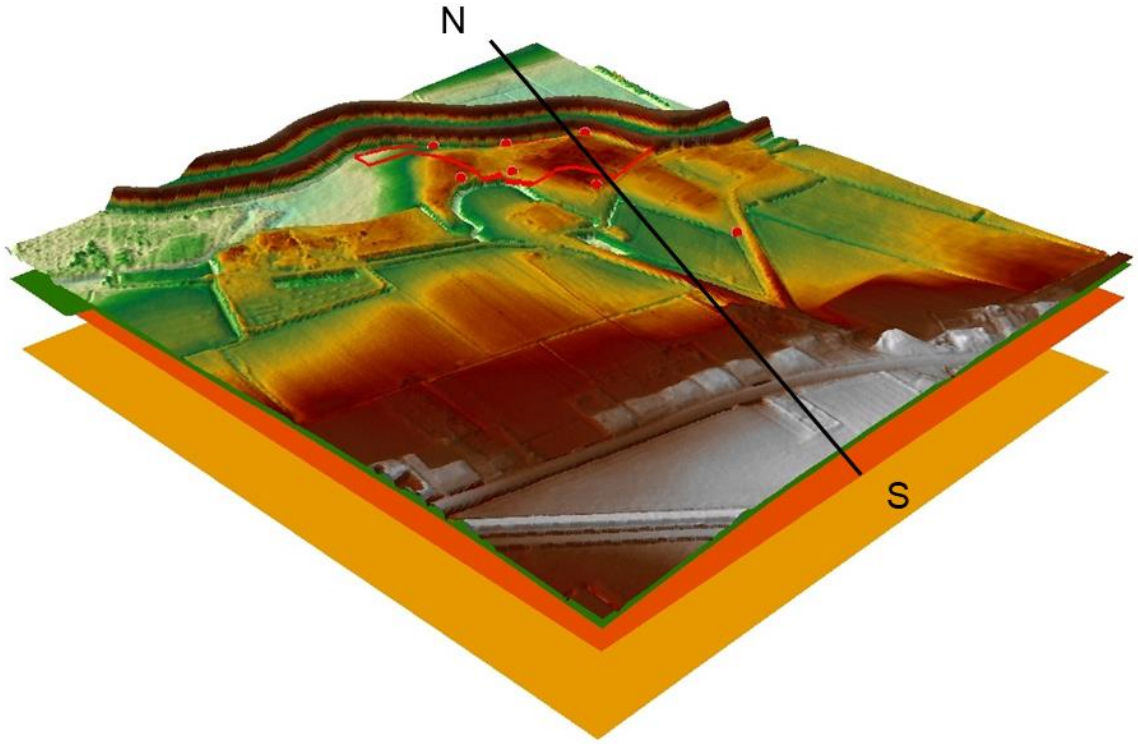

Figure 4-9. A three-dimensional visualisation of the surface and geological layers of the Berlaar site.

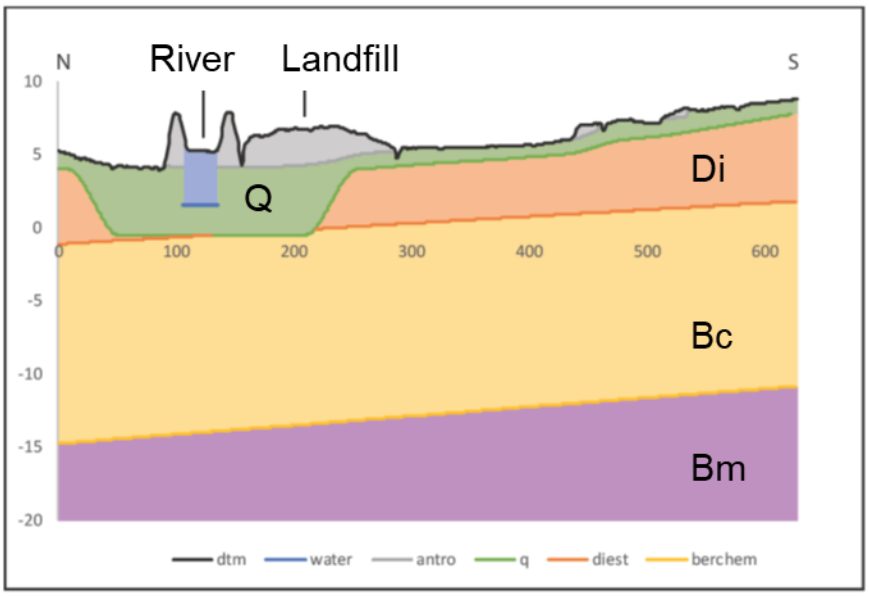

Figure 4-10. Geological cross-section profile of the Berlaar site (Q= Quaternary, Di= Diest Formation, Bc = Berchem Formation, Bm = Boom Formation). Position of the profile line is indicated in Figure 4-9; distance and elevation are displayed in meters.

4.3.2 Zillebeke site

The geology of the Zillebeke site is characterized by a cover of sandy-silty deposits belonging to the Quaternary and Tielt Formation above Ypresian clay of the Kortrijk Formation (see Figure 4-11 and

Figure 4-12). The limited inflow observed in the piezometers (section 4.2.2) can be attributed to the existence of heavy clay at shallow depth beneath the surface.

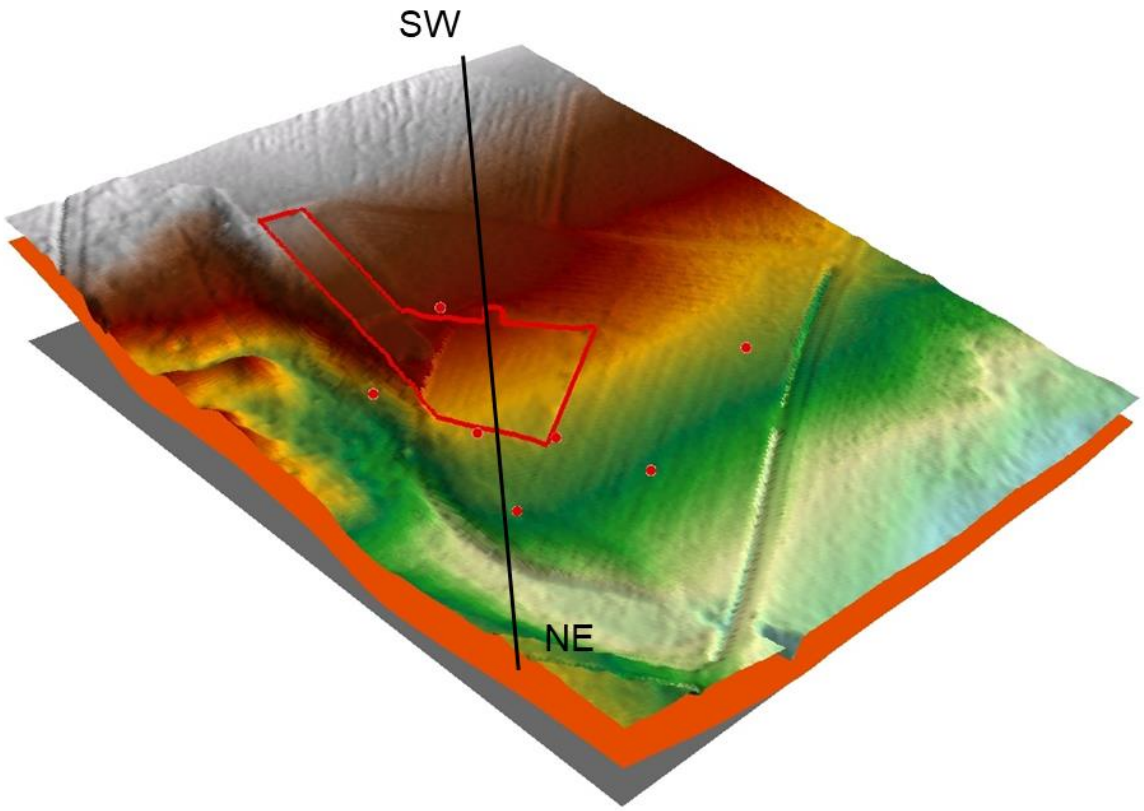

Figure 4-11. A three-dimensional visualisation of the surface and geological layers of the Zillebeke site.

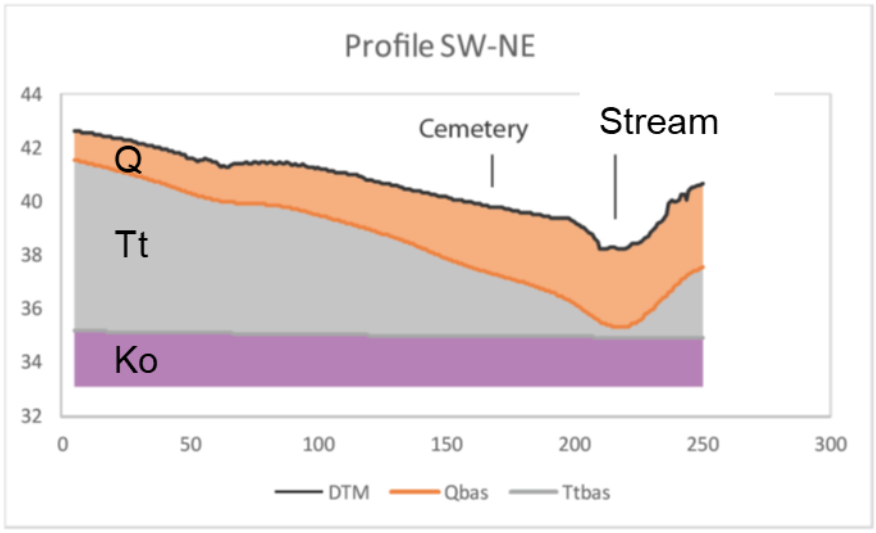

Figure 4-12. Geological cross-section profile of the Zillebeke site (Q= Quaternary, Tt= Tielt Formation, Ko= Kortrijk Formation). Position of the profile line is indicated in Figure 4-11; distance and elevation are displayed in meters.

4.3.3 Villers-Deux-Eglises site

The geology of the Villers-Deux-Eglises site is characterized by a thin cover of loamy slope deposits overlying weathered bedrock (schists) of the Famenne Formation (see Figure 4-13 and Figure 4-14). The steepness of the slope combined with the thin soil cover suggests that the groundwater observed is likely indicative of a perched groundwater table situated above the bedrock. This condition explains the limited inflow observed in the piezometers, particularly during dry summer months (cf. section 4.2.2).

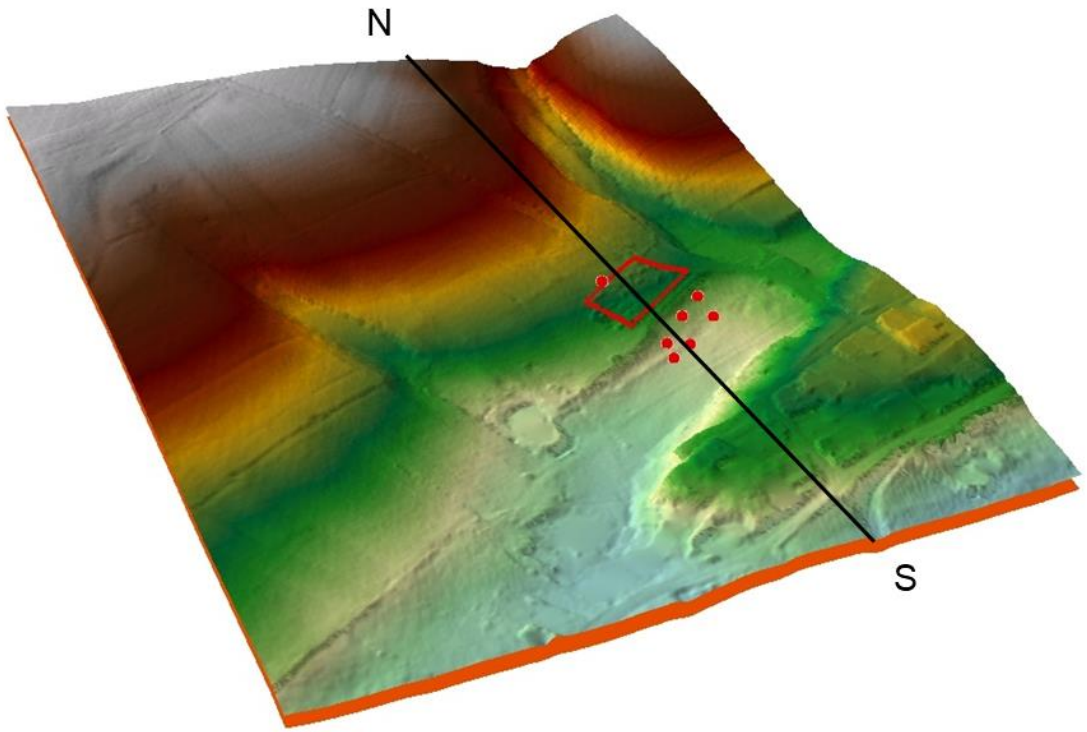

Figure 4-13. A three-dimensional visualisation of the surface and geological layers of the Villers-Deux-Eglises site.

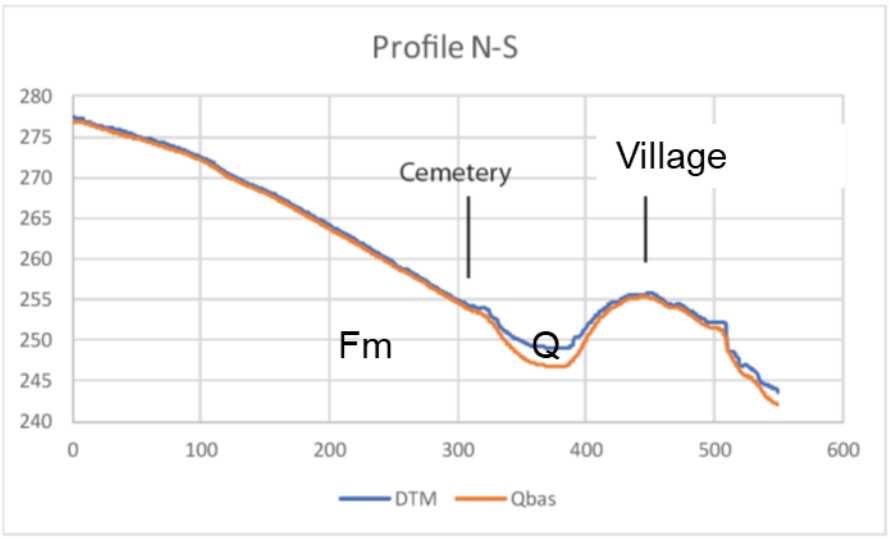

Figure 4-14. Geological cross-section profile of the Villers-Deux-Eglises site (Q= Quaternary, Fm= Famenne Formation). Position of the profile line is indicated in Figure 4-13); distance and elevation are displayed in meters.

4.4 Model building for contamination transport in an aquifer system

The four sections hereafter describe the steps followed in the model building for assessing the spatial-temporal evolution of the pollution from the Canivet landfill site:

- Evaluating the model described in section 3.5.2.3 (*i.e.,* model build from available data without calibration) using the available data (section 3.3.2).
- Sensitivity study
- Calibration
- Evaluation of increasing model complexity and simplification

4.4.1 Model results and evaluation

The **flow model** is evaluated with the residuals (difference between observation and calculated values) and related statistics as mean error, sum of squared errors etc. The comparison between calculated and observed values (Figure 4-15A) shows that the model reproduces the observed average spatial trends quite well, simulating low values of hydraulic head in the north and higher values towards the south, corresponding to the measured heads (Figure 4-15, Top). Diagnostic plots (Figure 4-15B-D) indicate that the residuals are scattered around a value of zero but with some bias with overestimation at the extraction wells (towards the north) and underestimation in the south (Figure 4-15B), errors are homoscedastic (Figure 4-15C, residual variance does not increase with observed head), and they are not normally distributed (Figure 4-15D, deviations at the tails). However, taken into account that the model was built from readily available information, in general, the flow model reproduces the observed hydrogeological features well given it objective to provide long-term saturated thicknesses and Darcy fluxes for the transport model.

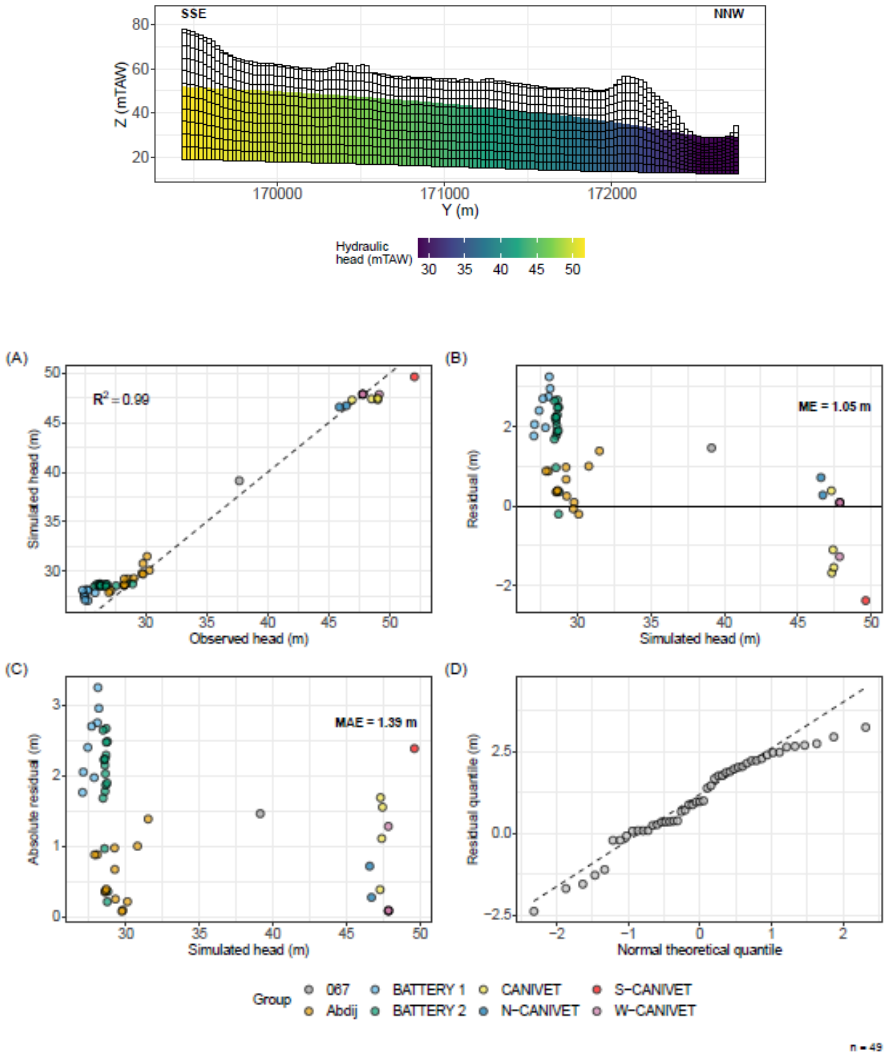

Figure 4-15 – (Top) Cross-section of the uncalibrated hydraulic head field at column 21 of the numerical grid, (Middle and bottom) Diagnostic plots for the flow model of the Canivet landfill site (A) Observed versus simulated heads, (B) residuals, (C) Absolute residuals, and (D) quantile plot (R^2 = coefficient of determination; ME = mean error; MAE = mean absolute error).

The **transport model** calculates the chloride concentration as a function of time and space between the period 1980 (year 0) to 2020. The contamination moves from the source in the landfill to the NNW (Figure 4-16). The shape of the plume and the concentrations levels only change marginally after 20 years. Comparison with observations is shown in Figure 4-17. Although general plume characteristics and concentration levels are reproduced by the model, detailed temporal and spatial variations are quite different. Note that this is not unexpected as the complex real system is simplified significantly in the conceptual model.

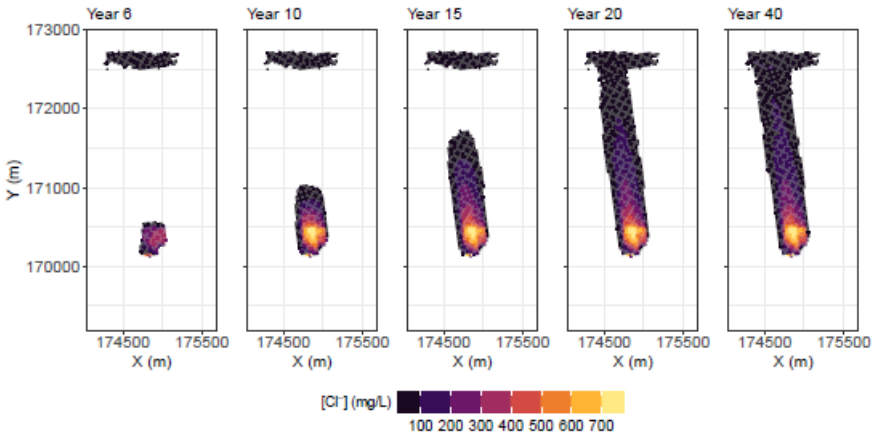

Figure 4-16 - Chloride concentrations at the water-table at selected times for the uncalibrated model. Cutoff value: 25 mg/L. Year 0 corresponds to 1980.

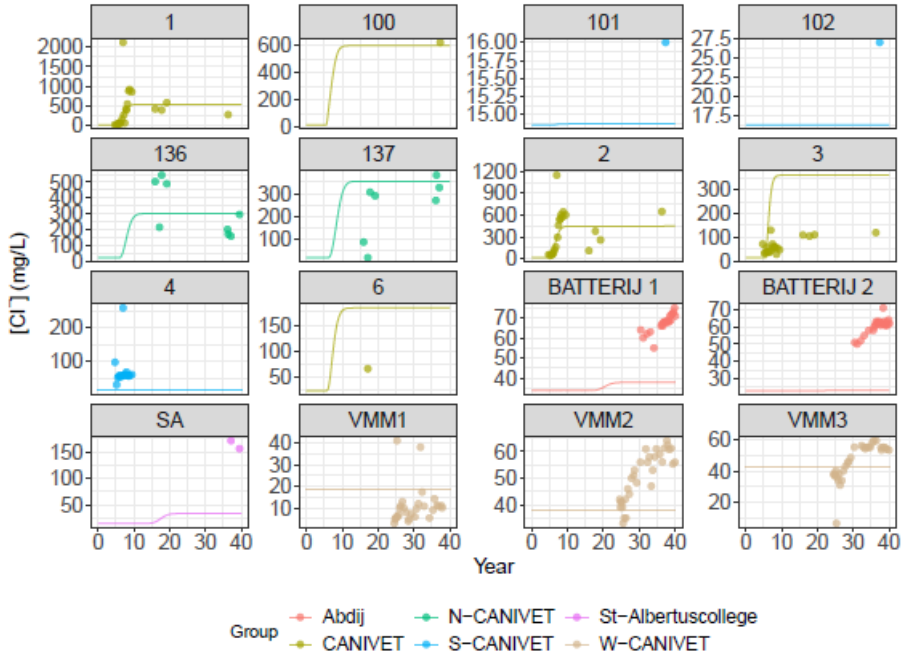

Figure 4-17 - Simulated breakthrough curves of chloride at the different piezometers. Observed values are plotted as points.

4.4.2 Sensitivity study

A sensitivity analysis was performed to assess the relative importance of parameters to certain relevant model output. Selected parameters and variables for the sensitivity analysis are:

- Parameters for which limited data was available (*e.g.*, horizontal hydraulic conductivity) but might have a large impact on the model outcome,
- Parameters for which no data was available, and values are based on expert knowledge (*e.g.,* longitudinal dispersivity) and thus their uncertainty is very large,
- Parameters without data and their value is arbitrarily set or estimated from interpretation of available data (*e.g.,* correction factor for recharge at landfill, start year of leaching).

Sensitivity of parameters may depend on the output variables that are selected. One convenient choice is the heads and concentrations measured in the piezometers; these variables are directly linked to measuring the performance of the model.

Local sensitivity measures are presented in Figure 4-18 in terms of composite scaled sensitivities (CSS). The exact meaning of this measure is beyond the scope of this report; the ranking is important with more sensitive parameters having higher CSS. The most sensitive parameters are the start of leaching from the landfill (after 1980) and the horizontal conductivity of the Brussel sands. These two parameters determine the breakthrough; the latter also influence the heads in the system. Together with the porosity (also a relative high sensitivity), these parameters are expected to have a large effect in an advective-dominated groundwater system. Note also that parameters related to concentrations, and then specifically close to the source, are also sensitive (porosity and the rechange concentration multiplier in landfill), whereas many parameters controlling the steady-state flow are less sensitive.

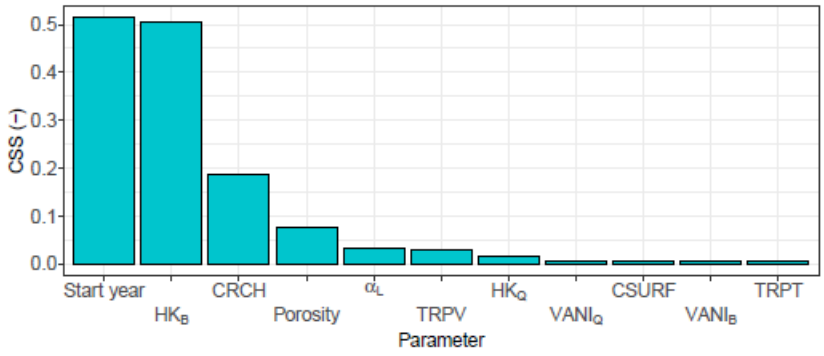

Figure 4-18 – Indication of sensitivity of parameters (measured by CSS) for heads and concentrations. Start year: year since 1980 to start leaching in landfill, HK_B: horizontal conductivity Brussel sands, CRCH: recharge concentration multiplier in landfill, a_L: longitudinal dispersivity, TRPV: ratio of vertical transverse dispersivity to longitudinal dispersivity; HK_Q: horizontal conductivity Quaternary deposits, $VANI_Q$: vertical anisotropy Quaternary deposits, CSURF: surface water concentration multiplier, $VANI_B$: vertical anisotropy of Brussels sands, TRPT: ratio of transverse transverse dispersivity to longitudinal dispersivity.

Beside output variables for model performance using state variables, other sets of output variables can be defined which are related to the migration and the extent of the contamination plume. As an example, sensitivities are calculated for (i) plume front measured by an 1.5 increase in concentration compared to the initial concentration (Figure 4-19, top) and (ii) arrival time measured by the earliest time of arrival of higher concentrations (1.5 increase) in a zone around the extraction wells (Figure 4-19, bottom). The horizontal hydraulic conductivity in the Brussels sands is now the most sensitive parameter, followed by the porosity and the starting year of leaching. Note also that hydraulic properties of the Quaternary deposits have higher sensitivity as it influences the plume front near the extraction wells. For arrival time (Figure 4-19, bottom), only three sensitive parameters are identified as these parameters strongly influence the advective properties of the system.

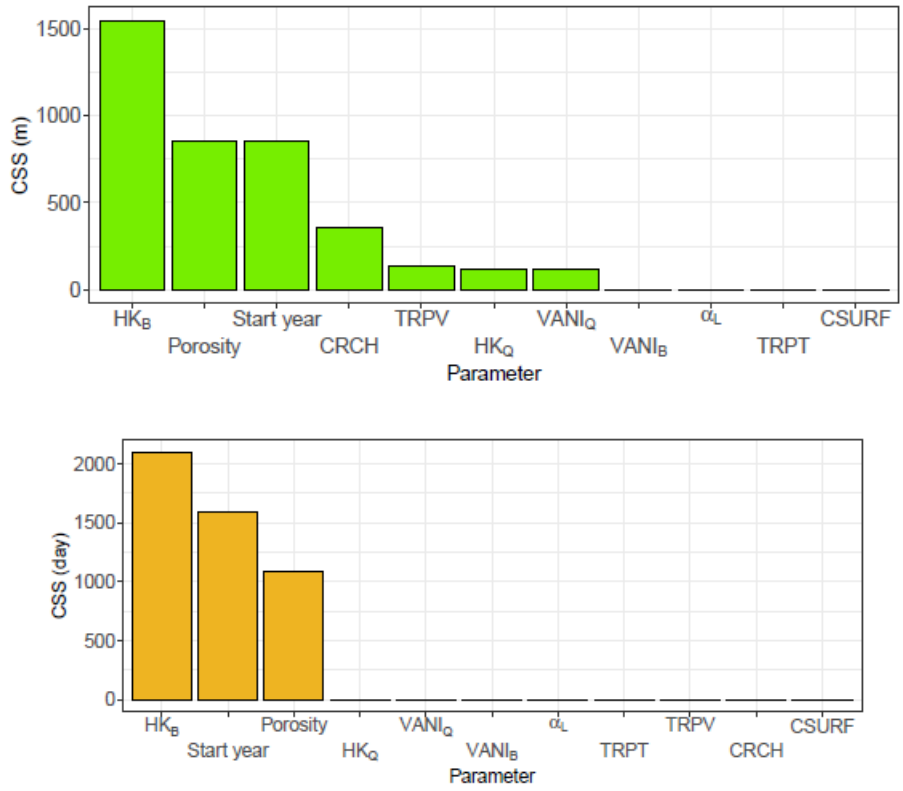

Figure 4-19 – Indication of sensitivity parameters (measured by CSS) for (Top) the plume front and (Bottom) arrival time. Parameter names are listed in the caption of Figure 4-18.

4.4.3 Calibration

When observations of state variables are available (Figure 4-17), model parameters can be adapted by minimizing the sum of squared errors between model predictions and observations; a process known as optimization or calibration. In this study, a global minimization algorithm called particle swarm optimization (PSO, Kennedy and Eberhart (1995), Zambrano-Bigiarini and Rojas (2013)) was used to minimize the weighted least-squared objective function. PSO is an evolutionary stochastic optimization method based on the behaviour of bird flocks, where candidate solutions (i.e. particles) are iteratively moved in the search space towards the optimum and gives a probability density function of the variables. Parameters that are optimized are those studied in the sensitivity analysis (section 4.4.2). Resulting probability functions are shown in Figure 4-20.

The parameters that were identified with a high sensitivity (previous section) exhibit a relative narrow distribution (HK_B, CRCH and start year). Other parameters are less well defined (e.g. those related to the Quaternary deposits) and/or their optimal value are close to their limits. Further analyses were done on local sensitivity at the optimal parameter set, comparison with observations, calculation of integrated variables (*e.g.*, different spatial moments), and residuals analysis. The local sensitivity at the optimal parameter set indicated a different set of sensitive parameters (beside conductivity of Brussel Sands, also conductivity of the Quaternary deposits as recharge multiplier become sensitive) indicating nonlinearity in the parameter sensitivities. Comparison with the observed breakthrough data and (unweighted) residual statistics were similar to those obtained with the uncalibrated model. Other targets (e.g. spatial moments) did change somewhat but could not be validated with observations. The calibrated model did not lead to a significant improved model, most probable by lacking observations at key locations or times (e.g. such as observations of chloride breakthroughs

along a well transect or more frequently sampled concentrations within the landfill at intermediate times). Available data for construction and parameterization of the model gave an acceptable model based on a comparison with available observations; for this example, calibration using the available observations did not result in an improved parameterization.

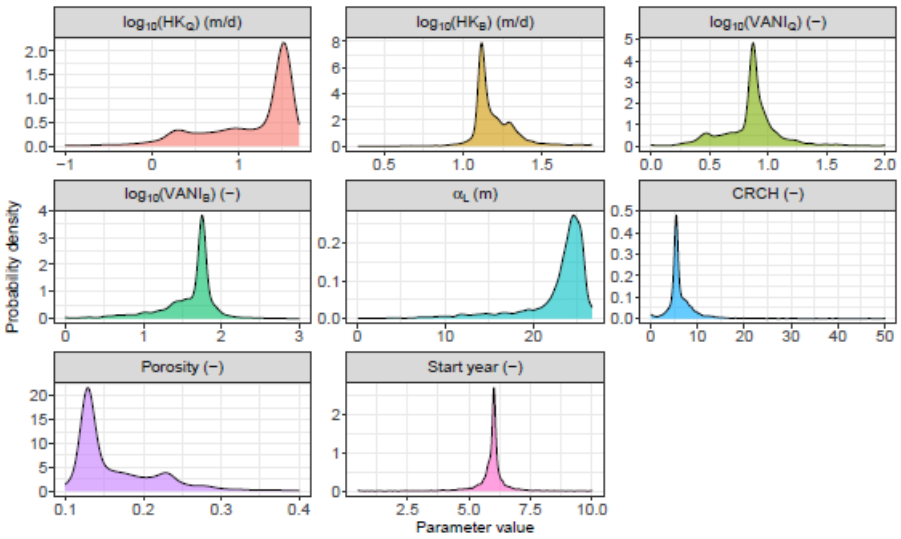

Figure 4-20 – Sampling probability densities of parameter values obtained during PSO

4.4.4 Simplifying and increasing complexity of model

4.4.4.1 Uniform recharge

The flow model used a spatially variable ground water recharge for which estimates were available for Flanders in an open database (Zomlot et al. 2015). When this information is not available, an estimate of a spatially averaged value is an alternative. The arithmetic mean in the modal domain is 190.1 mm/y which is mostly lower in the zone of the Canivet landfill (Figure 4-21, Top Left). For the piezometer locations, the effect of the simulated hydraulic heads is systematic as the uniform recharge results in lower heads at all locations (Figure 4-21, Top Right) – this is a direct consequence of slightly smaller total recharge in the domain (due to averaging and neglecting recharge and constant head nodes). However, the difference is smaller than 10 cm which is lower than the measurement errors. Overall, the flow model using uniform recharge behaved almost identical to the model with the spatially variable recharge. Also, the concentrations are lower when simulated with a uniform recharge. This is a direct consequence of the lower recharge at the landfill site in case of the uniform recharge which reduces the mass load into the system significantly. Further from the landfill (contamination source), the differences are much smaller. It is expected that for long-term steady-state flow problems, the overall effect might be small as the net influx in the system remains the same. For issues related to transient conditions or depending on local condition (*e.g.,* point source for contamination as the Canivet landfill site), the effect on some variables can be large.

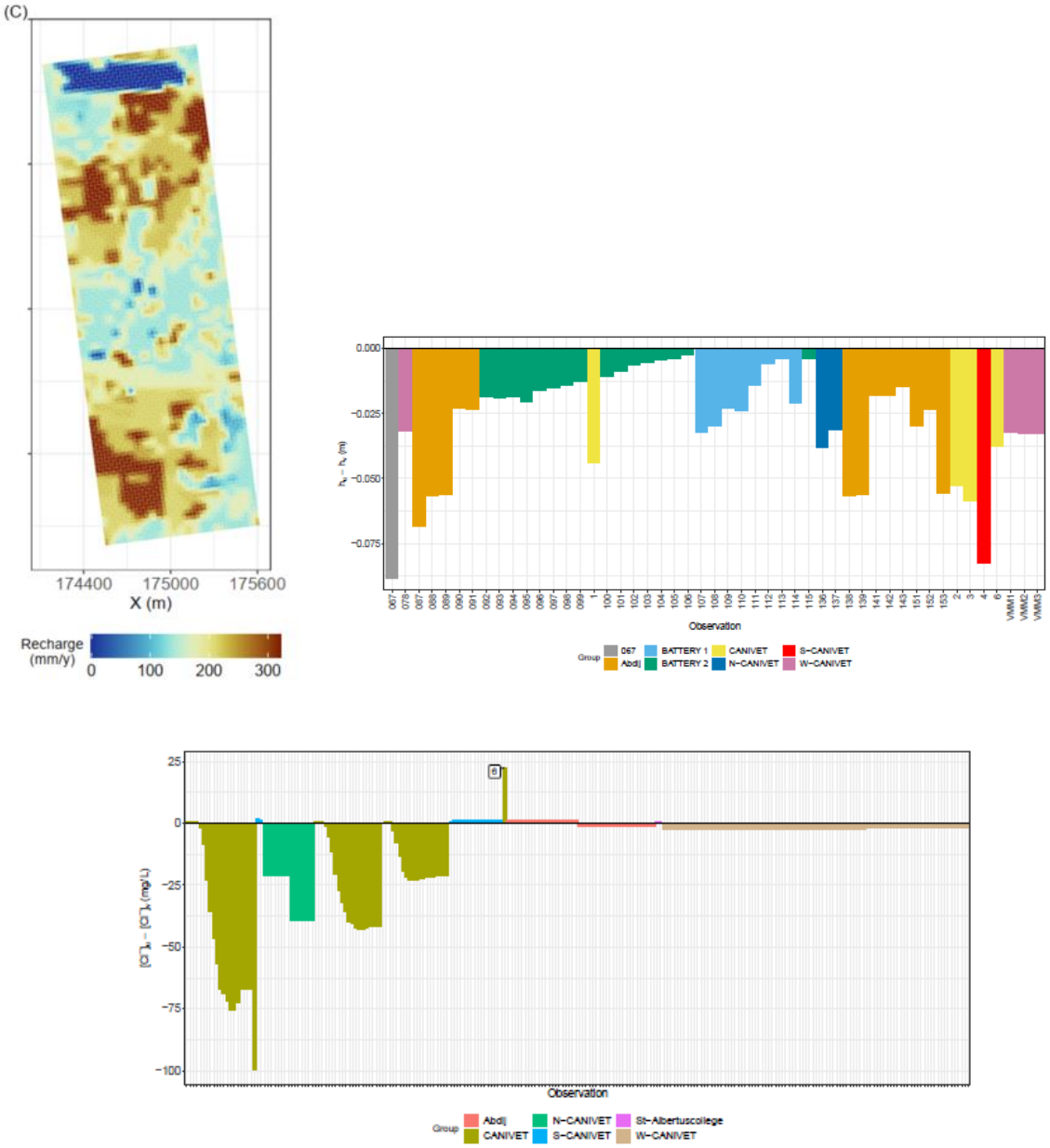

Figure 4-21 – Analysis of effect of uniform recharge. (Top Left) Distribution of spatially varying recharge, (Top Right) Difference in simulated hydraulic heads using the uncalibrated flow model with uniform recharge (h_u) and the model with spatially variable recharge (h_v), estimated at the locations of groundwater, (Bottom) Difference in simulated chloride concentrations using the uncalibrated flow model with uniform recharge ($[Cl^-]_u$) and the model with spatially-variable recharge ($[Cl^-]_v$), estimated at the locations and times of chloride concentration observations. X axis labels are omitted for visualization purposes.

4.4.4.2 Heterogeneity of hydraulic conductivity

Given the importance of spatial variability of hydraulic conductivity on field-scale solute transport (Rubin 2003), the high sensitivity of the hydraulic conductivity of the Brussels sands (section 4.4.2), and the observed variability of the hydraulic conductivity of the Brussels sands (Huysmans et al. 2014; Huysmans and Dassargues 2012; Possemiers et al. 2012; Huysmans and Dassargues 2009), the model complexity is increased by accounting for a heterogeneous hydraulic conductivity field in order to evaluate its effect on different aspects of solute transport in the aquifer.

The basis for a stochastic spatial data analysis is the variogram (Cressie 1993) which is available for the hydraulic conductivity of the Brussels sands from (based on 72 slug tests performed over the entire extent of the Brussels Formation, Figure 4-22, (Peeters 2010)). Random fields of the hydraulic conductivity were constructed using unconditional and conditional sequential Gaussian simulation (Pebesma 2004) where for the latter measured values obtained by pumping tests previously conducted at the wellfield extraction site are used. For each set, 100 fields were generated as input to flow and transport simulations.

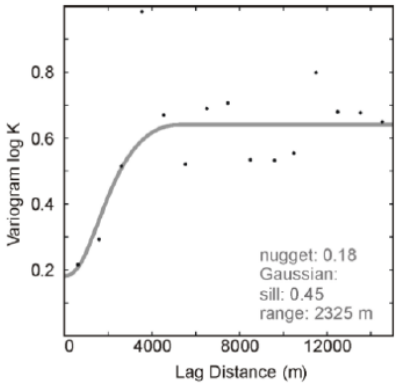

Figure 4-22 – Experimental and theoretical variogram of the hydraulic conductivity based on 72 slug tests performed in the Brussels sands (Peeters 2010)

The probability of presence of the contamination is captured the maps shown in Figure 4-23. It is very likely that contamination will be present near the Canivet landfill site and at the extraction wells. The potentially contaminated area is in a narrow band between the landfill and the extraction wells and slightly wider for the conditional fields. As above for the sensitivity analysis, arrival times at the extraction wells can be a model result of interest. Histograms for the unconditional and conditional realizations are shown in Figure 4-24. The effect of considering a spatially variable hydraulic conductivity in the Brussels sands has a large effect on the arrival time. Most of the values for the heterogeneous fields are lower than the estimated arrival time for the homogeneous model. Flow and transport in spatially heterogeneous field of hydraulic conductivity a typically concentrated in some high conductive channels in the domain which acts as preferential paths for the migration of solutes. Heterogeneous fields have only a minor impact on general features such as the main direction of flow and order of concentration levels are less affected. However, specific features might be influenced such as variations in plume geometry and concentration distributions. Consequently, some integrated variable such as the spatial moments can be influenced as well. As such, the effect of including heterogeneity in the hydraulic conductivity field for this kind of advection-dominated system is apparent in certain outcome variables and features, and depending on the selected model target, might become crucial. Conditioning the heterogeneity on measurements can become important locally and results in more narrow distributions of variables. If the measurements are reliable, this might result in reduced uncertainty in model outcomes.

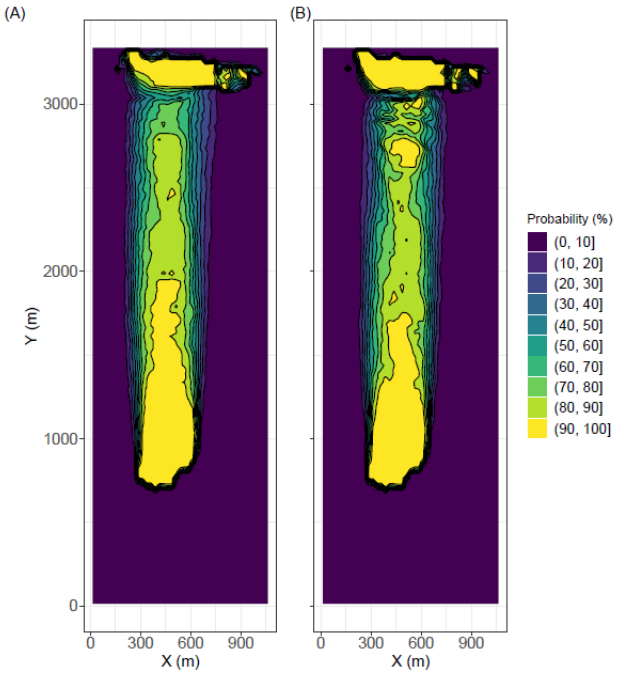

Figure 4-23 – Spatial probability maps of presence of contamination from the Canivet landfill after 40 years unconditional (A) and conditional (B) fields of the hydraulic conductivity of the Brussels sands. Local model coordinates are used instead of real-world projected coordinates for visualization purposes.

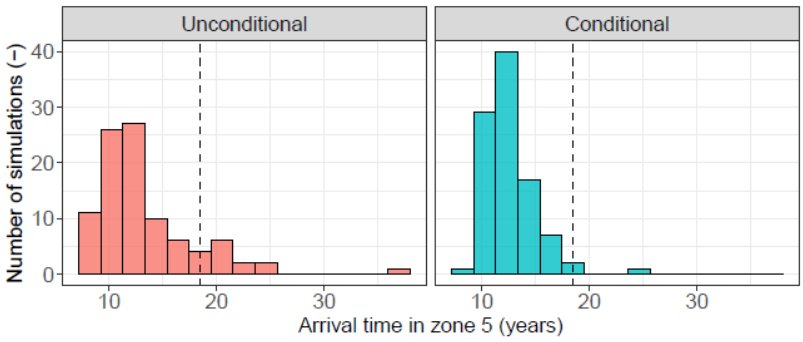

Figure 4-24 – Time of first arrival at the extraction wells using 100 unconditionally and 100 conditionally generated hydraulic conductivity fields (Brussel sands). The arrival time of the model using the homogeneous field is shown as a vertical dashed line.

4.4.4.3 Source term

The sensitivity analysis in section 4.4.2 revealed that source term parameters (timing, magnitude, geometry-location) are quite sensitive. Unfortunately, information on the source term is very limited and thus uncertainty large. Several complexities were added to the model to investigate the different aspects:

- Leaching time and magnitude – reproducing possible randomness of leachate concentrations entering the groundwater system by a Brownian motion signal, and
- Geometry and location of source term – by defining different scenarios for the source term.

Starting at the assumed time of leaching (5.5 y) and the best guess of initial concentration, 1000 Brownian motion signals were produced with a time step of 14d of a period of 40 y. To constrain the signals to plausible values, a set of four selection criteria was defined resulting in 73 signals (Figure

4-25). Negative signals were set to a zero concentration. Figure 4-26 shows the contamination plume at different times for two scenarios. These show the large influence of the source signal magnitude and timing on the resulting simulated plume. However, the advection-dominated system responds quickly to changes in leachate concentrations. Overall, source term timing and magnitude does not affect the geometry of the plume that much, which is controlled more by the boundary conditions and flow regime.

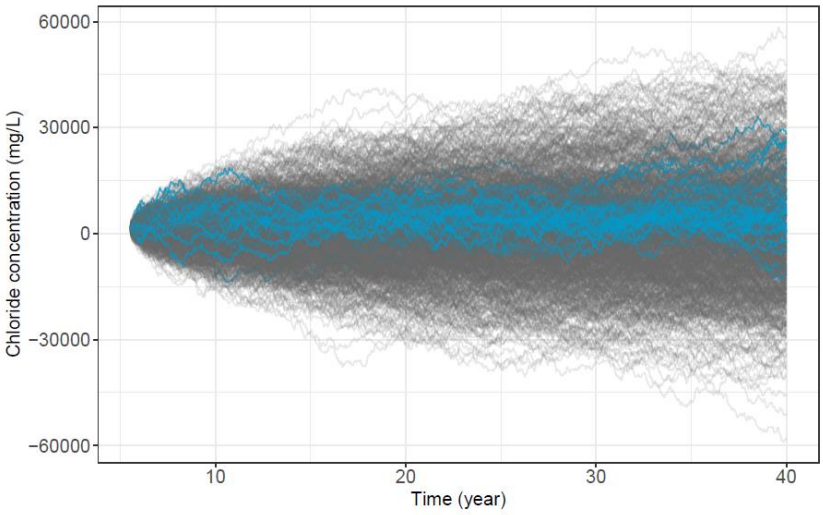

Figure 4-25 – One thousand Brownian motion signals generated for the landfill source term using a discretization length of 14 days. The 73 accepted signals are shown in blue. Note that the signals originate at year 5.5 corresponding to the start of leaching.

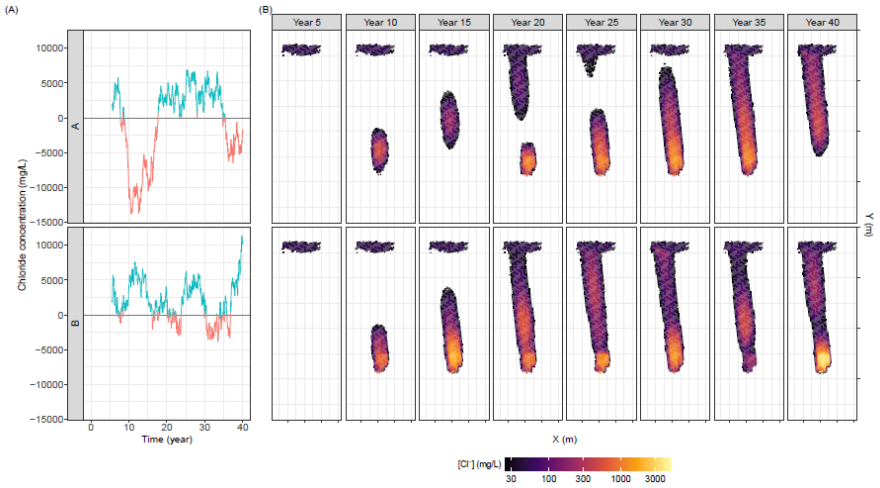

Figure 4-26 - Two Brownian motion signals for the source term concentrations (A) and their resulting chloride concentrations at the water-table for selected times (B). Negative values for the source signals were set to zero as input for the transport model. Note the logarithmic scale for the water-table concentrations and cutoff value: 25 mg/L

Seven scenarios were defined to analyse the impact of uncertainty on the contamination plume by defining different distributions of contaminant recharge to the ground water within the landfill site (Figure 4-27, Top). Figure 4-27 (bottom) shows the relative concentrations calculated as plume concentration divided by maximum concentration for each scenario, at the water-table after 40 years using the seven source term geometry scenarios. The source term geometry primarily affects plume geometry near the landfill in this advection-dominated system and is of less importance

downgradient. However, there is also an effect of the exact location of a contamination in a landfill on the overall placement and geometry as is clear from scenario 1 and 2.

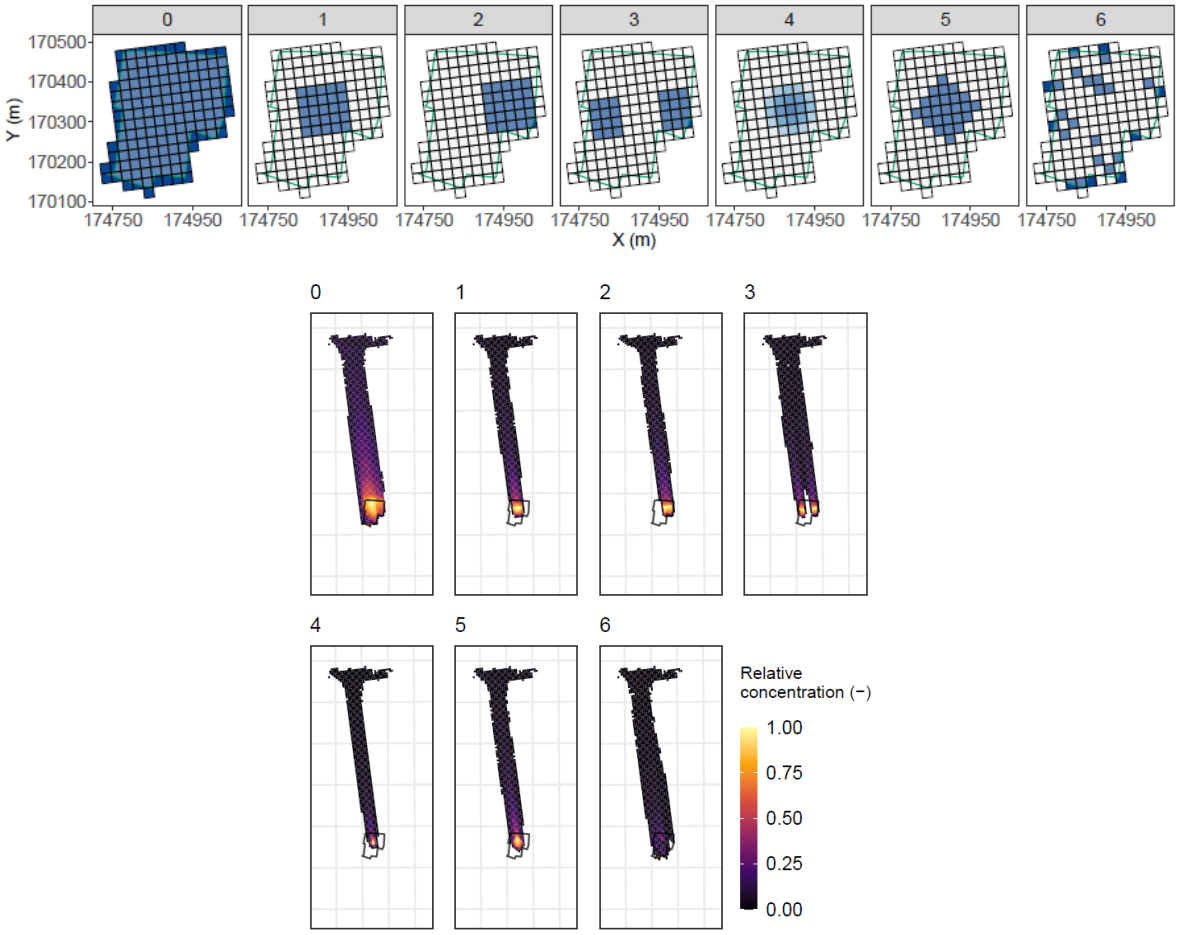

Figure 4-27 – (Top) Source term geometry scenarios highlighting the cells within the landfill cadastre (shown as a coloured line) receiving polluted recharge, (Bottom) Relative water-table concentrations after 40 years under seven different source term geometry scenarios. The landfill cadastre outline is shown in black. Axis labels are omitted for visualization purposes.

4.4.4.4 Redox processes

When organics are leached from a contaminated place, they will be subject to oxidation reactions by a series of different electron-acceptors. Measured redox potentials in the VMM piezometers in the area indicate that in the pristine aquifer, oxygen is reduced and that iron and sulphate species not. Nitrate and pyrolusite reactions are possible in the range of measured redox potentials.

The model to simulate the oxidation of organics in the subsurface follows in essence the description in section 3.4.1 – the redox reactions are set up for an organic represented by the formula CH_2O. The rate equations follow the general formalism of Eq. (13) with a first-order dependence of the electron donor and neglecting the factors *B*, $\left(\frac{K_B}{K_B + B}\right)^{\alpha}$, and *T*. The water flow and solute transport models were simplified to a two-dimensional model mainly for reasons of computational speed – in this advection dominated system, a NNW-SSE transect through the landfill towards the extraction wells was taken. Initial conditions of electron acceptors were obtained from available studies with site-specific data; model parameters from the open scientific literature (and are thus not site-specific).

However, the model was calibrated by optimizing half-saturation, rate constants, and inhibition constants for different electron acceptors (O_2, NO_3^-, MnO2, and FeOOH; inhibition constant was not calibrated for the latter) and the concentrations of DOC and MnO_2. A global Latin Hypercube – One-at-the Time (LH-OAT) sensitivity analysis identifies concentration of DOC and MnO_2, the decay rates of FeOOH and MnO_2 as the most sensitive parameters, followed by the half saturation and inhibition constant of MnO_2 and the rate of O_2 (Figure 4-28). The sensitivity coefficients are mainly linked to the importance of the FeOOH electron acceptor in the system. Parameters related to O_2 and NO_3^- are insensitive as they were already consumed in the pristine system.

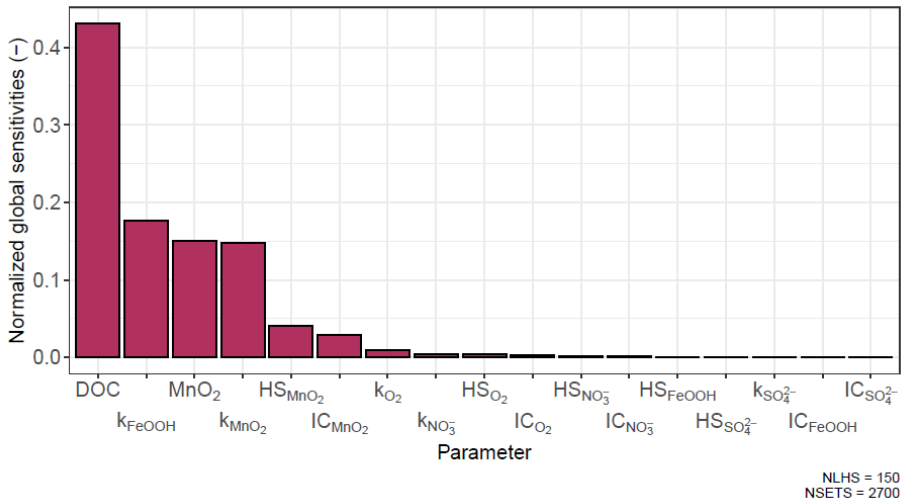

Figure 4-28 – Global parameter sensitivities for the 2D reactive transport model (shown as average sensitivities normalized by their sum) obtained using LH-OAT analysis using 150 Latin hypercube samples and a perturbation factor of 1 % resulting in 2700 parameter sets (HS represents half saturation, IC the inhibition constant, and k the rate constant).

In general, there was not sufficient data to constrain the model parameters by calibration. The available data is sufficient if targets are related to "orders-of-magnitude" of the concentration (*e.g.,* Figure 4-29 for DOC and Mn), but insufficient for a detailed picture of the oxidation-reduction processes in the groundwater system – for that, high quality breakthrough curves for all redox sensitive species across several wells along a flow path are needed. If one suffices with the target of order of magnitudes for the concentrations or basic TEA sequencing, the model shows the spatial distribution and evolution of the electron donor and acceptors (Figure 4-30), and the sequence of redox reactions: a split sequence where oxygen and nitrate are degraded concurrently followed by the simultaneous reductive dissolution of manganese- and iron-oxides (Figure 4-31, top). It seems that a first-order dependence on the electron-acceptors is sufficient to describe the available data. Oxygen is the largest contributor to the degradation of DOC whereas goethite provides the largest buffer in the system as the constant injection of DOC over almost 35 years has not yet resulted in the depletion of iron-oxides in the aquifer system (Figure 4-31, bottom).

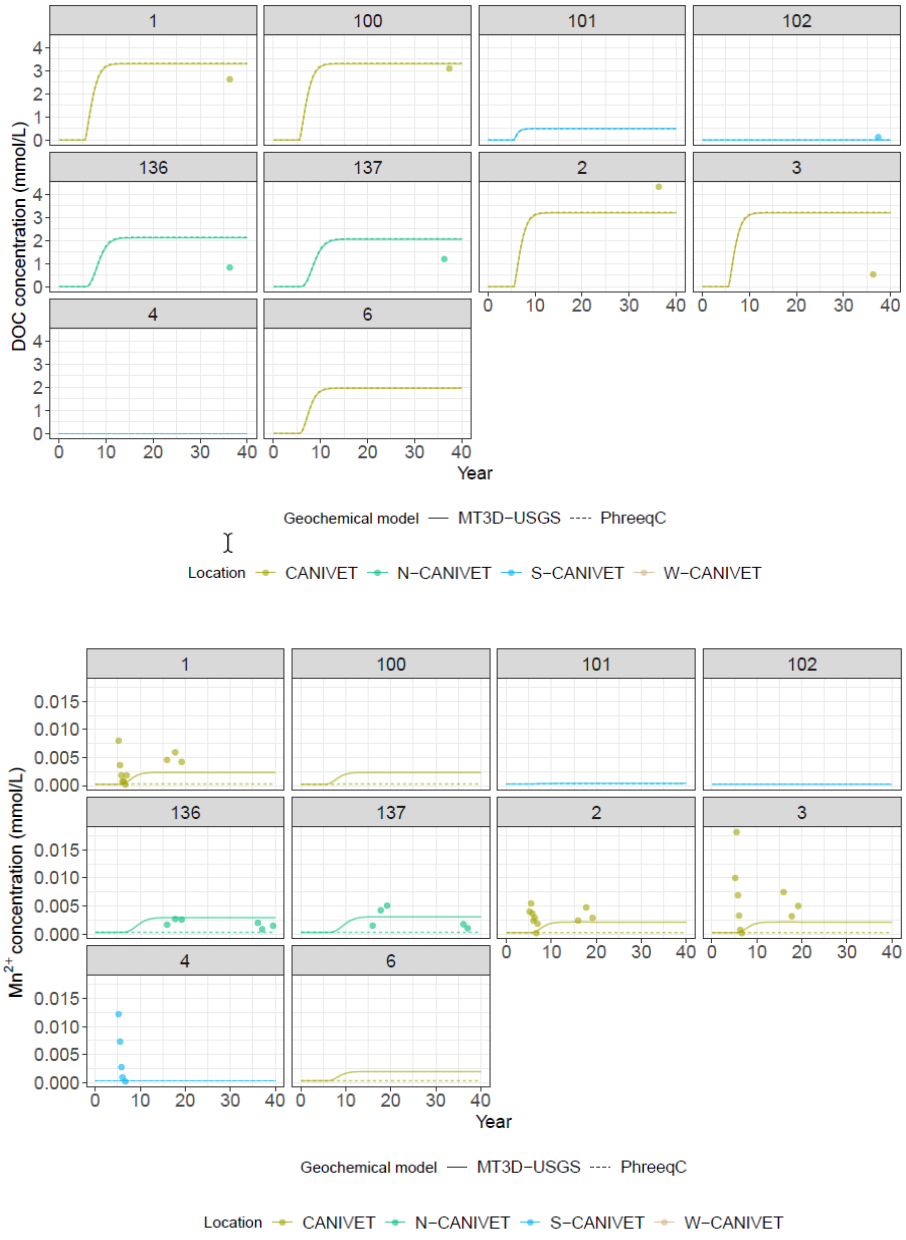

Figure 4-29 – Simulated (line) and observed (point) aqueous DOC (top) and $Mn2+$ (bottom)concentrations at the observation wells using the 2D reactive transport model with the MT3D (neglect Phreeqc calculations).

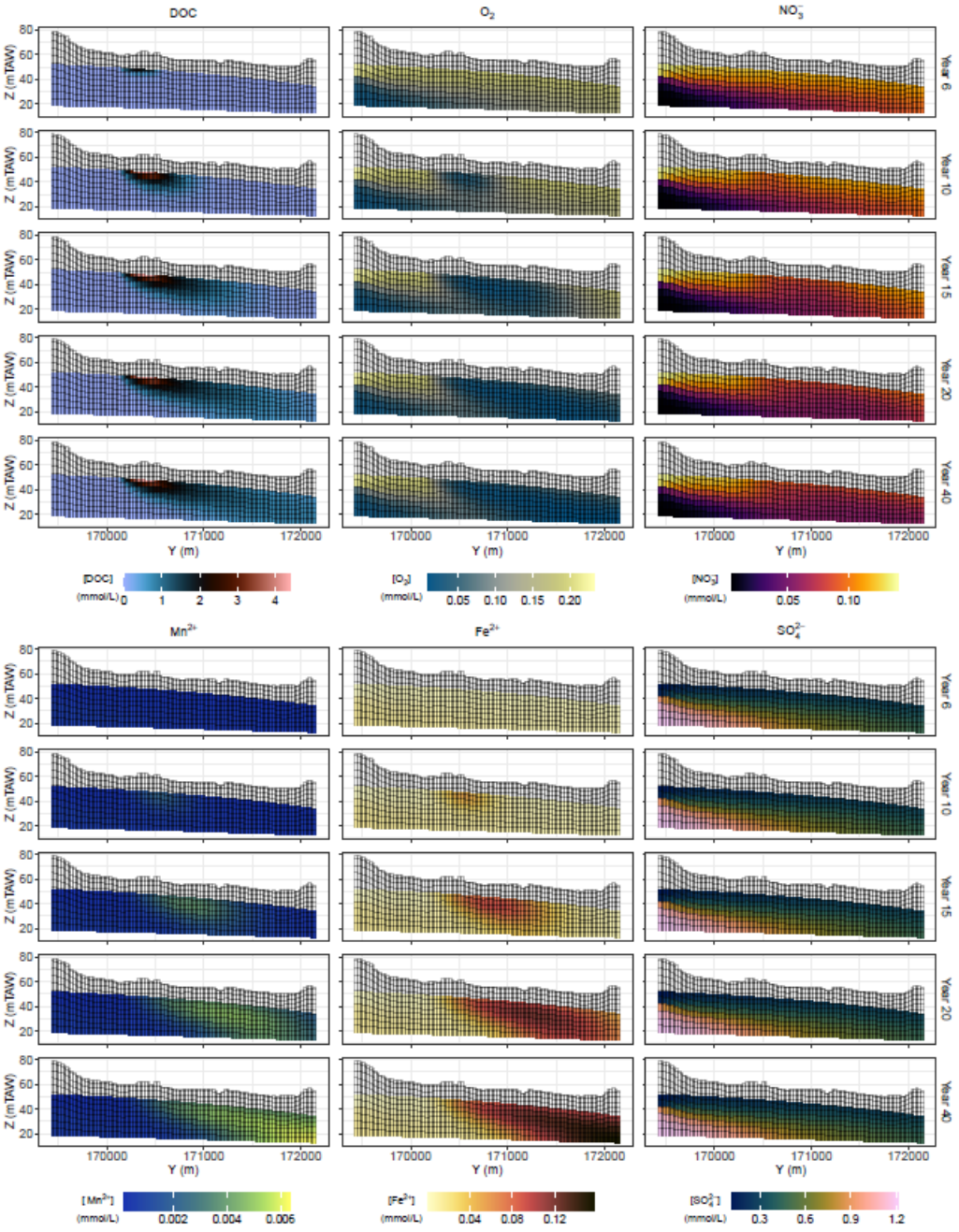

Figure 4-30 – Concentrations of redox sensitive species at selected times simulated by the 2D reactive transport model using the geochemical capabilities of MT3D-USGS.

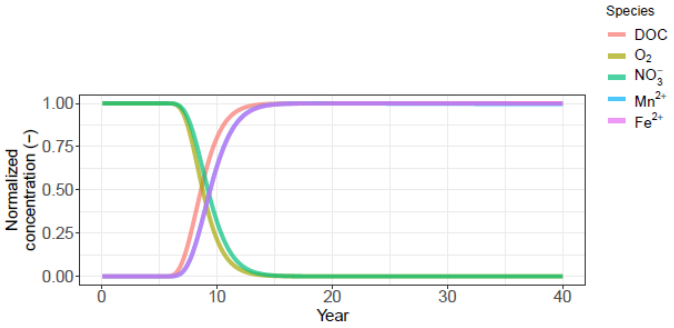

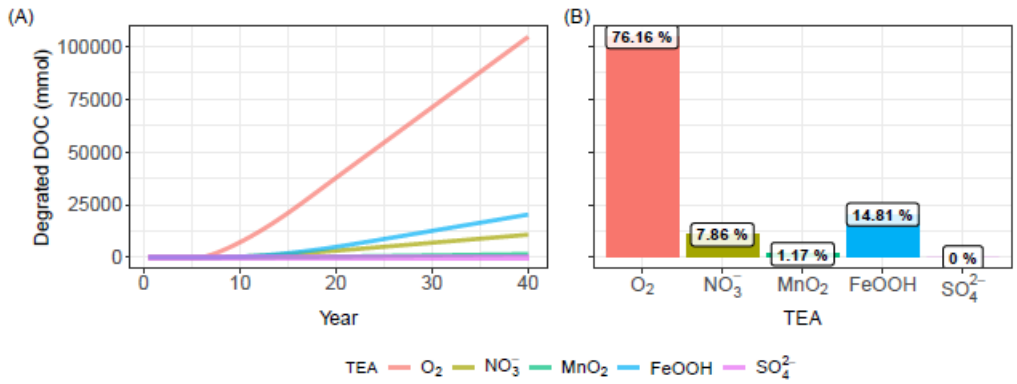

Figure 4-31 – (Top) Normalized concentrations at a selected location downgradient of the landfill in the middle of the aquifer, and (Bottom) Contribution of each TEA to the degradation of DOC (A) as a time series and (B) after 40 years using the calibrated 2D reactive transport model and the geochemical capabilities of MT3D-USGS.

4.5 Coupled reactive transport models

4.5.1 Benchmarks to verify MTHP

4.5.1.1 Mineral and inorganic redox equilibria in an anaerobic carbonate aquifer (pht3D)

A first benchmark consists of example 3 from the pht3D manual that was based on the study by Walter et al. (1994). The benchmark involves mineral and inorganic redox equilibria in an anaerobic carbonate aquifer that is leached with acidic mine tailing water in a one-dimensional transport set-up. An aquifer initially at almost neutral pH conditions is leached with a solution at pH 3 with different concentration in different elements (C, S, Fe, Mn, Ca, Mg, Na, K, Cl, Al, Si). The aquifer consists of a number of minerals (calcite, siderite, gibbsite, $Fe(OH)_3$, gypsum, SiO_2). Some geochemical information obtained with MTHP is compared with output from pht3D as shown in Figure 4-32. We observed an excellent correspondence between the two codes. A clear sequence of mineral buffering reactions is simulated: first calcite dissolution with precipitation of gypsum and siderite; followed by siderite dissolution when calcite is exhausted, and gibbsite dissolution when also siderite is exhausted. These three buffering steps lead to different levels in pH and pe.

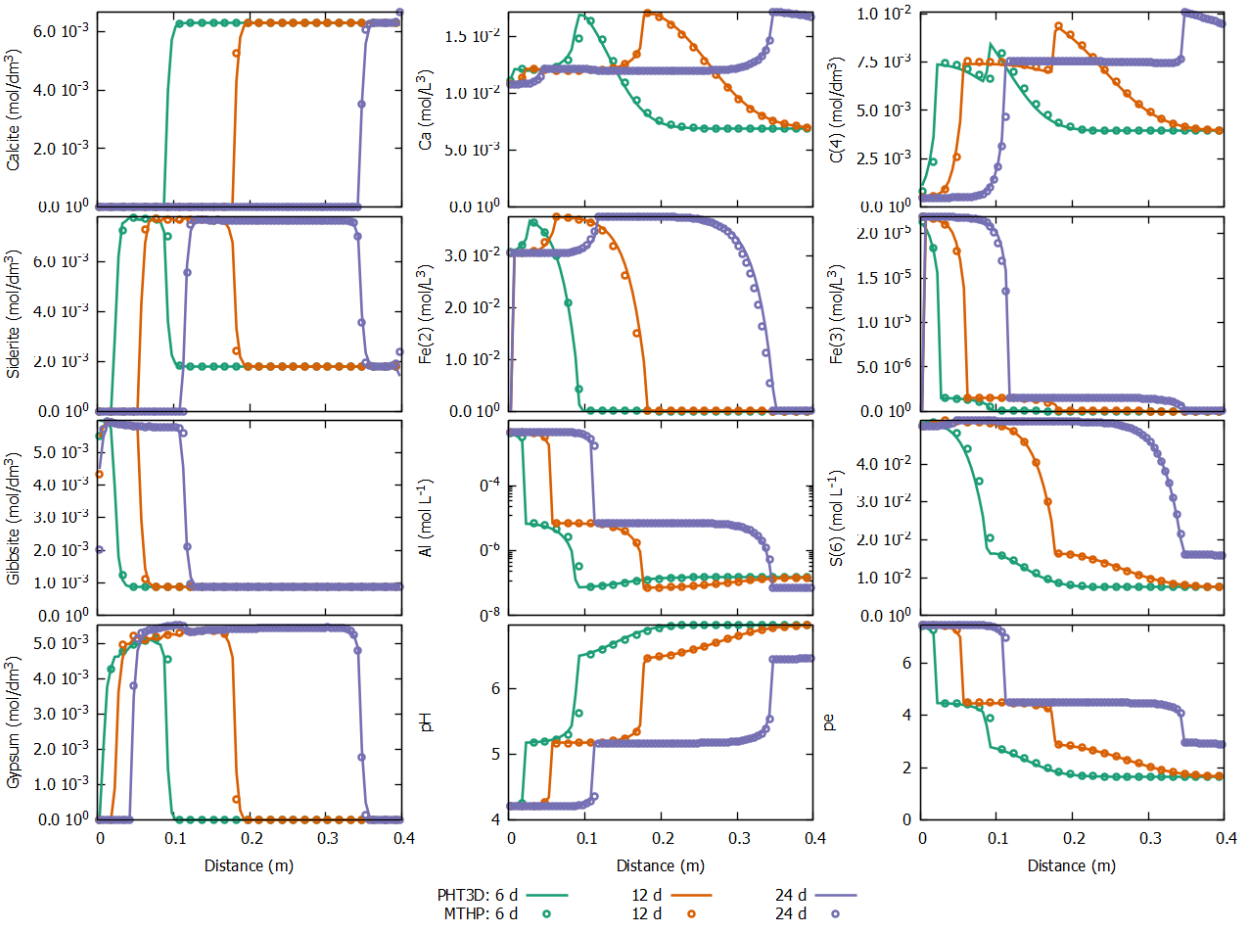

Figure 4-32 – Profiles of selected aqueous components, minerals, pH and pe at three time (6, 12 and 24 days) obtained with PHT3D (lines) and MTHP (dots)

4.5.1.2 Transport of an anionic tenside (pht3D)

Figure 4-33 shows an example initially presented by Sardin, Krebs, and Schweich (1986), featuring the transport and reactions of an anionic tenside (alkylbenzenesulfonates of sodium). The process of tenside injection is used for enhanced oil recovery in (i) oilfields and (ii) at oil-product contaminated sites. Sardin, Krebs, and Schweich (1986) carried out a range of batch and column experiments and analysed the results using a one-dimensional reactive multi-species transport model. The model uses multi-component transport with equilibrium dissolution/precipitation and cation exchange. We can see in Figure 4-33 that observations are quite well reproduced, but more importantly for us the MTHP simulation is almost identical to the PHT3D output.

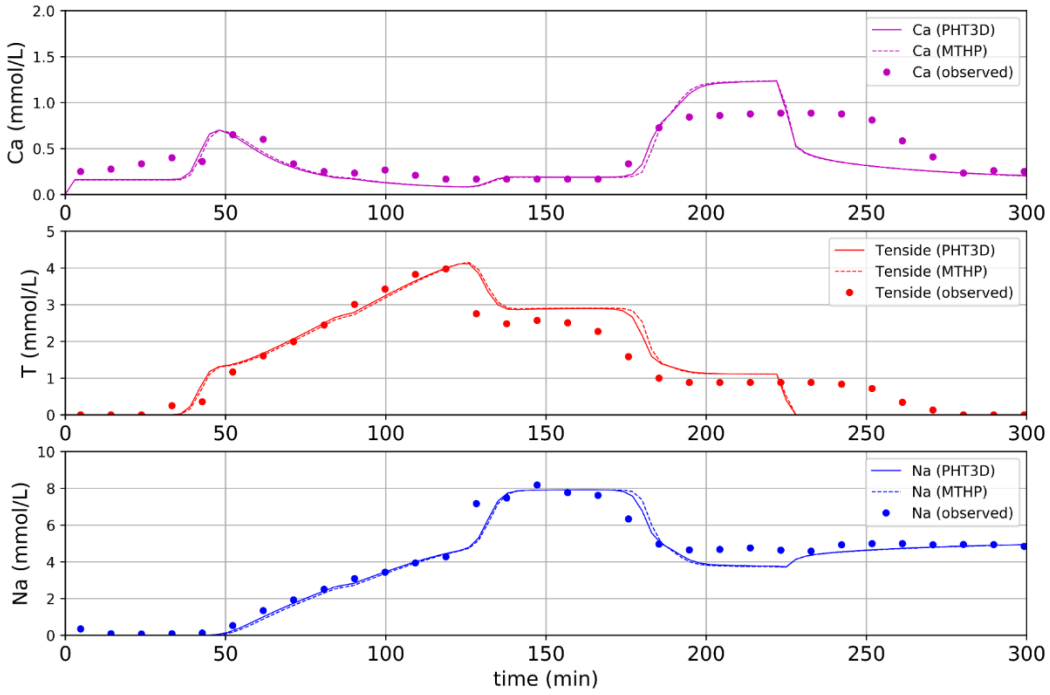

Figure 4-33 – Benchmarking MTHP against example 06 from the PHT3D manual: Transport and reactions of an anionic tenside through a column. The geochemical reactions included in this example include sorption (ion exchange), aqueous complexation reactions and dissolution / precipitation of calcium tenside (CaT2) (from Prommer and Post (2010)).

4.5.1.3 Kinetic sequential degradation of TCE (pht3D)

Figure 4-34 shows a two-dimensional example of the kinetic, sequential degradation of PCE (perchloroethylene) to TCE (trichloroethylene), then to DCE (dichloroethylene), then to VC (vinyl chloride), and finally of VC to ethylene. The simulations assume a steady flow field, with hydraulic heads of 100 m and 99 m at the left and right sides of the domain (10 m thick aquifer, n = 0.3 and K = 50 m d−1), respectively. A well with a small flux of 2 m d−1 is positioned 155 m downstream of the influent boundary. It is used to inject a specific PCE mass per time in order to simulate in a rather simplistic way the contaminant source (details in Prommer and Post (2010)). Here again, the match between the MTHP and PHT3D simulations is perfect, which allows us to conclude that the MT3D – PHREEQC coupling has been correctly implemented in our code.

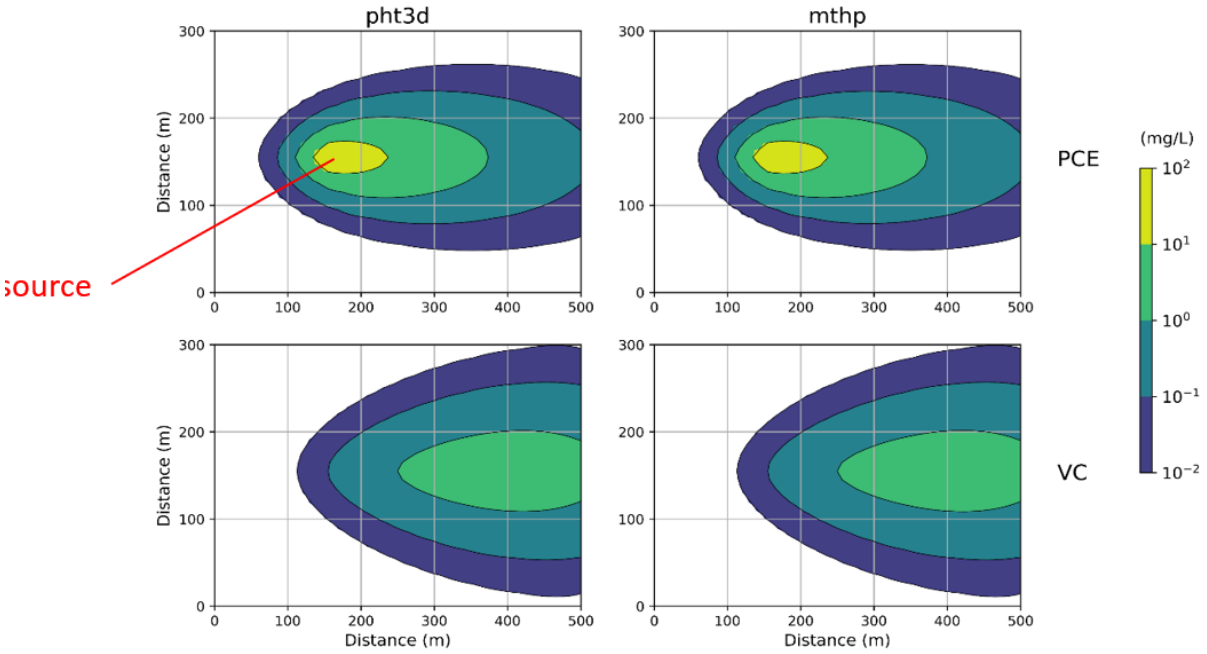

Figure 4-34 – Benchmarking MTHP (right) against example 08 from the PHT3D (left) manual: Kinetic, sequential degradation of chlorinated hydrocarbons (PCE at the top and vinyl chloride at the bottom). Concentrations after 300 days (from Prommer and Post (2010)).

4.5.1.4 Cation exchange reactions (HPx in HYDRUS-2D)

An aquifer containing initially a NaBr solution is injected with a $CaCl_2$ solution (limited injection region at the upstream boundary) including also other major cations that are subject to cation exchange reactions within the aquifer. Spatial contours and time series at three observation points are shown in, respectively, Figure 4-35 and Figure 4-36. The benchmark showed only a small discrepancy between MTHP and HPx which is probably the result of a different dispersion caused by a different transport solver and the coarser grid resolution of MTHP.

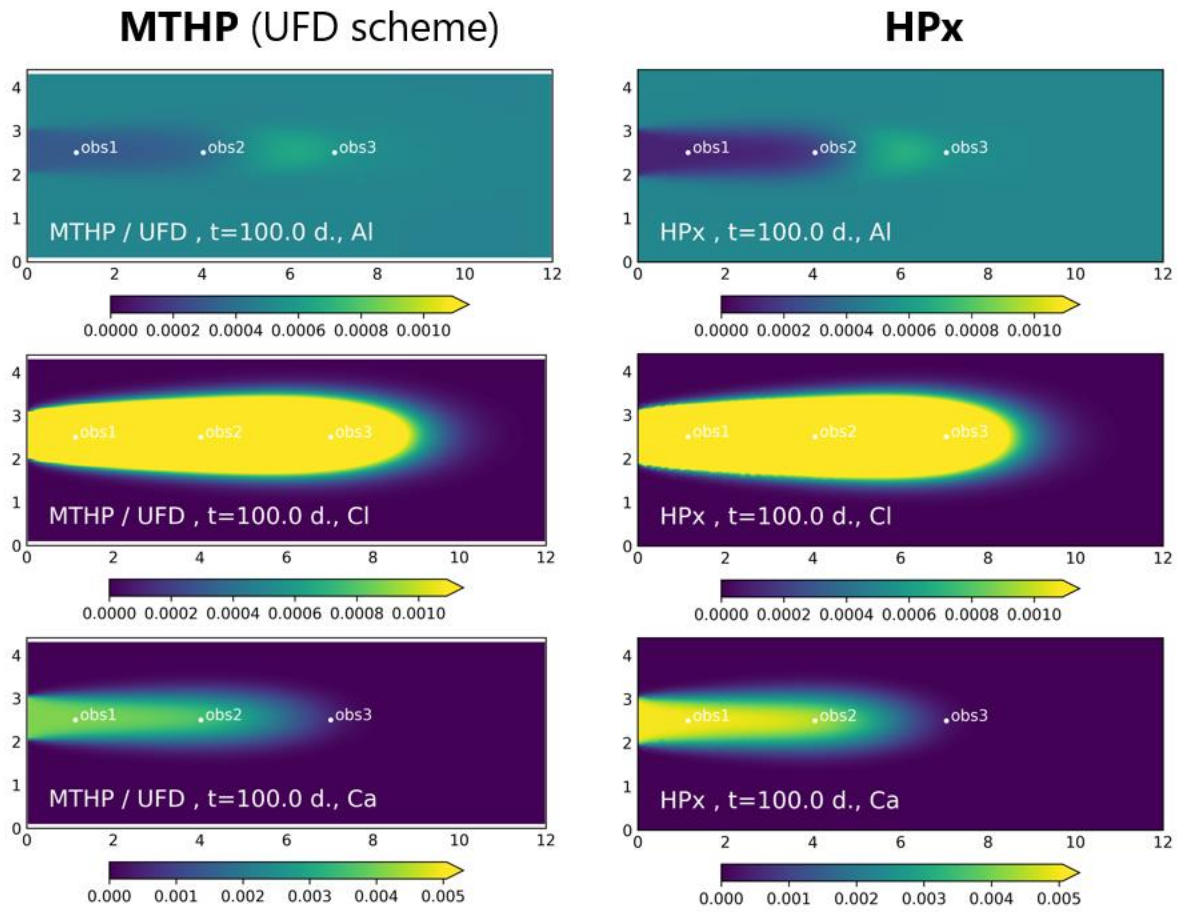

Figure 4-35 - Al, Cl and Ca concentration contours (mol/kgw) after 100 days obtained with MTHP (left) and HPx (with HYDRUS-2 as the transport solver).

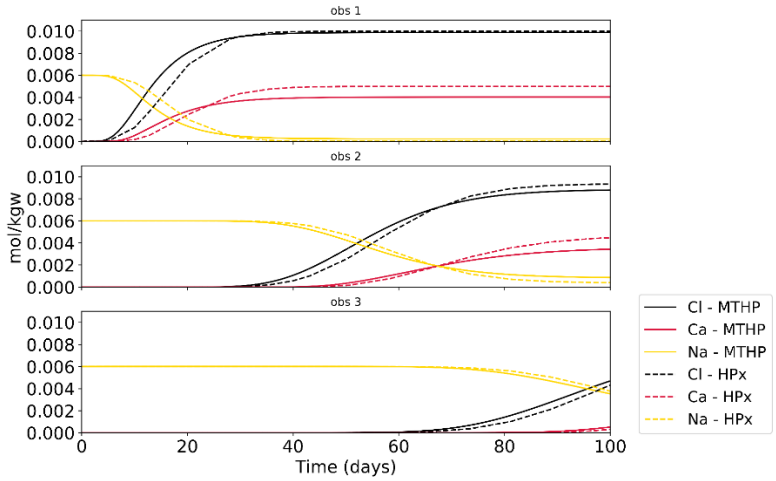

Figure 4-36 - Cl, Ca and Na concentrations over time at three observation points, MTHP vs. HPx. (with HYDRUS-2 as the transport solver).

4.5.2 Building reactive models from scientific knowledge

In this section, example calculations are given for geochemical and reactive transport simulations including the models for microbiological-driven kinetically-controlled redox degradation of organics

(section 3.4.1) and sorption of metals on organic material/humic acid (section 3.4.2). The examples are for illustrative purposes only but could serve as a starting point for further model development or applications.

4.5.2.1 Kinetic model for organic species degradation

A simplified batch-type of example calculation is shown in Figure 4-37. In this calculation, a zero-order dependence assumed on the electron donor (the DOM) is assumed. Also, biomass is not considered as a limited factor and is thus neglected in the example. Thus, Eq. (13) is simplified to (by setting the options and parameters in the input form shown in Figure 3-16):

$$R = Q_{\max} \frac{[E_A]}{K_A + [E_A]} I \tag{24}$$

The partial pressure of CO_2 is buffered at a constant value of $10^{-3.5}$ atm. All electron acceptors described in section 3.4.1 are present in the system (O, N, and S as aqueous components, Mn and Fe as solid phases). Parameters are taken from literature but should be adapted for specific conditions. The top figure shows the cumulative degradation of CH_2O. The amount of a particular electron acceptor is determined by its initial amount in the system. The maximum rates (shown in the bottom figure) are defined by the different parameters (Q_{max}, K_A, and the inhibition term I). When $K_{I;j}$ in I (see Eq. (14)) is low, the next redox reaction will only become significant if the concentration of the previous redox acceptor is very low; e.g., the manganese electron acceptor is only significant if nitrate concentrations are very low. A higher value of the inhibitor term parameter will result in an overlap of two (or more) redox reactions; e.g., the manganese inhibitor term parameter in the iron reduction rate equation is set two orders of magnitude higher than nitrate in the manganese rate resulting in an overlap between organic degradation by manganese and iron.

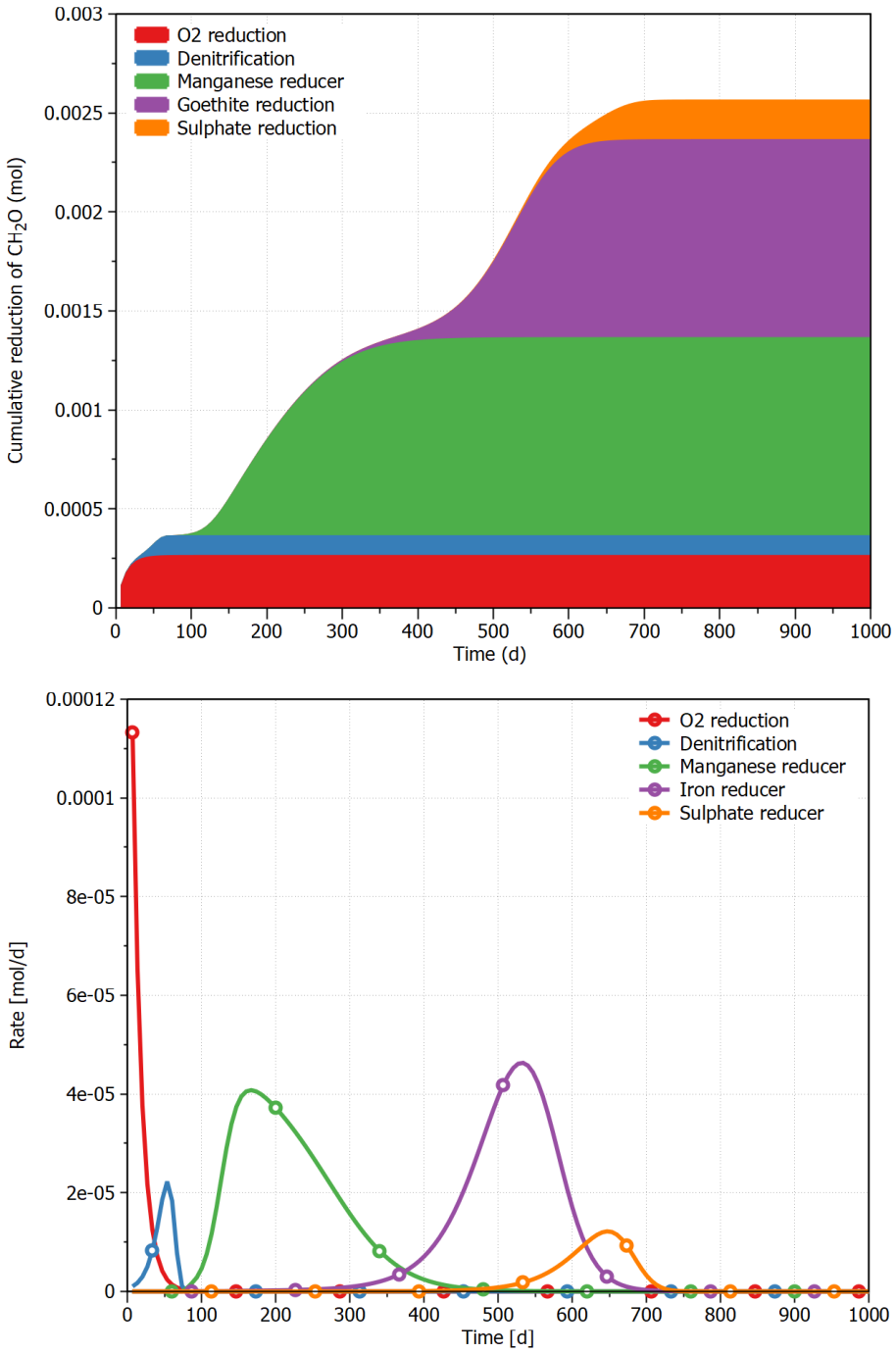

Figure 4-37 – Example calculation of microbiologically-driven kinetic degradation of an organic by different electron acceptors: (Top) cumulative CH_2O degradation by different electron acceptors, and (Bottom) rates of individual redox reactions.

The next example illustrates the combination of the biochemical model for oxidation of organics with a two-dimensional water flow and transport system. We consider a simple rectangular saturated transport problem (Figure 4-38) where the pristine aquifer contains different electron acceptors (O(0), N(5), S(6) and solid Fe(3)). An organic pollutant-rich, oxygen-poor water solution is infiltrating in the middle of the left boundary; in the other parts the fresh groundwater is infiltrating. The organic pollutant is reduced by the different oxidants in the aquifer clearly illustrated in Figure 4-39. Compared

to a tracer (Figure 4-39, left), the spatial extension of the organic pollutant (Figure 4-39, right) is smaller.

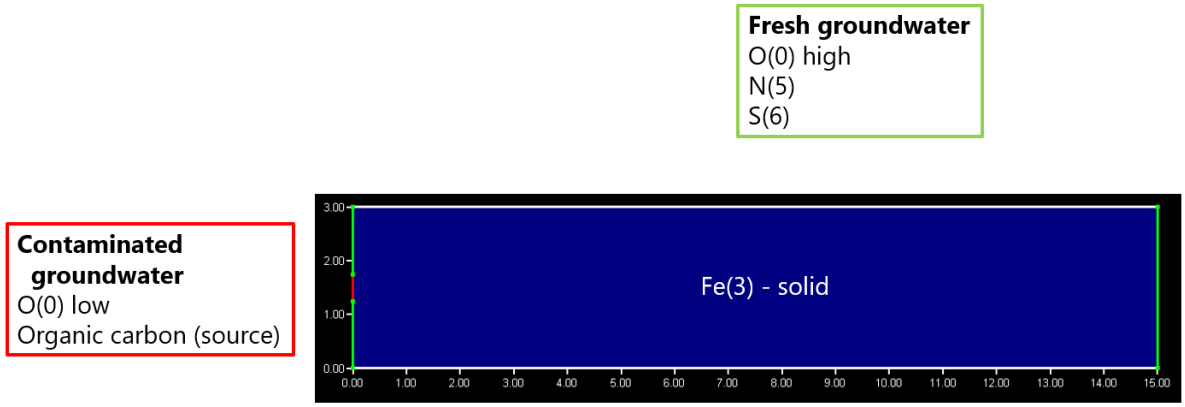

Figure 4-38 – Two-dimensional flow and transport domain with initial and boundary conditions.

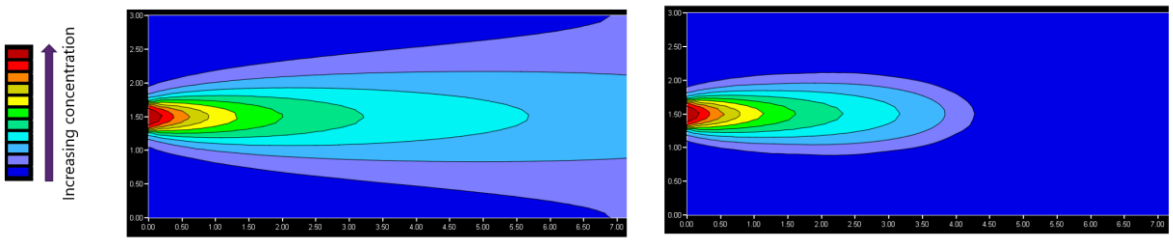

Figure 4-39 – Spatial extent of a plume for (left) an inert tracer, and (right) an organic pollutant subject to reductive degradation reactions (concentration scale is relative, thus different for left and right plots).

Figure 4-40 shows the spatial distribution of the electron acceptors. O(0) is consumed first followed by N(5). For the three aqueous electron acceptors, a depletion zone is visible outside the organic pollutant zone (compare Figure 4-40 with Figure 4-39) indicating transversal transport of the electron acceptor to the zones with the pollutant. The depletion zone for the immobile electron acceptor (goethite for iron) is of course localized where the pollutant is. The overall picture illustrates the plume fringe concept (Meckenstock et al. 2015) – degradation rates of the different electron acceptors are the highest at the fringe of the plume (Figure 4-41).

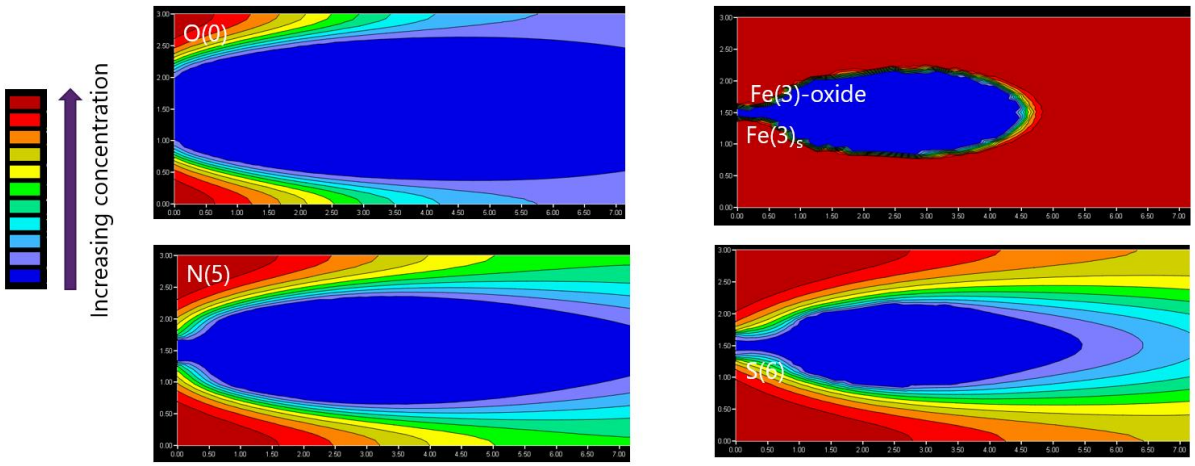

Figure 4-40 – Spatial extent of a plume for different electron acceptors in the aquifer (concentration scale is relative, thus different absolute values for different electron acceptors).

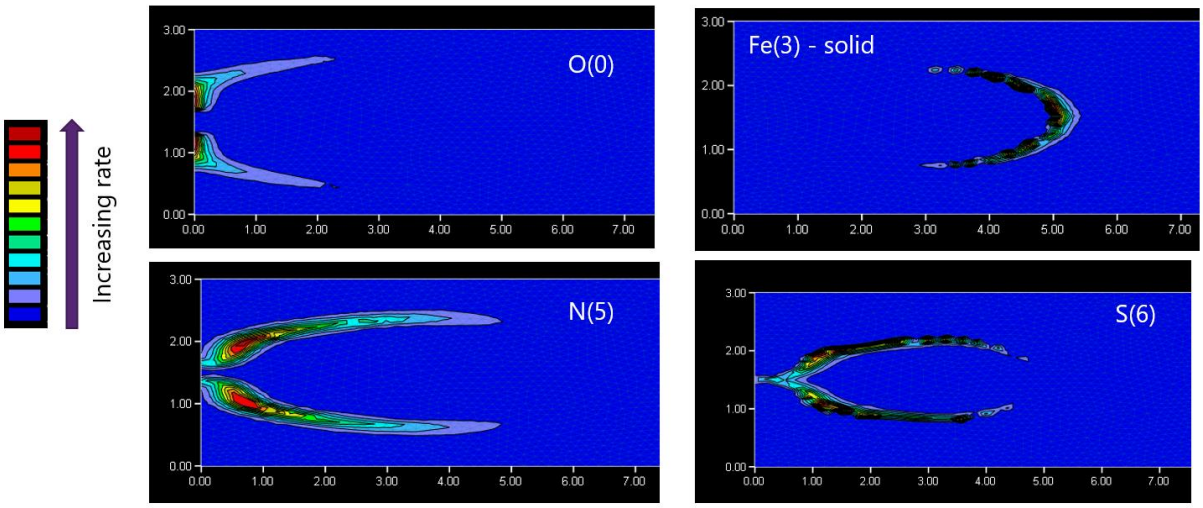

Figure 4-41 – Zones of degradation rate by different electron acceptors (scale of the degradation rate is relative, thus different absolute values for different electron acceptors).

4.5.2.2 Sorption of metals on subsurface organic matter

In this section, the humic-ion binding model VII (Tipping, Lofts, and Sonke 2011) is illustrated with an simple example. For a soil with a bulk density of 1.8 kg/dm³ and 2% of organic matter (with a fraction of fulvic acid of 0.6), sorption of Cd, Pb and Ca on soil organic matter is calculated for different NaCl background concentrations and pH values. Figure 4-42 shows sorption of Cd for different background concentrations of NaCl and pH values without competition of Ca and Pb. Variation in pH leads to almost two orders of magnitude variations in K_d; the ionic strength (a result of the NaCl background) has a smaller influence. Competition with Ca (for one NaCl background concentration) is shown in Figure 4-43. There is a clear influence of Ca concentration, and thus competition between Ca and Cd for the available sites. The effect of pH is smaller than the effect of Ca concentration on the K_d. The last example accounts also for the competition with Pb (Figure 4-44) which sorbs more efficient to organic matter than Cd.

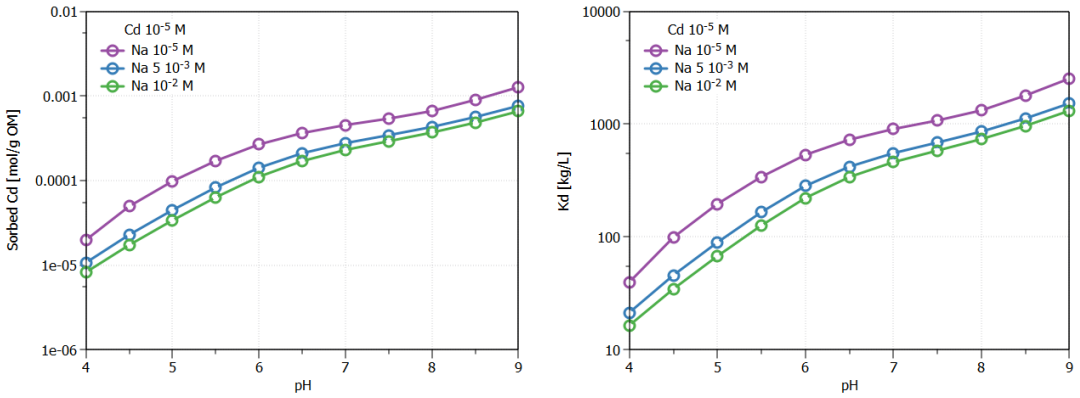

Figure 4-42 – Effect of ionic strength on sorption of Cd for different NaCl background concentrations: (left) sorbed Cd concentration, (right) K_d.

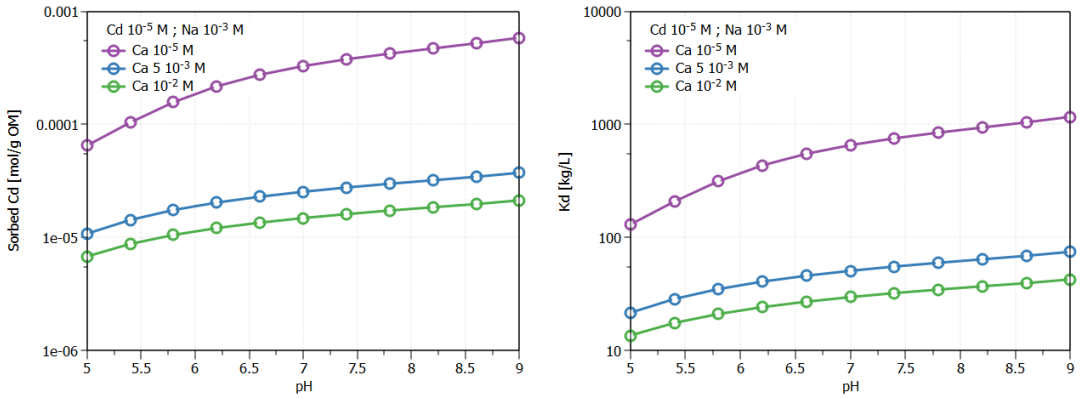

Figure 4-43 – Competition with Ca for Cd sorption for one background concentration of NaCl: (left) sorbed Cd concentration, (right) K_d.

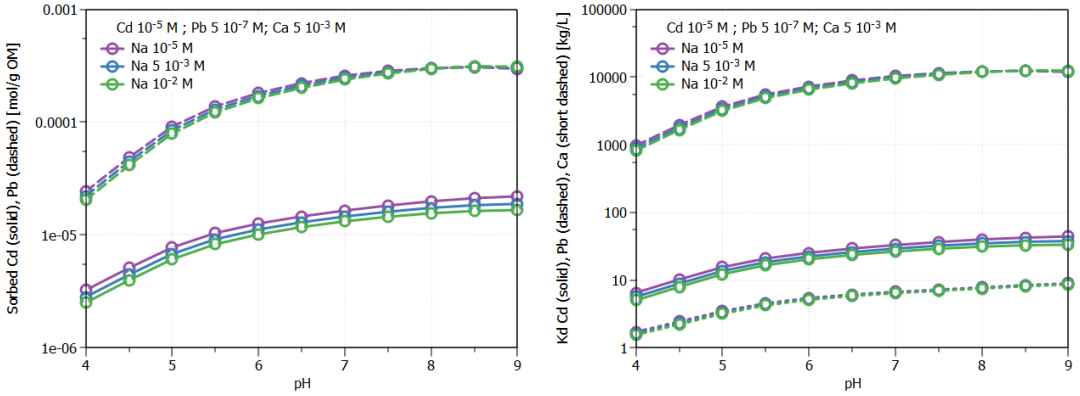

Figure 4-44 – – Competition of Cd sorption with Ca and Pb for one background concentration of NaCl: (left) sorbed Cd concentration, (right) K_d.

4.6 Site specific investigations in support of Model

4.6.1 Mobility of contaminates under changed conditions – flooding

Contaminated riverbanks pose significant environmental challenges, particularly in regions impacted by historical industrial activities and prone to increasing climate change consequences. Constructed wetlands have emerged as a potential solution for managing floodings from storm surges. However, the mobility and fate of elements such as arsenic (As) and cobalt (Co) under dynamic redox conditions remain poorly understood. This study investigates the potential for upward migration of these elements despite the formation of iron (Fe) crusts at the sediment-water interface (SWI), which may act as a barrier to their dispersion (Figure 4-45). To address this, undisturbed soil from a riverbank with historical contamination from phosphate and metal industries were sampled in the Grote Nete Valley (Flanders, Belgium). The soils, characterized by high levels of phosphorus (P), cadmium (Cd), and As, along with moderate Co contamination, were collected as intact 35 cm cores from a natural grassland. The cores (initial pH 7, 15.9% organic carbon in the top soil) were subjected to flooding for up to 100 days, with periodic sampling of soil solution using rhizon samplers and monitoring of the overlying water via pipetting and Diffusive Gradients in Thin Films (DET). The results involve the evolution of redox potential (Eh) and dissolved oxygen (DO) in the overlying water, and confirmed the formation of Fe crusts at the SWI. Trends in Fe, As, and Cd mobility were observed, with distinct patterns noted for Mn and Co. While upward diffusive migration of mobilized elements was confirmed, flux calculations based on Fick's law indicated limited dispersion into the overlying water for Fe, As, and potentially P due to their entrapment in the Fe crust. In contrast, Co demonstrated a different behaviour, with a permanent mobility at all waterlogging times and strongly linked with the reductive dissolution and mobilization of Mn-oxides. This study underscores the importance of understanding geochemical dynamics in the design of effective constructed wetlands and provides insights into managing contamination in historically impacted riverbank ecosystems. Shallow wetlands might be considered as an appropriate strategy to avoid most contaminants being further delivered into the riverflow.

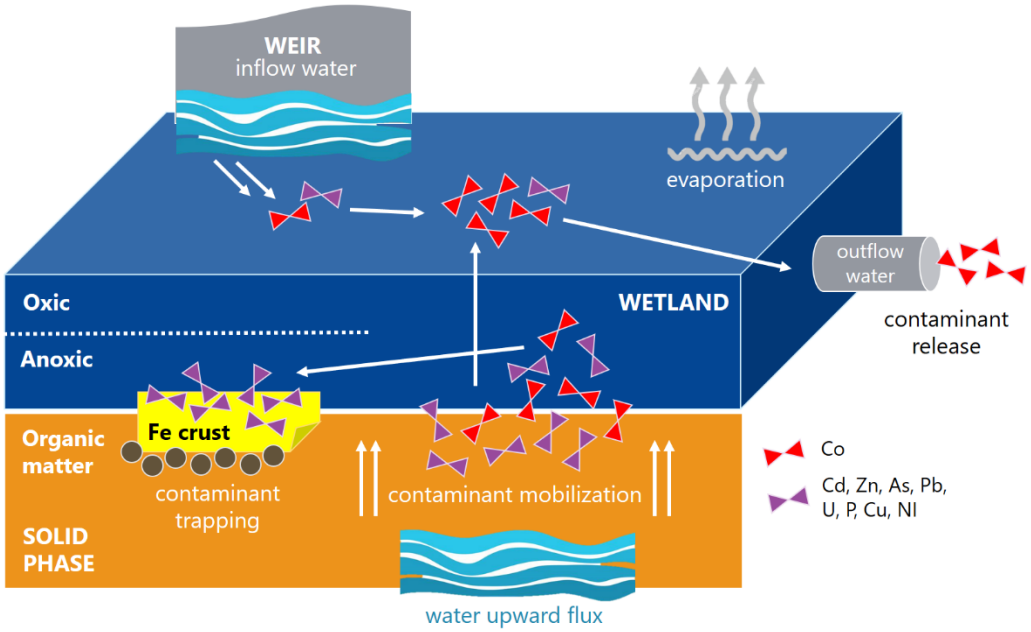

Figure 4-45 – Schematic overview of the processes in flooded contaminated land.

Table 4-5 – Average total solid concentrations of the heavy metals and trace elements (in mg·kg dry soil^{-1}) in the top 30 cm of the Grote Nete Valley oil columns in comparison with the P_{90} background value of the European Union grasslands (Reimann et al. 2014) and its corresponding ratio.

Element	Total concentration (mg·kg^{-1})		Ratio (Grote Nete Valley/ background)
	Grote Nete Valley	Natural EU background	
Cd	96.6 ± 7.2	0.57	169
As	1570 ± 224	16	98
Pb	891 ± 131	41	22
Cu	320 ± 28	37	9
U	12.9 ± 2.6	2.2	6
Co	81.6 ± 17.8	17	5
Ni	138 ± 20	43	3
Zn	1810 ± 224	642	3
Cs	4.05 ± 0.5	3	1.4
P	17600 ± 2220	1390	13

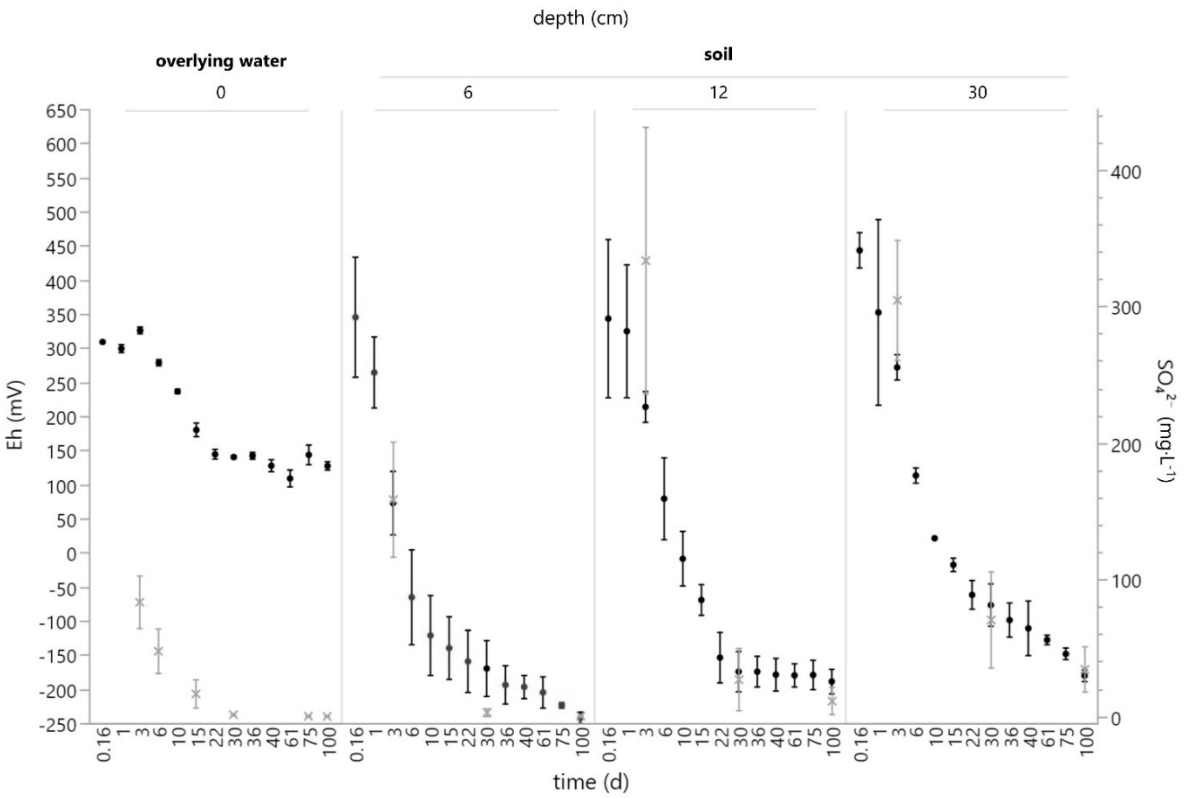

Figure 4-46 – Evolution over time (d) of redox potential Eh (• , in mV) and the rhizon SO_4^{2-} concentration (✕, in mg·L^{-1}) in the overlying water and in the soil columns at different depths (cm). Means and xxx (sd, SEM, n=x)

Table 4-6 – Dissolved concentrations (in µg·L^{-1}) and their standard errors of selected contaminants in the overlying water at the end of the 3-day and 100-day waterlogging period. The values are the averages of the pipetting samples at two depths in all three columns (N=6) of each waterlogging period. The data are compared with the legal freshwater limits established by the Milieukwaliteitsnorm (MKN, VLAREM II) from the Vlaamse Milieumaatschappij (Flemish Government 2024) (for Cs there is no limit established).

Element	Overlying water concentration (µg·L^{-1})			Ratio Grote Nete Valley/limit (-)	
	limit in Flanders (VLAREM II)	Grote Nete Valley			
		3-day	100-day	3-day	100-day
Co	0.5	439 ± 81.5	500 ± 118	880	1000
Zn	20	3220 ± 275	35 ± 18	160	1.75
Cd	0.45	66 ± 16.1	0.28 ± 0.05	145	0.6
As	3	276 ± 52.3	16.1 ± 3.75	90	5.4
Cu	7	209 ± 38.5	8.79 ± 2.24	30	1.3
Ni	34	436 ± 14	226 ± 16	13	6.6
U	1	0.74 ± 0.07	1.11 ± 0.36	0.7	1.1
Pb	10	4.11 ± 1.44	0.35 ± 0.13	0.4	0.04
Cs	-	0.13 ± 0.01	0.05 ± 0.003	-	-
P	140	3192 ± 694	157 ± 19.3	25	1.1

4.6.2 Biodegradation of XOC.

4.6.2.1 BAM biodegradation in soils in and near graveyards.

Based on the groundwater analyses of the investigated sites (see above), it was decided to focus on pesticide residue compounds referring to both the parent compound or possible transformation products. 2,6-dichlorobenzamide (BAM) was one of the most frequently encountered pesticide residues. BAM is a transformation product of dichlobenil, a broad-spectrum herbicide that was mainly used for clearing weeds in non-agricultural areas such as private and public places like courtyards, pavements, industrial sites, private gardens, railways and graveyards. The use of the compound has been banned in the EU since 2008 but BAM remains an issue likely because dichlobenil remains in the soil and the recalcitrant character of BAM. Therefore, we examined the top soils of four different grave yards for BAM biodegradation capacity as well soils from neighboring areas where dichlobenil was used in the past, by incubating soil samples (in total around 40 from 4 different sites) in minimal medium containing 10 mg/L BAM. However, the capacity to degrade BAM was poor with only one soil sample originating from a dichlobenil treated public area near the church of Wespelaar (WES17), showing BAM degradation. The result confirm the recalcitrance character of BAM and the corresponding extremely rarity of microbiota able to degrade the compound. Because of that rarity (up to now only 3 bacterial isolates have been described that degrade and use BAM as a C-source, all isolated from Danish soils) and to identify the mechanism of degradation in the WES17 soil, enrichment cultures were started to isolate the responsible organism by enrichment for cultures that use BAM as sole C-source. From this enrichment culture, we obtained several isolates that grow on BAM and catabolize it. In a first effort, contaminations of the dichlobenil /BAM degrader *Aminobacter* sp. MSH1, an organism isolated from the courtyard of a plant nursery in Denmark (Sorensen et al. 2007) and an important study object in the KU Leuven laboratory in other research projects, were recovered. Therefore, the complete experiment was repeated with new soil samples taking from two areas including the Wespelaar area. BAM degradation was again rare and only observed with sample taken from the WES17 location. A new enrichment of BAM degraders from that sample was performed and resulted into the isolation of 7 BAM degrading isolates. The sequence of the 16S rRNA gene of the new strains showed 100% identity with this of *Aminobacter* sp. MSH1 but also with another soil isolate *Aminobacter* strain (*Aminobacter niigataensis*), demonstrating that the new organisms are phylogenetically strongly related to *Aminobacter* sp. MSH1 but not necessary the same. This is not unexpected since such a specialization in biodegradation has been observed before for other pesticide residues and besides strain MSH1, also the two other Danish BAM catabolic strains reported in literature, are *Aminobacter niigataensis* species (Sorensen et al. 2007). A genomic fingerprint of the strains using BOX-PCR revealed small but clear differences between the new strains and strain MSH1 (Figure 4-47) indicating that the new isolates are true novel strains and not *Aminobacter* sp. MSH1 contaminants. Currently, we are performing a full genome sequence comparison between the new strains and *Aminobacter* sp. MSH1 to confirm this. The aim is to turn these findings into a peer-reviewed publication.

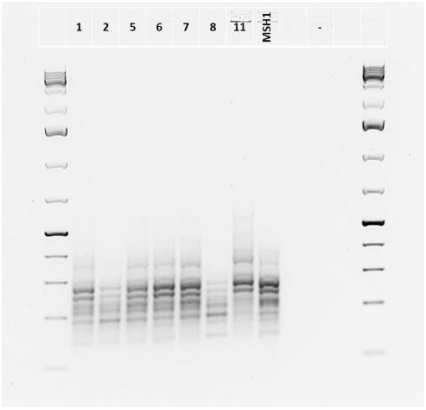

Figure 4-47 – BOX-PCR genome profiling of 7 BAM-degrading isolates obtained from the WES17 soil sample and of Aminobacter sp. MSH1. The isolates relate to lanes marked with 1, 2, 5, 6, 7, 8 & 11.

4.6.2.2 Pesticide biodegradation governed by microbiota adapted to degrade recalcitrant organic carbon.

Several observations from the KU Leuven group and others indicate that the presence of recalcitrant assimilable organic carbon (AOC) might improve degradation and mineralization of xenobiotics. It is hypothesized that such recalcitrant AOC will enrich for microbiota with enzymes optimized towards recalcitrant AOC (for instance aromatic compounds) and that these enzymes will lead to fortuitous (i.e., co-metabolic) biodegradation of the xenobiotica. To study this hypothesis, two different approaches were intended. One approach looks for correlations between soil characteristics including recalcitrance of the dissolved organic carbon (DOC) and the capacity of the soil communities to mineralize pesticides. In the second approach, soil communities will be enriched for degraders of recalcitrant AOC by feeding them with recalcitrant DOC and monitored for their pesticide mineralizing capacity. In both cases, pesticide mineralization was scored by examining the production of $^{14}CO2$ from a range of ^{14}C-labeled pesticide compounds in an inventive high-throughput microtiter plate assay. Recalcitrance of the DOC was scored by determining the Specific UV Absorption (SUVA) of extracted DOC. Only work was done on the first approach. In the previous report, we focused on examining the relationship between soil parameters and pesticide mineralization capacity of top soils (taken from the grave yard sites) but no direct relation was found. In the work presented here, we examined deeper soil samples along a vertical profile up to 3 m deep. We hypothesized that DOC becomes enriched in more recalcitrant DOC while migrating through the soil and hence that microbiota in deeper layers will become enriched in degraders of more recalcitrant DOC and show increased capacity to mineralize pesticides. Up to now, samples were taken from two sites, i.e., a vertical profile in an agricultural field (Ter Munck) and a vertical profile in a small forest downstream (according to groundwater flow direction) of the graveyard of Wespelaar. At each sampling site, a vertical soil profile was taken from 0 – max. 3 m depth using a gauge and soil samples at 0, 0.5, 1, 1.5, 2, 2.5, and 3 m at Ter Munck and 0, 0.1, 0.2, 0.4, 0.6, 0.8, 1.0, 1.25, 1.5 and 1.65 m at Wespelaar were retained for analysis. Measured soil characteristics were pH, moisture content, C/N ratio, DOC content, SUVA & total elemental analysis of pore water extracts. Tested pesticides for mineralization were carbofuran, BAM, 2,4 dichlorophenoxyacetic acid (2,4-D), linuron, isoproturon, endofuran, bentazon, and atrazine. $^{14}CO_2$ emission was monitored over a period of 63 days. Unexpectedly, no clear differences were found in SUVA along the vertical profile with the highest SUVA in the top soil sample and highly identical SUVAs in the deeper samples (Table 1). On the other hand, mineralization

of several pesticides was observed. The upper soil samples showed the highest range of pesticides that were mineralized. Moreover, mineralization pesticide rates of soils from 0 m to 0.5 m showed relatively high values while soils of 2.5 m and 3.0 m showed slow mineralization for all pesticides. Carbofuran and bentazon showed the highest mineralization rate at the top layer soil, while the mineralization of 2,4 D and isoproturon showed maximal mineralization rate at the depth of 0.5 m (Table 4-5, Figure 4-48 and Figure 4-49). BAM was not mineralized showing again its recalcitrant nature. Because of the nature of the site, we expect more variation in SUVA along the vertical profile. We conclude that pesticides can be mineralized along the vertical soil profile but that this cannot be related to DOC quality as determined by SUVA. Otherwise, other factors might play, i.e., the number of pesticide degrading microbes that might be higher at the top soil because of initial higher pesticide concentrations, higher oxygen concentrations etc.

Table 4-5. Soil properties (pH, SUVA, ICP, C/N) and mineralization parameters determined for the soil samples taken along a 3 m vertical soil profile at the Ter Munck site.

Depth		0 m	0.5 m	1.0 m	1.5 m	2.0 m	2.5 m	3.0 m
pH		6.45	5.94	5.87	5.73	5.70	8.06	8.28
NPOC (mg C/L)		18.43	6.87	4.21	4.57	2.34	1.82	1.97
C/N		10.00	6.84	7.94	6.79	7.88	112.96	145.09
Total C (mg C/L)		0.12	0.04	0.03	0.02	0.02	0.19	0.28
Total N (mg N/L)		0.012	0.005	0.003	0.004	0.002	0.002	0.002
SUVA		0.118	0.093	0.099	0.093	0.078	0.085	0.075
Carbofuran	a	4.58	3.56	3.67	2.72	1.60	1.61	1.89
	μ	0.19	0.10	0.11	0.08	0.06	0.05	0.08
	λ	25.96	28.07	27.70	24.87	31.58	24.34	29.24
2,4 D	a	24.69	6.92	5.86	16.86	8.80	1.58	0.74
	μ	0.87	16.91	0.50	0.68	0.29	0.06	2.12
	λ	6.79	3.51	16.59	8.36	7.14	36.76	13.04
Linuron	a	4.01	3.10	3.40	1.40	4.14	2.79	0.85
	μ	0.14	0.08	0.10	0.08	0.08	0.14	50.00
	λ	22.58	27.11	31.84	37.05	36.89	28.82	30.14
Isoproturon	a	7.56	18.91	9.84	2.14	7.18	1.68	1.33
	μ	1.31	2.75	0.36	0.12	0.41	0.08	0.09
	λ	21.85	23.25	20.15	32.21	10.45	36.33	36.90
Bentazon	a	8.96	27.09	2.82	2.73	2.10	2.60	2.55
	μ	1.10	0.23	0.57	0.41	0.71	0.18	0.15
	λ	19.79	9.23	19.14	17.32	21.27	17.60	15.09

*a: mineralization extent, μ: max. mineralization rate, λ:lag phase before mineralization started. These parameters were calculated using the modified Gompertz model ($P = Ae^{-e^{\frac{e}{A}(\mu\lambda-(\mu-c)t)+1}} + ct$).

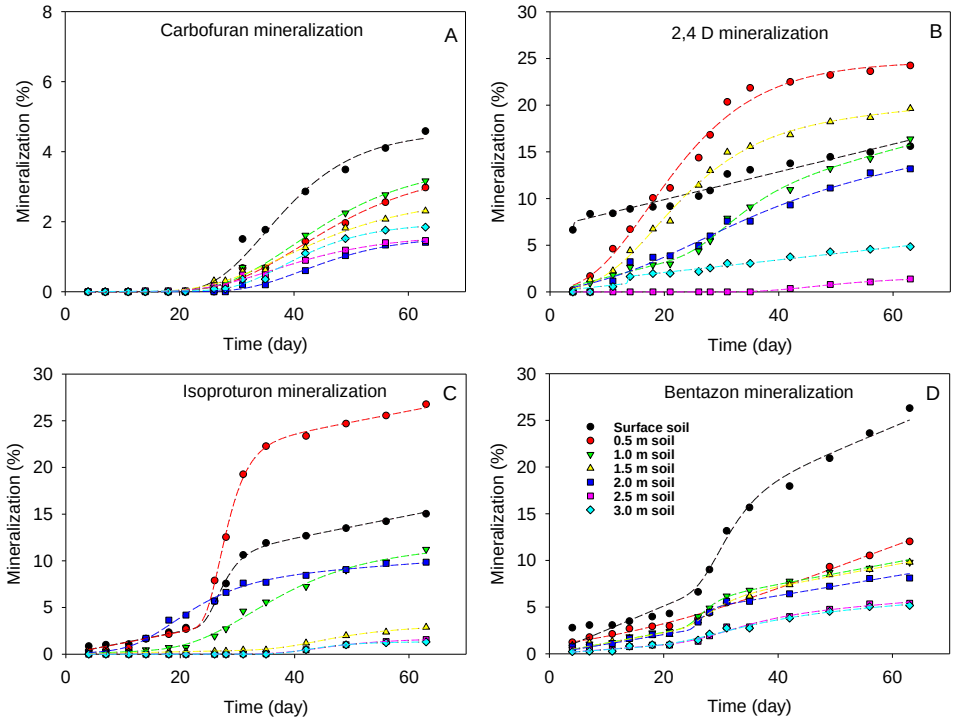

Figure 4-48 – Recorded mineralization of the pesticides carbofuran, 2,4 D, isoproturon, and bentazon for soil samples taken along a vertical profile at the Ter Munck site.

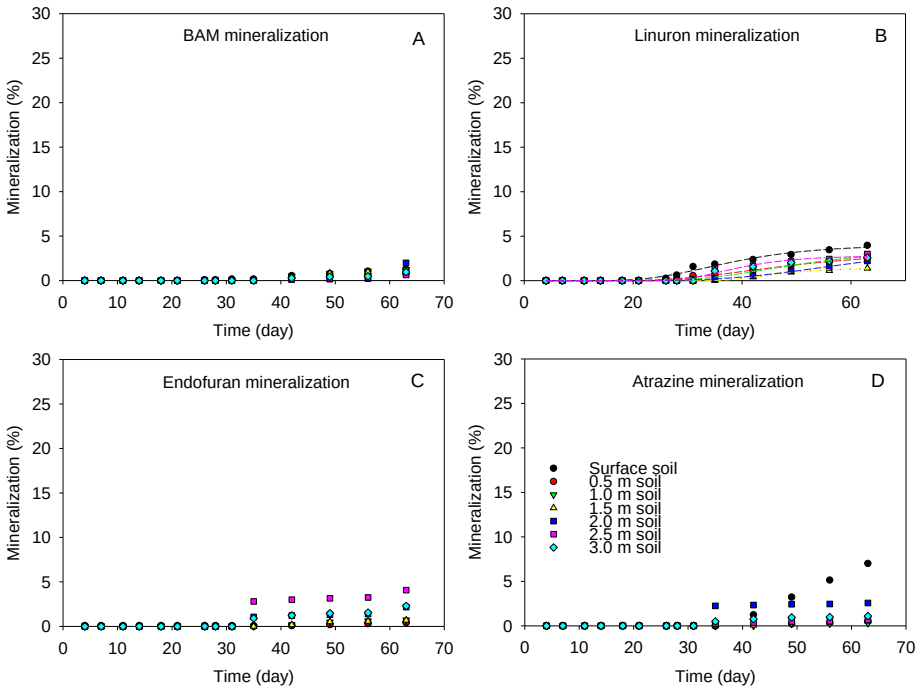

Figure 4-49 – Recorded mineralization of the pesticides BAM, linuron, endofuran, and atrazine for soil samples taken along a vertical profile at the Ter Munck site.

4.6.2.3 Kinetics of BAM degradation by Aminobacter sp. MSH1 and its growth on BAM

Detailed information on the BAM degradation kinetics at the relevant trace concentrations that the compound is present in waters and groundwater is currently lacking while for modeling purposes, this

knowledge is required for predicting and optimizing the degradation process. Since BAM was not well degraded in the tested soils including Wespelaar, we decided to start using a BAM degrading organism to explore BAM degradation kinetics at relevant trace concentrations at µg – ng/L scale. This is extremely important since kinetics might differ between low (i.e. µg – ng/L scale) and high concentrations (mg/L) and the degradation of pollutants at trace concentrations as they occur in the environment (including the examined sites) has been hardly explored (Helbling et al., 2014). As a BAM degrading organism, we selected rather the well-described *Aminobacter* sp. MSH1 instead of the new isolate from Wespelaar which showed later on instable BAM degradation. However, contaminating assimilable organic carbon (AOC) in media makes the biodegradation experiment a mixed-substrate assay and hampers exploring pollutant degradation at trace concentrations (Helbling et al., 2014). Therefore, we examined how the BAM concentration affects MSH1 growth and BAM substrate utilization kinetics under AOC-restricted conditions to avoid mixed-substrate conditions. To this end, MSH1 was incubated in AOC restricted MMO medium in the presence of a range of BAM concentrations (25 to 1200 1200 µg-C/L) and growth of MSH1 as well as BAM removal was monitored in time. To compare, also growth on and degradation of benzoate was examined as well as growth on glucose at different concentrations. For all BAM concentrations, a clear lag phase in growth was observed as cell densities remained fairly constant up to 125 hours including the condition without BAM (Figure 4-50). Final cell densities on 25, 45, 100, and 180 µg-C/L of BAM (Figure 4-50a--d) were similar to the final cell density observed when no supplemental carbon was added. Only in case of initial BAM concentrations of 320 and 1200 µg-C/L, final cell densities were higher compared to MMO without supplemental carbon (Figure 4-50e and f). Growth was characterized by two exponential growth phases, independent of the BAM concentration, i.e., one from approximately 125 to 160 hours, followed by a second, longer and slower growth phase. The first growth phase occurred simultaneously with the growth phase on MMO without additional carbon (Figure 4-50), indicating that the first growth phase was due to growth on background AOC.

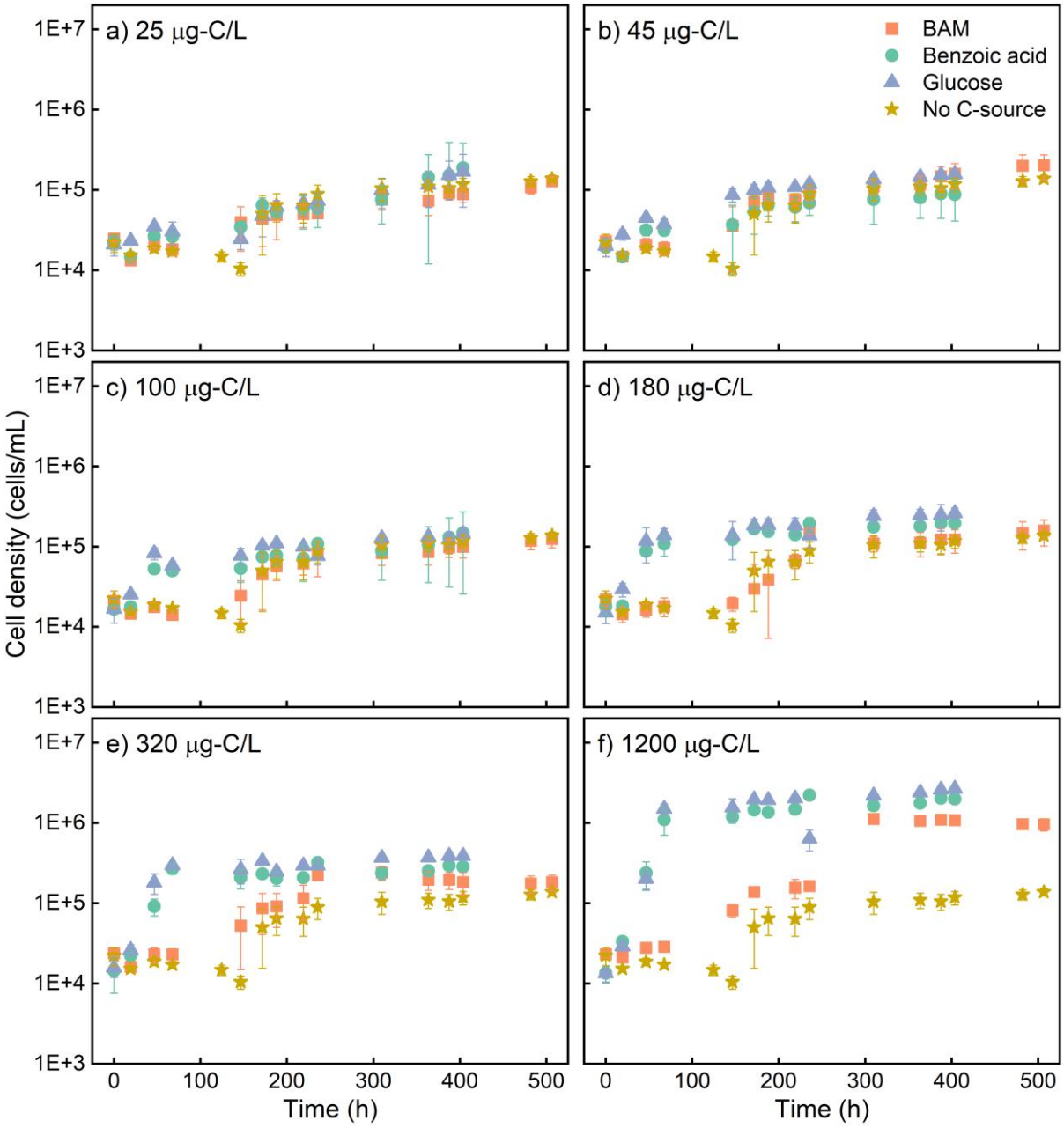

Figure 4-50 – Growth of MSH1 in BAM, benzoic acid and glucose amended MMO under AOC-restricted conditions with different initial concentrations of carbon sources, i.e., a) 25 µg-C/L, b) 45 µg-C/L, c) 100 µg-C/L, d) 180 µg-C/L, e) 320 µg-C/L, and f) 1200 µg-C/L. Conditions without added C-source were included to show the growth of MSH1 in AOC-restricted MMO medium without additional carbon source.

Growth of MSH1 on benzoic acid and glucose was comparable, but differed from the growth on BAM, irrespective of the carbon concentration (Figure 4-50). A lag phase was observed for growth on 25 and 45 µg-C/L of benzoic acid and glucose (Figure 4-50a and b) that was similar to the condition without added carbon substrate. For growth on 100 µg-C/L and higher concentration levels of benzoic acid and glucose, no lag phase was observed as growth started immediately (Figure 4-50c-f). We conclude that, in contrast to glucose and benzoic acid, the growth linked to BAM degradation at lower concentrations is difficult to assess, since the MSH1 cell densities did not increase above those obtained on residual

background AOC despite the relatively low concentrations of AOC (11.6 µg/L) after the AOC-restricting treatment.

BAM degradation is shown in Figure 4-51. Complete BAM degradation after 500 hours was only observed at initial BAM concentrations of 320 and 1200 µg-C/L (Figure 4-51eand f). While at initial BAM concentrations of 100 and 180 µg-C/L, complete BAM removal was observed at 560 hours (Figure 4-51cand d) and at initial BAM concentrations of 25 and 45 µg-C/L, 100% removal was not reached (Figure 4-51a and b). In contrast to BAM, benzoic acid was rapidly and completely degraded within 200 hours at all initial concentrations (Fig. 4-33).

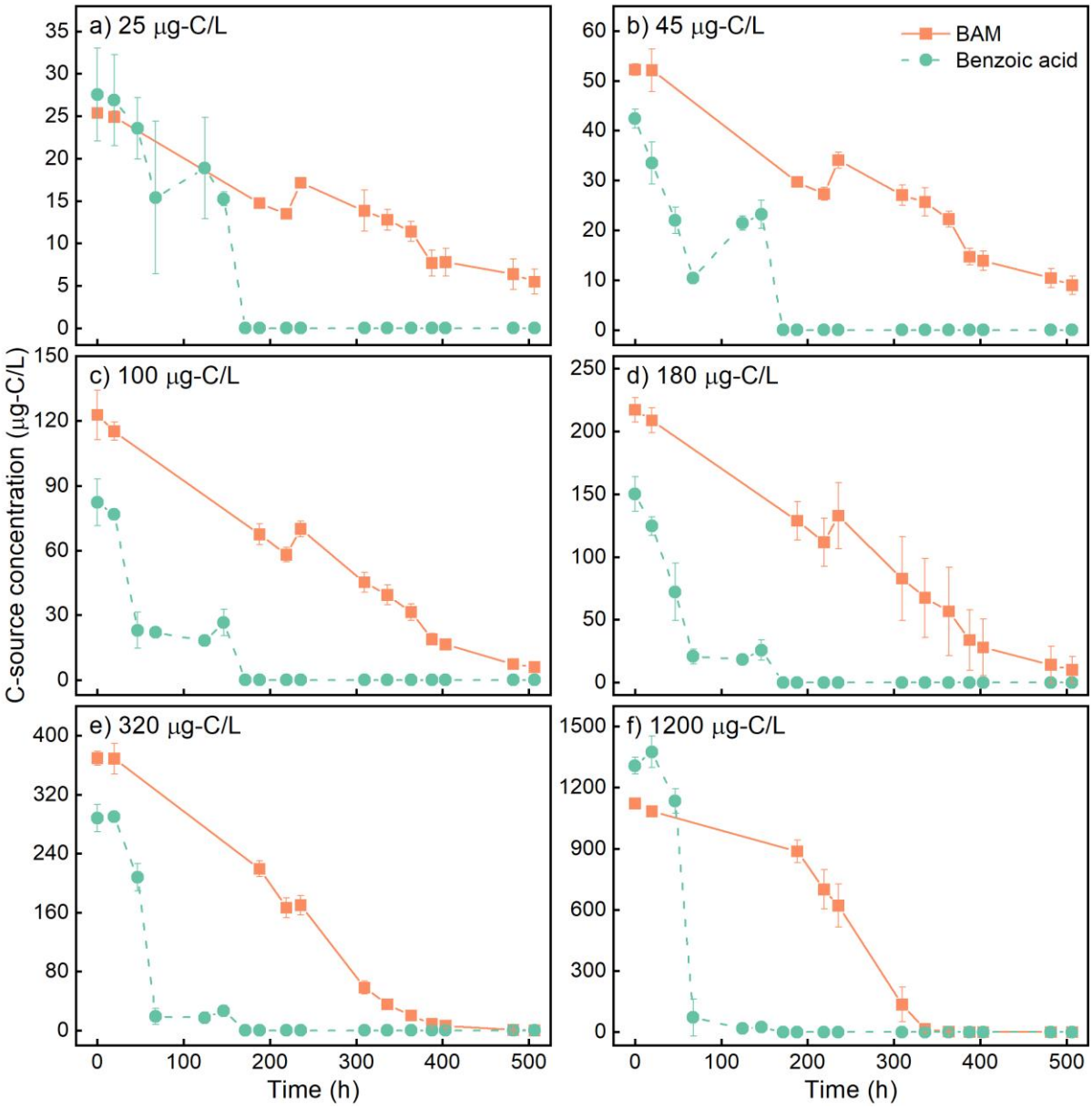

Figure 4-51 – BAM and benzoic acid degradation by strain MSH1 in AOC-restricted MMO in experiment 5. a) 25 µg-C/L, b) 45 µg-C/L, c) 100 µg-C/L, d) 180 µg-C/L, e) 320 µg-C/L and f) 1200 µg-C/L of BAM and benzoic acid.

Overall, the results showed that growth yields on BAM were concentration-dependent and decreased substantially at trace concentrations, i.e., growth of MSH1 diminished until undetectable levels at

BAM concentrations below 217 µg-C/L and hence that BAM was removed by MSH1 through non-growth-linked biodegradation below this concentration. Nevertheless, BAM degradation continued. Decreasing growth yields at lower BAM concentrations might relate to physiological adaptations to low substrate availability or decreased expression of downstream steps of the BAM catabolic pathway beyond 2,6-dichlorobenzoic acid (2,6-DCBA) that ultimately leads to Krebs cycle intermediates for growth and energy conservation. This research revealed a new aspect of the recalcitrant character of BAM in oligotrophic waters as groundwater, i.e., the fact that catabolic degraders are not able to grow on the compound at the concentrations encountered in the environment and as such have to acquire their carbon from elsewhere like other DOC. The results of this part were published in Environmental Science and Technology (Raes et al., 2024).

4.6.2.4 Influence of sand filter community on MSH1 growth and BAM degradation.

Subsequently, we focused our research on the effect of DOC on BAM biodegradation. Again, we used the BAM-degrading *Aminobacter* sp. MH1 to study this rather than a soil community. More specifically, experiments were performed to examine how DOC and the presence of other resident microbiota affects biodegradation of BAM at low relevant environmentally concentrations in natural waters hypothesizing (i) that the presence of additional DOC as an auxiliary carbon source will support BAM biodegradation by increasing the biomass of the BAM degrader but that (ii) this can be counteracted by other bacteria that compete for the additional DOC. Growth of MSH1 and concomitant BAM degradation was monitored in three different freshwaters (water-KL, water-ZW, and water-SI) in either the presence or the absence of co-existing bacterial resident community, to understand how co-existing endogenous bacteria affect MSH1 growth and BAM degradation. The experiment was performed with two different sand filter communities derived from drinking water production plants, named as SFC-KL and SFC-HA. MSH1 growth and BAM degradation curves are shown in Figure 4-52. In all the three water matrixes, the presence of both SFCs suppressed the growth of MSH1. Compared with the conditions without SFC, the maximum cell densities of MSH1 were approximately 75-fold and 19-fold lower in the presence of SFC-KL and SFC-HA, respectively (Figure 4-52a and b). Consequently, the AOC available for MSH1 (AOC_{MSH1}) was significantly reduced when SFCs and MSH1 were co-incubated (p-value < 0.05) (data not shown). In addition, the presence of SFCs seriously affected BAM biodegradation. BAM was completely degraded at the end of the experiment without SFCs whereas approximately 57.9 % and 43.9 % of BAM remained in the presence of SFC-KL and SFC-HA, respectively (Figure 4-52c and d). On the other hand, the presence of MSH1 did not significantly influence the growth of SFC-KL and SFC-HA (data not shown) and the concentrations of AOC_{SFC} remained at the same level whether MSH1 was present or not (data not shown). It was concluded that MSH1 has a clear competitive disadvantage for growth on AOC in the presence of co-incidental microbiota (i.e., SFCs). This shows another aspect of the recalcitrance of organic micropollutants in freshwaters, i.e., that degradation might be hampered by competition of the organic micropollutant degraders for other DOC by resident microbial community members. This has to be taken into account when examining and predicting pesticide degradation. Moreover, solutions have to be found for solving this bottle neck of recalcitrance.. A publication for Environmental Science and Technology is being prepared.

Next steps should extend this work towards soil environments including both vadose zone and aquifer for instance in soil columns simulating conversion of dichlobenil to BAM and leaching of BAM through the soil column accompanied by modeling efforts as previously done for atrazine (Cheyns et al. 2010).

Moreover, solutions have to be found for resolving the observed bottle neck of organic micropollutant biodegradation. Several projects (FWO and ERA-NET) at the KU Leuven focus on this now.

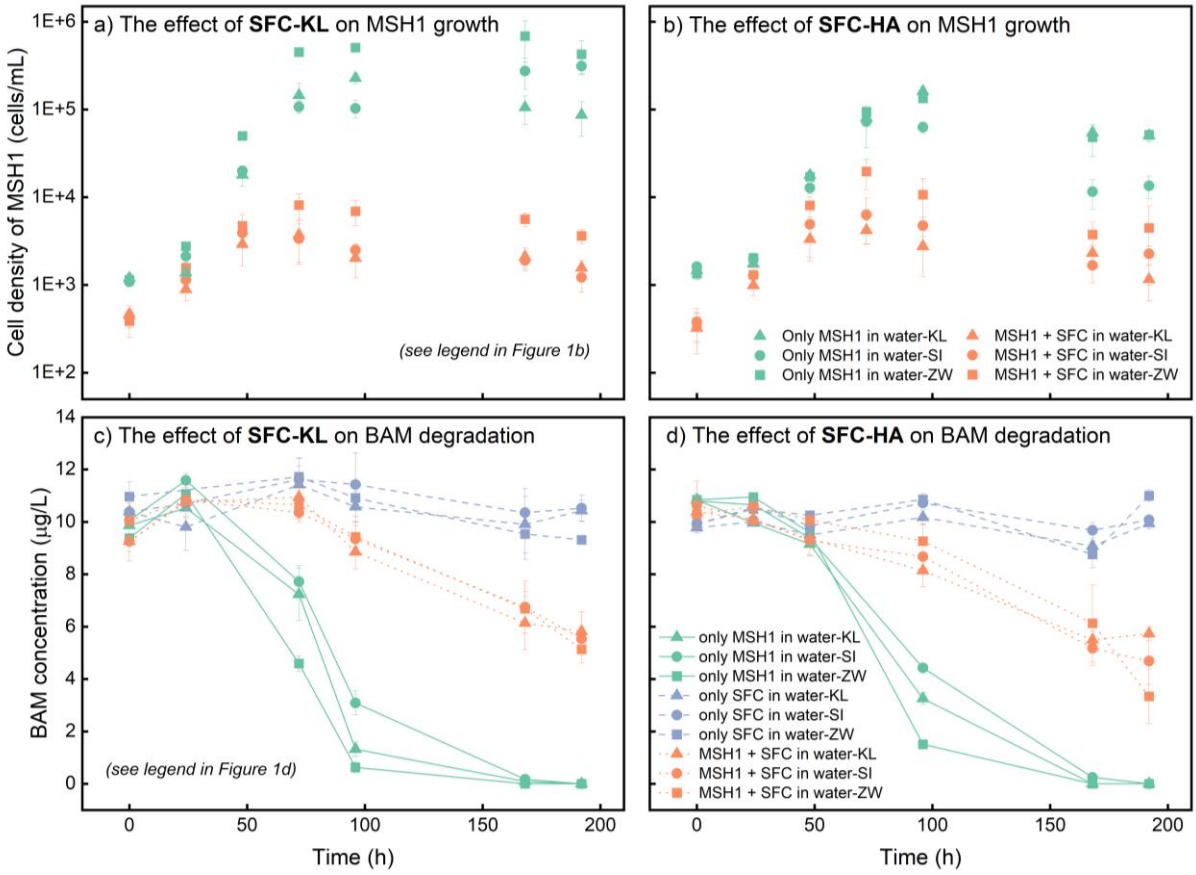

Figure 4-52 – Effect of the presence of two SFCs (i.e., SFC-KL and SFC-HA) on the growth of MSH1 (a, b) and MSH1-mediated BAM degradation (c, d) in three different freshwaters.

4.7 Conclusions and Recommendations

Assessing the susceptibility of a site for ground water pollution. We carried out a screening at national scale for the suitability of monitoring schemes to detect the risk of pollution to the shallow groundwater of thousands of cemeteries and landfill sites and checked this suitability through site visits. Several georeferenced databases exist for this purpose. The most important criteria were: drainage class from the digital soil map, distance to water courses and slope of more than 4.5° in Flanders.

Setting up subsurface geological models as input to flow and transport models. Geological models are essential for the development of three-dimensional groundwater flow and transport models. When dealing with relatively small study areas (as is the case here for the point sources such as cemeteries and landfills) and a requirement of high-resolution spatial data (e.g. due to variability inherent to shallow Quarternary geology), publicly available data is lacking with sufficient levels of detail and therefore information from boreholes at the site itself and additional information (soil maps, digital elevation models) are essential.

Although publicly available data is crucial for building a geological model, specific site characterization and information seems to be inevitable as well.

Constraining a model describing the transport of a leachate from a landfill The case study of this modeling study was a landfill leachate plume in a sandy phreatic aquifer potentially threatening a groundwater extraction site to the south of Leuven, Belgium. As a first step, a composite database was constructed from existing sources and included hydraulic head measurements, geochemical field parameters, and concentrations of geochemical species, among others. The data show elevated concentrations of several species indicative of groundwater pollution due to landfill contamination. A three-dimensional flow and transport model was built using site-specific data available in the open literature. the long-term average hydraulic head field and hydrogeological features can be simulated reasonably well. The general spatial trends in chloride (Cl) could also be reproduced; however, using only readily available chloride data could not reproduce the more detailed variations in the observations.

Model output as regards model complexity was studied for different aspects. Assuming a uniform variable recharge rate (instead of a spatially variable recharge rate) did not affect the flow model output. However, as the load of Cl from the landfill in the aquifer is directly related to the recharge rate through the landfill, Cl concentrations are sensitive to the assumed recharge, although differences are much smaller further from the landfill. Using a homogeneous instead of a heterogeneous hydraulic conductivity field does not greatly affect general plume characteristics. Uncertainties on source term magnitude and timing are often quite large for legacy landfills (and many other point sources). Uncertainties of timing and magnitude of the contamination source are quite important as they persist throughout time and space and affect concentration in receptors. On the other hand, source geometry might influence concentrations near the point source but can be dampened at larger distances or at longer time scales. Finally, also the degradation of dissolved organics by redox reactions was simulated with a limited number of site-specific information, but available measurements did not allow for validation of the simulations.

The case study gave insights into how available data and model abstraction can help build models. However, further research is required on the acceptable degree of data and process abstraction when modelling field-cases of subsurface flow and reactive transport. Although general suggestions are made with regard to sensitive model input and processes for several targets, a lack of specific data prevented a more refined identification of the required levels of data and model complexity. Obtaining an exact level of acceptable abstraction could, for example, be achieved by constructing a (or taking an existing) highly detailed and well-tested model with well-defined goals and adding (stripping) model complexity step-by-step while monitoring model performance to determine when acceptable results are achieved (forfeited). Furthermore, alternative sites and cases should be investigated to determine the dependence of these general conclusions on the type of system (e.g. advection- or diffusion-dominated, transient or steady-state, the absence of large vertical gradients), pollution source, and type (e.g. leachate infiltration or subsurface storage, mobile versus sorbing contaminants) and system scale (e.g., field-scale and plot-scale). The latter might also influence the dominating processes, e.g., locally around a shallow pollution source; water-table fluctuations or reactive transport in the unsaturated zone can control the fate of contaminants, but for kilometre-scale long-term plume migration, these processes might become less important. If more knowledge on these subjects becomes available, conceptually simple models could be augmented by highly targeted

insertions of model complexity. This could lead to a more accessible approach to modelling complex subsurface flow and transport.

Deriving conceptual model and its implementation in (coupled) reactive transport models. Implementing the HPx framework for coupled reactive transport modeling into the groundwater solute transport code MT3D-USGS resulted in a new versatile and powerful tool (MTHP) for assessing the fate and migration of organic and inorganic pollutants in subsurface saturated systems based on a mechanistic understanding of the governing processes including thermodynamic equilibrium calculations and microbiologically driven kinetic degradation processes. The new code was benchmarked for typical coupled reactive transport problems, including redox equilibria, cation exchange, mineral dissolution, and kinetic degradation networks in one- and two-dimensional transport problems.

To ease the use of complex biogeochemical models in coupled reactive transport models, user-friendly input forms were made for two important sets of processes without compromising on the versatility of the software. The first process is the microbiological-driven kinetic degradation of organic pollutants or organic matter for C-H-O components by a set of different electron acceptors (O(0), N(5), Mn(4), Fe(3), and S(6)) also linked to microbiological growth and death. The second process concerns the sorption of (heavy) metals to subsurface organic matter using the discrete humic-ion binding interaction model from Tipping, Lofts, and Sonke (2011) (model VII). Examples were provided to illustrate these models in a batch-type set-up and, for the first process, in a two-dimensional flow and transport set-up. The latter also illustrated the plume fringe concept.

The developed code and the two process implementations – all available in a public software repository – form a good starting point for developing (site-specific) models for assessing pollutant movement from point sources. Following the templates for these processes, other similar templates could be developed to capture additional processes or other emerging types of contaminants. Some limited work could be done to keep the tool (MTHP) current or use a similar framework for other codes with specific application domains. It is also needed to provide further suitable parameterisation of such models by laboratory studies, calibration and database development.

Screening the actual dispersion of contaminates from a point source Screening and monitoring was done around several selected cemeteries and landfills for measuring several heavy metals and organic compounds (pesticides, BTEX). Unfortunately, the monitoring scheme was not executed as initially planned due to various practical and logistical challenges, including staff availability, travel restrictions imposed by the COVID-19 pandemic and constraints caused by diminished groundwater levels during the dry summer months. BAM was monitored for Zillebeke and Villers-Deux-Eglises for a few sampling dates and confirmed the presence of BAM at these sites. Monitoring data is summarized and available in Walstra et al. (2024).

Gaining insight into contamination / metal remobilization after land change (flooding flood mitigation strategy by artificial wetlands) Artificial wetlands are one of the measures considered in the strategy for flood mitigation in view of climate change. Intermitted flooding of these artificial wetlands may induce changes in the mobility of contaminants when a (hidden) point-source contamination (or any other type, such as a diffuse contamination) is present. In RESPONSE, the consequence of intermittent flooding on inorganic contaminants (heavy metals) was investigated using samples from the Grote Nete site. It was observed that a significant remobilization is possible

under such land use changes. Therefore, it is important to assess consequences of land use changes for specific sites where contamination is present or expected to be present. This can be based on an experimental program and/or with numerical assessments based on mechanistic understanding of processes (of which some examples were developed in RESPONSE).

Gaining insight on biodegradation of organic pollutants that originates from pesticides applied at given sites such as cemeteries The research performed in RESPONSE showed the occurrence of multiple pesticide residues including pesticide transformation products like 2,6-dichlorobenzamide (BAM) in the groundwater near the examined cemeteries at concentrations higher than implemented threshold concentrations although it is not clear whether they originated from (former) pesticide use in the cemeteries. We decided to focus on BAM degradation since (i) it is a major recalcitrant groundwater organic micropollutant (occurring at trace concentrations) in Europe, and (ii) not much is known about its genesis as a transformation product in soil and about its fate/behaviour in natural systems while being extensively studied in the KU Leuven lab as a model for micropollutant biodegradation. The research performed, although not coming to fate modelling in soil, demonstrated some new aspects of the compounds' recalcitrance towards catabolism in groundwater systems when present at relevant environmental trace concentrations, i.e., occurrence of BAM degraders in natural soils is poor, degraders do not grow on the compound at low concentrations indicating that they should acquire the carbon/nitrogen for growth from other organics (i.e. other dissolved organic compounds (DOC)) and that BAM degraders, when present, have to compete for this DOC with other local resident organisms. As such, our research revealed new aspects of mechanisms of recalcitrance of organic micropollutants and bottle necks of organic micropollutant degradation in oligotrophic freshwater systems like groundwater. We are currently working on solutions to solve such bottle necks for instance for application in drinking water treatment systems treating micropollutant contaminated groundwater.

5 DISSEMINATION AND VALORISATION

Workshop "Contaminant migration from point sources to groundwater: from data to models", 12 May 2023, Leuven

Approximately 80 participants joined this workshop. There were two speakers from outside the project:

R. Meckenstock (University of Duisburg-Essen, Germany): How microorganisms overcome limitations of anaerobic degradation of polycyclic aromatic hydrocarbons in groundwate.

R. Eppinger (VMM, Belgium): The quality of the groundwater in Flanders based on the monitoring network of the Flanders Environment Agency

There were 6 presentation from the project partners:

B. Van Wesemael and J. Schoonejans (UCLouvain): Selection of graveyards and landfills ensuring variation in soil, ground water and geological conditions

J. Walstra and V.M.A. Heyvaert (GSB-RBINS): From field to models: Creating a geological framework for groundwater modelling

D. Springael (KULeuven): Pesticide residues around graveyards: BAM, the omnipresent micropollutant and a hard nut to crack

E. Smolders (KULeuven) F. Dengra Grau (SCK CEN, KULeuven): Upward migration of metals from contaminated soils to constructed wetlands

C. Neyens and M. Huysmans (VUB)Reactive transport modelling of point source contaminations in groundwater: model input and process abstraction

D. Jacques (SCK CEN): Modelling coupled reactive transport in soil & groundwater systems

Code and models:

Three github repositories are created for sharing the code and model developments within RESPONSE:

- MTHP code and examples: https://github.com/dphjacques/MTHP
- Module for sorption modelling with model VII: https://github.com/dphjacques/HPx-SorptionModels
- Module for microbiological driven degradation of organics: https://github.com/dphjacques/HPx-KRN

6 PUBLICATIONS

Publications

Raes B., Wang, J., Horemans B., Dirckx L., Waldherr S., Kohler H.-P. E., Springael D. (2024). The growth yield of *Aminobacter niigataensis* MSH1 on the micropollutant 2,6-dichlorobenzamide decreases substantially at trace substrate concentrations. Environmental Science and Technology. *58* (6), 2859–2869.

PhD-Dissertation

Neyens, C., 2022. 'Reactive transport modelling of point source contaminations in groundwater: Model input and process abstraction', Vrije Universiteit Brussel.

Poster and presentations

Neyens, C., et al., (2019) Coupling HYDRUS - MT3D to PHREEQC for reactive transport simulations across a fluctuating groundwater table. Computational Methods in Water Resources XXII, June 3-7, 2018 (http://cmwrconference.org/).

Walstra J., Leterme B., Geukens L., Heyvaert V., Huysmans M., Jacques D., Neyens C., Schoonejans J., Smolders E., Springael D. & Van Wesemael B. (2018). The RESPONSE project: Reactive transport modelling of point source contamination in soils and groundwater In: Geophysical Research Abstracts, vol. 20, pp. EGU2018-15217, EGU (8–13 April 2018, Vienna, Austria)

Walstra J., Leterme B., Geukens L., Goovaerts T., Heyvaert V., Huysmans M., Jacques D., Neyens C., Schoonejans J., Smolders E., Springael D. & Van Wesemael B. (2018). The RESPONSE project: Reactive transport modelling of point source contamination in soils and groundwater In: 6th Geologica Belgica Meeting 2018, Geologica Belgica (12–14 September, Leuven, Belgium)

Geukens G., Verreydt B., Walstra J., van Wesemael B., Heyvaert V., Huysmans M., Neyens C., Schoonejans J., Leterme B., Jacques D., Smolders E., Springael D. (2019). Occurrence of pesticides in groundwater in and around graveyards and pesticide biodegradation capacity of the corresponding top soils. Poster presented at AquaConSoil (20–24 May 2019, Antwerp, Belgium)

Leterme B., Geukens L., Jacques D., Heyvaert V., Huysmans M., Neyens C., Smolders E., Springael D., Van Wesemael B. & Walstra J. (2019). RESPONSE project: Reactive transport of point source contamination in soils and groundwater In: Sustainable Use and Management of Soil, Sediment and Water Resources: 15th International Conference, pp. 54-61, AquaConSoil (20–24 May 2019, Antwerp, Belgium)

Leterme, B., Neyens, C., Huysmans, M., Jacques, D., (2019) MTHP: coupling PHREEQC to MT3D-USGS for reactive transport. GQ2019, Liège, Belgium.

Neyens, C., Jacques, D., Leterme, B., Huysmans, M., (2019) A coupled HYDRUS-MT3D-PHREEQC tool for simulating variably-saturated reactive solute transport. EGU General Assembly 2019, Vienna, Austria.

Neyens, C., Jacques, D., Leterme, B., Huysmans, M., (2019) Coupling HYDRUS and PHREEQC to MT3D-USGS. Modflow and More 2019, Golden, Colorado, USA.

Neyens, C., Jacques, D., Leterme, B., Huysmans, M., (2019) Simulating variably-saturated solute transport with a coupled HYDRUS - MT3D-USGS tool. GQ2019, Liège, Belgium.

Leterme, B., Neyens, C., Jacques, D. (2021) Coupling unsaturated and saturated zone reactive transport: Development and benchmarking of the MTHP tool. Third International Soil Modelling Consortium Conference, 2021 (Virtual).

Neyens, C., Leterme, B., Huysmans, M., Jacques, D. (2021) A new MCP package for reactive transport modelling in MT3D-USGS. 48th IAH conference, Brussels, September 2021.

Jacques, D., and Gedeon M. (2023) HPx as the geochemical solver in MT3D-USGS. 7th International Conference 'Hydrus Software Applications to Subsurface Flow and Contaminant Transport Problems', Prague.

Reports

Walstra J., Goovaerts T. & Heyvaert, V.M.A. (2024). Screening, monitoring and geological modelling of selected contaminated sites in Belgium. Contributions to the RESPONSE project. GSB report 2024/XXX, Scientific Reports Series, Royal Belgian Institute of Natural Sciences – Geological Survey of Belgium.

ACKNOWLEDGEMENTS

Figures in the sections related to the Canivet landfill site (sections 3.3.2 and 4.4) are from Neyens (2022)

REFERENCES

Appelo, C. A. J., and D. Postma. 2005. *Geochemistry, groundwater and pollution, 2nd edition* (A.A. Balkema Publishers: Amsterdam, The Netherlands).

Bea, S. A., H. Wainwright, N. Spycher, B. Faybishenko, S. S. Hubbard, and M. E. Denham. 2013. 'Identifying key controls on the behavior of an acidic-U(VI) plume in the Savannah River Site using reactive transport modeling', *Journal of Contaminant Hydrology*, 151: 34-54.

Bedekar, V., E.D. Morway, C.D. Langevin, and m. Tonkin. 2016. "MT3D-USGS version 1: A U.S. Geological Survey release of MT3DMS updated with new and expanded transport capabilities for use with MODFLOW: U.S. Geological Survey Techniques and Methods 6-A53, 69 p., http://dx.doi.org/10.3133/tm6A53." In.

Bhanja, S. N., J. Wang, N. K. Shrestha, and X. Zhang. 2019a. 'Microbial kinetics and thermodynamic (MKT) processes for soil organic matter decomposition and dynamic oxidation-reduction potential: Model descriptions and applications to soil N 2 O emissions', *Environ Pollut*: 812-23.

Bhanja, Soumendra N., Junye Wang, Narayan K. Shrestha, and Xiaokun Zhang. 2019b. 'Modelling microbial kinetics and thermodynamic processes for quantifying soil CO2 emission', *Atmospheric Environment*, 209: 125-35.

Cressie, N.A.C. 1993. *Statistics for Spatial Data* (John Wiley & Sons, Inc).

DOV. 2021. 'Databank Ondergrond Vlaanderen - Geologisch 3D-model (v3)', Accessed 2021-07-23. http://dov.vlaanderen.be.

Essaid, H. I., B. A. Bekins, E. M. Godsy, E. Warren, M. J. Baedecker, and I. M. Cozzarelli. 1995. 'Simulation of aerobic and anaerobic biodegradation processes at a crude oil spill site.', *Water Resources Research*, 31: 3309–27.

Essaid, H. I., I. M. Cozzarelli, R. P. Eganhouse, W. N. Herkelrath, B. A. Bekins, and G. N. Delin. 2003. 'Inverse modeling of BTEX dissolution and biodegradation at the Bemidji, MN crude-oil spill site', *Journal of Contaminant Hydrology*, 67: 269-99.

Fetter, C.W. 2001. *Applied Hydrogeology (4th ed.)* (Prentice Hall).

Flemish Government. 2024. 'EMIS Navigator. https://navigator.emis.vito.be/detail?woId=10071&woLang=nl&woVersion=2024-12-12. Vlaamse Navigator Milieuwetgeving', Accessed 12 March 2024.

GDI-Vlaanderen. 2021. 'Geografische data-infrastructuur Vlaanderen', Accessed 2024-08-28. https://www.vlaanderen.be/geopunt/vlaams-geoportaal/gdi-vlaanderen.

Greskowiak, J., J. Gwo, D. Jacques, J. Yin, and K. U. Mayer. 2015. 'A benchmark for multi-rate surface complexation and 1D dual-domain multi-component reactive transport of U(VI)', *Computational Geosciences*, 19: 585-97.

Hammes, F., and T. Egli. 2007. "A Flow Cytometric Method for AOC Determination. Techneau, 1-20. Report No.: 3.3.1." In.

Hunter, K. S., Y. F. Wang, and P. Van Cappellen. 1998. 'Kinetic modeling of microbially-driven redox chemistry of subsurface environments: coupling transport, microbial metabolism and geochemistry', *Journal of Hydrology*, 209: 53-80.

Huysmans, M., and A. Dassargues. 2009. 'Application of multiple-point geostatistics on modelling groundwater flow and transport in a cross-bedded aquifer (Belgium)', *Hydrogeology Journal*, 17: 1901-11.

———. 2012. 'Modeling the effect of clay drapes on pumping test response in a cross-bedded aquifer using multiple-point geostatistics', *Journal of Hydrology*, 450: 159-67.

Huysmans, M., P. Orban, E. Cochet, M. Possemiers, B. Ronchi, K. Lauriks, O. Batelaan, and A. Dassargues. 2014. 'Using Multiple-Point Geostatistics for Tracer Test Modeling in a Clay-Drape Environment with Spatially Variable Conductivity and Sorption Coefficient', *Mathematical Geosciences*, 46: 519-37.

Jacques, D., J. Simunek, D. Mallants, and M. T. van Genuchten. 2002. "Multicomponent transport model for variably-saturated porous media: application to the transport of heavy metals in soils." In *14th International Conference on Computational Methods in Water Resources*, 555-62.

———. 2005. "Long term uranium migration in agricultural field soils following mineral P-fertilization." In *ICEM05: The 10th International conference on Environmental Remediation and Radioactive Waste Management*. Glasgow, United Kingdom.

Jacques, D., J. Šimůnek, D. Mallants, and M. Th van Genuchten. 2006. 'Operator-splitting errors in coupled reactive transport codes for transient variably saturated flow and contaminant transport in layered soil profiles', *Journal of Contaminant Hydrology*, 88: 197-218.

———. 2008a. 'Modeling Coupled Hydrologic and Chemical Processes: Long-Term Uranium Transport following Phosphorus Fertilization', *Vadose Zone Journal*, 7: 698-711.

———. 2008b. 'Modelling coupled water flow, solute transport and geochemical reactions affecting heavy metal migration in a podzol soil', *Geoderma*, 145: 449-61.

Jacques, D., J. Simunek, D. Mallants, and M. Th. van Genuchten. 2018. 'The HPx software for multicomponent reactive transport during variably-saturated flow: Recent developments and applications', *JOURNAL OF HYDROLOGY AND HYDROMECHANICS*, 66: 211-26.

Jia, M., D. Jacques, F. Gérard, D. Su, K. U. Mayer, and J. Šimůnek. 2019. 'A benchmark for soil organic matter degradation under variably saturated flow conditions', *Computational Geosciences*.

Kennedy, J., and R. Eberhart. 1995. 'Particle swarm optimization', *1995 Ieee International Conference on Neural Networks Proceedings, Vols 1-6*: 1942-48.

Koopal, L. K., T. Saito, J. P. Pinheiro, and W. H. van Riemsdijk. 2005. 'Ion binding to natural organic matter: General considerations and the NICA–Donnan model', *Colloids and Surfaces A: Physicochemical and Engineering Aspects*, 265: 40-54.

Laloy, E., and D. Jacques. 2022. 'Speeding Up Reactive Transport Simulations in Cement Systems by Surrogate Geochemical Modeling: Deep Neural Networks and k-Nearest Neighbors', *Transport in Porous Media*.

MacQuarrie, K. T. B., E. A. Sudicky, and E. O. Frind. 1990. 'Simulation of biodegradable organic contaminants in groundwater: 1. Numerical formulation in principal directions', *Water Resources Research*, 26: 207-22.

MacQuarrie, K. T. B., and E.A. Sudicky. 2001. 'Multicomponent simulation of wastewater-derived nitrogen and carbon in shallow unconfined aquifers: I. Model formulation and performance', *Journal of Contaminant Hydrology*, 47: 53-84.

Marsac, Rémi, Nidhu L. Banik, Johannes Lützenkirchen, Charlotte Catrouillet, Christian M. Marquardt, and Karen H. Johannesson. 2017. 'Modeling metal ion-humic substances complexation in highly saline conditions', *Applied Geochemistry*, 79: 52-64.

Mayer, K. U., P. Alt-Epping, D. Jacques, B. Arora, and C. I. Steefel. 2015. 'Benchmark problems for reactive transport modeling of the generation and attenuation of acid rock drainage', *Computational Geosciences*, 19: 599-611.

Mayer, K. U., E. O. Frind, and D. W. Blowes. 2002. 'Multicomponent reactive transport modeling in variably saturated porous media using a generalized formulation for kinetically controlled reactions', *Water Resources Research*, 38: 1174, doi:10.029/2001WR000862.

Meckenstock, Rainer U., Martin Elsner, Christian Griebler, Tillmann Lueders, Christine Stumpp, Jens Aamand, Spiros N. Agathos, Hans-Jørgen Albrechtsen, Leen Bastiaens, Poul L. Bjerg, Nico Boon, Winnie Dejonghe, Wei E. Huang, Susanne I. Schmidt, Erik Smolders, Sebastian R. Sørensen, Dirk Springael, and Boris M. van Breukelen. 2015. 'Biodegradation: Updating the Concepts of Control for Microbial Cleanup in Contaminated Aquifers', *Environmental Science & Technology*, 49: 7073-81.

Meersmans, J., K. Van Weverberg, S. De Baets, F. De Ridder, S. J. Palmer, B. van Wesemael, and T. A. Quine. 2016. 'Mapping mean total annual precipitation in Belgium, by investigating the scale of topographic control at the regional scale', *Journal of Hydrology*, 540: 96-105.

Meeussen, J. C. L. 2003. 'ORCHESTRA: An object-oriented framework for implementing chemical equilibrium models', *Environmental Science & Technology*, 37: 1175-82.

Meyus, Y., O. Batelaan, and F. De Smedt. 2000. "Concept Vlaams Groundwater Model (VGM): Deelrapport 1: Hydrogeologische Codering van de Ondergrond van Vlaanderen (HCOV)." In.

Neyens, C. 2022. 'Reactive transport modelling of point source contaminations in groundwater: Model input and process abstraction', Vrije Universiteit Brussel.

Nguyen, T. P. O., M. A. Hansen, L. H. Hansen, B. Horemans, S. J. Sorensen, R. De Mot, and D. Springael. 2019. 'Intra- and inter-field diversity of 2,4-dichlorophenoxyacetic acid-degradative plasmids and their tfd catabolic genes in rice fields of the Mekong delta in Vietnam', *Fems Microbiology Ecology*, 95.

Nmor, S. I., E. Viollier, L. Pastor, B. Lansard, C. Rabouille, and K. Soetaert. 2022. 'FESDIA (v1.0): exploring temporal variations of sediment biogeochemistry under the influence of flood events using numerical modelling', *Geosci. Model Dev.*, 15: 7325-51.

Parkhurst, D. L., and C. A. J. Appelo. 1999. "User's guide to PHREEQC (version 2) - A computer program for speciation, batch-reaction, one-dimensional transport, and inverse geochemical calculations." In.

———. 2013. "Description of Input and Examples for PHREEQC Version 3 — A Computer Program for Speciation , Batch-Reaction , One-Dimensional Transport , and Inverse Geochemical Calculations " In *Chapter 43 of Section A, Groundwater Book 6, Modeling Techniques*, 519. U. S. Geological Survey.

Pebesma, E. J. 2004. 'Multivariable geostatistics in S: the gstat package', *Computers & Geosciences*, 30: 683-91.

Peeters, L. 2010. 'Groundwater and geochemical modelling of the unconfined Brussels aquifer, Belgium', KULeuven.

Peters, L. 2010. 'Groundwater and geochemical modelling of the unconfined Brussels aquifer', K.U.Leuven.

Possemiers, M., M. Huysmans, L. Peeters, O. Batelaan, and A. Dassargues. 2012. 'Relationship between sedimentary features and permeability at different scales in the Brussels Sands', *Geologica Belgica*, 15: 156-64.

Prommer, H., and Vincent Post. 2010. "pht3D - A Reactive Multicomponent Transport Model for Saturated Porous Media. User's Manual v2.10." In.

Raes, B., B. Horemans, D. Rentsch, J. T'Syen, M. G. K. Ghequire, R. De Mot, R. Wattiez, H. P. E. Kohler, and D. Springael. 2019. 'sp. MSH1 Mineralizes the Groundwater Micropollutant 2,6-Dichlorobenzamide through a Unique Chlorobenzoate Catabolic Pathway', *Environmental Science & Technology*, 53: 10146-56.

Raes, B., J. S. Wang, B. Horemans, L. Dirckx, S. Waldherr, H. P. E. Kohler, and D. Springael. 2024. 'The Growth Yield of Aminobacter niigataensis MSH1 on the Micropollutant 2,6-Dichlorobenzamide Decreases Substantially at Trace Substrate Concentrations', *Environmental Science & Technology*, 58: 2859-69.

Reimann, Clemens, Manfred Birke, Alecos Demetriades, Peter Filzmoser, and Patrick O'Connor. 2014. "Chemistry of Europe's Agricultural Soils: Part A : Methodology and Interpretation of the GEMAS Data Set." In.: Bundesanstalt für Geowissenschaftem und Rohstoffe.

Rubin, Y. 2003. *Applied Stochastic Hydrogeology* (Oxford University Press).

Salmon, S. U., A. W. Rate, Z. Rengel, S. Appleyard, H. Prommer, and C. Hinz. 2014. 'Reactive transport controls on sandy acid sulfate soils and impacts on shallow groundwater quality', *Water Resources Research*, 50: 4924-52.

Sardin, M., R. Krebs, and D. Schweich. 1986. 'Transient Mass-Transport in the Presence of Nonlinear Physicochemical Interaction Laws - Progressive Modeling and Appropriate Experimental Procedures', *Geoderma*, 38: 115-30.

Šimůnek, J., G. Brunetti, D. Jacques, M. Th. van Genuchten, and M. Šejna. 2024. 'Developments and applications of the HYDRUS computer software packages since 2016', *Vadose Zone Journal*: doi.org/10.1002/vzj2.20310.

Simunek, J., D. Jacques, G. Langergraber, S. A. Bradford, M. Sejna, and M. Th van Genuchten. 2013. 'Numerical Modeling of Contaminant Transport Using HYDRUS and its Specialized Modules', *Journal of the Indian Institute of Science*, 93: 265-84.

Simunek, J., M. Sejna, G. Brunetti, and M. T. van Genuchten. 2022. "The HYDRUS Software Package for Simulating One-, Two-, and Three-Dimensional Movement of Water, Heat, and Multiple Solutes in Variably-Saturated Porous Media, Technical Manual I, Hydrus 1D, Version 5.x." In, 334. Prage, Czech Republic: PC Progress.

Simunek, J., M. Sejna, H. Saito, K. Sakai, and M. T. van Genuchten. 2018. " The HYDRUS-1D Software Package for Simulating the Movement of Water, Heat, and Multiple Solutes in Variably Saturated Media, Version 4.17." In *HYDRUS Software Series 3*, 348. Department of Environmental Sciences, University of California Riverside, Riverside, California, USA.

Šimůnek, J., M. T. van Genuchten, and M. Šejna. 2016. 'Recent Developments and Applications of the HYDRUS Computer Software Packages', *Vadose Zone Journal*, 15.

Šimůnek, Jiří, Diederik Jacques, and Miroslav Šejna. 2013. "HP2 / 3 : Extensions of the HP1 Reactive Transport Code to Two and Three Dimensions." In *4th International Conference Proceedings of the HYDRUS Software Applications to Subsurface Flow and Contaminant Transport Problems*, 345-54.

Simunek, Jiri, Diederik Jacques, M. Th van Genuchten, and D. Mallants. 2006. 'Multicomponent geochemical transport modeling using HYDRUS-1D and HP1', *Journal Of The American Water Resources Association*: 1537-47.

Šimůnek, Jirka, Diederik Jacques, Navin K. C. Twarakavi, and Martinus Th Genuchten. 2009. 'Selected HYDRUS modules for modeling subsurface flow and contaminant transport as influenced by biological processes at various scales', *Biologia*, 64: 465-69.

Simunek, Jirka, M. Sejna, and M. T. van Genuchten. 2012. "The DualPerm Module for HYDRUS (2D/3D) - Simulating Two-Dimensional Water Movement and Solute Transport in Dual-Permeability Variably-Saturated Porous Media, Version 1." In *PC Progress, Prague, Czech Republic,*.

Sorensen, S. R., M. S. Holtze, A. Simonsen, and J. Aamand. 2007. 'Degradation and mineralization of nanomolar concentrations of the herbicide dichlobenil and its persistent metabolite 2,6-dichlorobenzamide by isolated from dichlobenil-treated soils', *Applied and Environmental Microbiology*, 73: 399-406.

Steefel, C. I., C. A. J. Appelo, B. Arora, D. Jacques, T. Kalbacher, O. Kolditz, V. Lagneau, P. C. Lichtner, K. U. Mayer, J. C. L. Meeussen, S. Molins, D. Moulton, H. Shao, J. Šimůnek, N. Spycher, S. B. Yabusaki, and G. T. Yeh. 2015. 'Reactive transport codes for subsurface environmental simulation', *Computational Geosciences*, 19: 445-78.

Steefel, Carl I., Steven B. Yabusaki, and K. Ulrich Mayer. 2015. 'Reactive transport benchmarks for subsurface environmental simulation', *Computational Geosciences*, 19: 439-43.

Tipping, E., P. M. Chamberlain, M. Fröberg, P. J. Hanson, and P. M. Jardine. 2011. 'Simulation of carbon cycling, including dissolved organic carbon transport, in forest soil locally enriched with 14C', *Biogeochemistry*, 108: 91-107.

Tipping, E., S. Lofts, and J. E. Sonke. 2011. 'Humic Ion-Binding Model VII: a revised parameterisation of cation-binding by humic substances', *Journal of Environmental Chemistry*, 8: 225-35.

Van Cappellen, P., and Y. Wang. 1996. 'Cycling of iron and manganese in surface sediments; a general theory for the coupled transport and reaction of carbon, oxygen, nitrogen, sulfur, iron, and manganese', *American Journal of Science*, 296: 197-243.

Van Keer, I., J. Bronders, and R. Smolders. 2001. "Oriënterend bodemonderzoek vormalige stortplaats CANIVET te Haasroode (Oud-Heverlee)." In.

Vandermaesen, J., S. Y. Du, A. J. Daly, J. M. Baetens, B. Horemans, B. De Baets, N. Boon, and D. Springael. 2022. 'Interspecies Interactions of the 2,6-Dichlorobenzamide Degrading

sp. MSH1 with Resident Sand Filter Bacteria: Indications for Mutual Cooperative Interactions That Improve BAM Mineralization Activity', *Environmental Science & Technology*, 56: 1352-64.

VMM. 2008. "Grondwater in Vlaanderen: het Brulandkrijtsysteem." In.

Walter, A. L., E. O. Frind, D. W. Blowes, C. J. Ptacek, and J. W. Molson. 1994. 'Modeling of multicomponent reactive transport in groundwater 1. Model development and evaluation', *Water Resources Research*, 39: 3137-48.

Watergroep, De. 2015. "Grondwaterwinningen Vlierbeek-HAC: modelinstrumentarium." In.

Watergroup. 2015. "Grondwaterwinningen Vlierbbeek-HAC: modelinstrumentarium." In.

Xie, Mingliang, K. Ulrich Mayer, Francis Claret, Peter Alt-Epping, Diederik Jacques, Carl Steefel, Christophe Chiaberge, and J. Šimůnek. 2015. 'Implementation and evaluation of permeability-porosity and tortuosity-porosity relationships linked to mineral dissolution-precipitation', *Computational Geosciences*, 19: 655-71.

Zambrano-Bigiarini, M., and R. Rojas. 2013. 'A model-independent Particle Swarm Optimisation software for model calibration', *Environmental Modelling & Software*, 43: 5-25.

Zomlot, Z., B. Verbeiren, M. Huysmans, and O. Batelaan. 2015. 'Spatial distribution of groundwater recharge and base flow: Assessment of controlling factors', *Journal of Hydrology: Regional Studies*, 4: 349–68.

ANNEX

6.1 Study sites report – Section of cementries and landfills – J. Schoonejans and B. van Wesemael, 2017.

6.2 Response – Installation of piezometers for screening (WP2) and monitoring (WP3)